# A Hierarchical Control Strategy for Hybrid Vehicles

**A THESIS**
**SUBMITTED TO THE FACULTY OF THE GRADUATE SCHOOL**
**OF THE UNIVERSITY OF MINNESOTA**
**BY**

**Felicitas Barbara Mensing**

**IN PARTIAL FULFILLMENT OF THE REQUIREMENTS**
**FOR THE DEGREE OF**
**Master of Science**

**July, 2010**

# Acknowledgements

I would like to thank my advisor Prof. Perry Li for his support of my studies at the University of Minnesota.

I wish to acknowledge the staff of the Center for Compact and Efficient Fluid Power for their financial and intellectual support. I would like to thank my fellow students for their help and advice when I needed it.

This research was funded by the Center for Compact and Efficient Fluid Power (CCEFP), a National Science Foundation Engineering Research Center.

## Abstract

With increasing gasonline prices and the rise of environmental concerns the demand for cleaner, more fuel efficient vehicles rises. The development of an environmentally friendly transportation technology is necessary. Hybrid vehicles were found to have high potential in decreasing fuel consumption in the transportation sector. Fuel efficiency increases with addtional flexibility in the drive train due to multiple power sources. With growing complexity in the drive train appropriate control is critical to achieve maximum fuel economy.

Research conducted by the Test Bed 3 group in the Center for Compact and Efficient Fluid Power at the University of Minnesota is investigating the potentials of fluid power power trains to drastically decrease fuel consumption in hybrid vehicles. In the scope of the Test Bed 3 project controls algorithms are developed for implementation on the hybrid vehicle.

In this thesis a control strategy based on hierarchical control is proposed. A generic three level control strategy that is applicable to any hybrid vehicle configuration is derived. On the example of two power split hybrid drive trains the use of this controls framework will be illustrated in simulation. Case studies were performed using an off-line simulation approach. These investigate optimal sizing of the power train, optimal operation of a power split configurated vehicle and the relationship of hydraulic efficiency and fuel consumption. Three hybrid architectures are compared in fuel economy. Fuel savings through hybridization of a conventional vehicle are discussed.

Using an input coupled hydraulic hybrid vehicle the implementation of the proposed strategy in real time is discussed. System level control implementation is shown and results from test drives are presented.

# Contents

# List of Tables

# List of Figures

# Chapter 1

# Introduction

In this chapter a background on hybrid vehicles and their controls will be presented. Relevant previous work will be discussed. The goals of the thesis will be defined and finally an overview of the thesis will be given.

## 1.1 Background

A hybrid vehicle is defined to be a vehicle that uses a mixture of power sources. The first hybrid was designed in the year 1899 by Ferdinand Porsche. The vehicle (Figure 1.1), called the *Lohnerporsche*, had two combustion engines as well as an electric motor and used a battery for intermediate energy storage ([1]). The vehicle never saw production because the simple internal combustion engine vehicles were selling too well. A popular dual-powered vehicle in the 1930 depression was the *haybrid*, which combined the output power of an internal combustion engine in a vehicle with the power of horses pulling it ([2]). In the early 19th century the internal combustion engine was competing with technologies like steam and electric vehicles like the Milburn Electric Car ([2]) which was produced by General Motors until 1930. At the time, oil was very cheap, plentifully available, and the combustion engine was considered to be relatively clean compared to coal and wood driven vehicles. This and the convenience of the liquid storage and very high energy content of gasoline finally made the production of alternative technologies unnecessary.

Today, although improved, vehicles still use the same technology invented 100 years

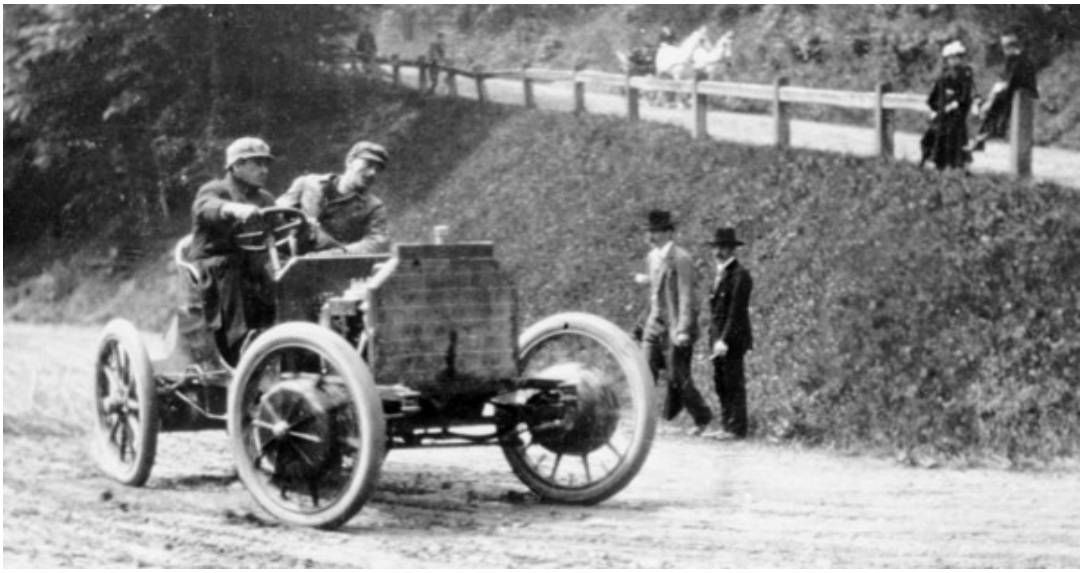

Figure 1.1: The 'Lohnerporsche'.

ago. Since then non-renewable fuels have become scarce, and therefore more costly, and it has been shown that the use of combustion engines threatens the health of the population and the environment. With these facts in mind researchers are investigating ways to reduce fuel consumption in transportation. Together with fuel cell drive trains and electric vehicles, hybrid vehicles were found to have potential to increase efficiency of fuel usage. Advancements in this technology have been achieved in recent years such that hybrid vehicles can be found on highways again today.

Hybrid vehicles save fuel and reduce emissions mainly by recovering braking energy that is usually lost into friction in conventional vehicles. Using regenerative braking the energy is stored and can be used for future propulsion. Further by using alternative power sources in hybrid vehicles the engine can be operated more efficiently and fuel consumption is therefore reduced. By using alternative power sources for start up the engine can be turned off when not used. This gets rid of idle losses and therefore increases fuel economy.

Electric hybrid vehicles, where a battery operates as energy storage and electric generators and motors are used to help propel the vehicle, are common in passenger

vehicle applications. In hydraulic hybrid vehicles the alternative energy storage consists of an hydraulic accumulator and hydraulic pumps and motors are used in addition to the engine. Hydraulic hybrid vehicles are often seen in large road vehicles like garbage trucks or delivery trucks. With the improvements of fluid power technologies some current research work considers hydraulic hybrid drive trains for passenger vehicle applications.

This research was funded by the NSF Center for Compact and Efficient Fluid Power (CCEFP). The goal of the CCEFP is to improve fluid power technology in efficiency, compactness and effectiveness. Specifically, the Test Bed 3 research project to develop a Hydraulic Hybrid Passenger Vehicle (HHPV) motivated this thesis work. The goal of the project is to design and build a fluid power drive train that is fuel efficient and comparable in drivability to other passenger vehicles in an urban environment. To achieve this goal a power split hydraulic hybrid drive train was chosen.

In comparison to electric hybrids fluid power has the advantage of power density while electrics achieve better energy density in the battery energy storage. Hydraulic components are generally considered more robust than their electric counterparts. On the market the weight and cost of the components will affect the demand. To draw a final comparison environmental issues should also be taken into consideration. The Test Bed 3 research group is investigating the potentials for hydraulic hybrids to compete with electric hybrids in passenger vehicles.

Hybrid power trains have been implemented in parallel, series and power split configuration. A parallel drive train can be seen in Figure 1.2. The engine is connected to the wheels by the mechanical carrier shaft, while a hydraulic unit is also coupled to the shaft. An accumulator can be used as energy storage to regenerate energy while braking. In this architecture all the power to the wheels is transmitted through the mechanical shaft. High efficiencies can therefore be achieved for power transmission. With one hydraulic pump/motor coupled to the carrier shaft the engine can be assisted in torque only. Engine management is therefore limited, which results in a non optimal efficiency of the combustion process.

In the series architecture, seen in Figure 1.3, the engine is driving a hydraulic pump to charge up the accumulator. The energy stored is then used by the hydraulic motor at the wheels to provide the desired power. In this configuration power to the wheels is transmitted through the possibly inefficient hydraulic line. Since the engine is decoupled

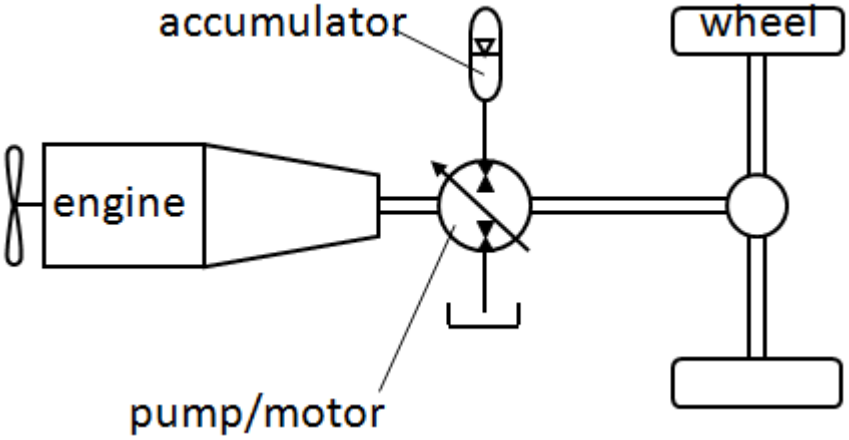


Figure 1.2: The parallel hybrid architecture.

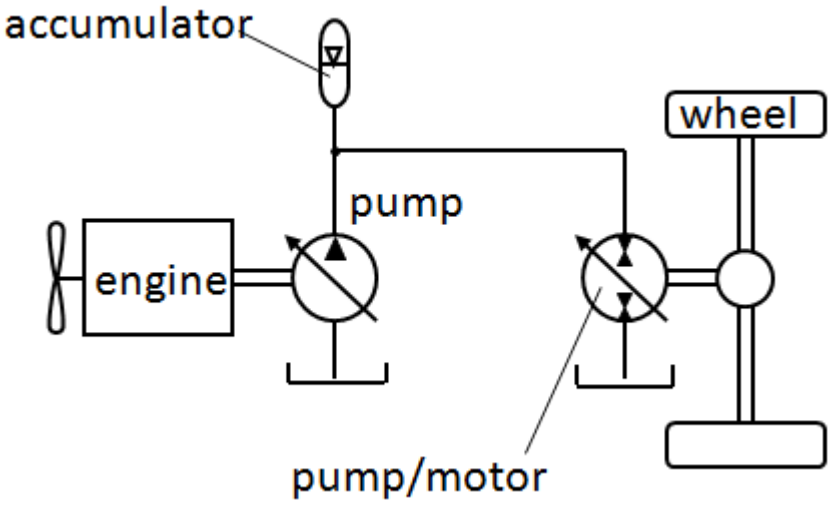


Figure 1.3: The series hybrid architecture.

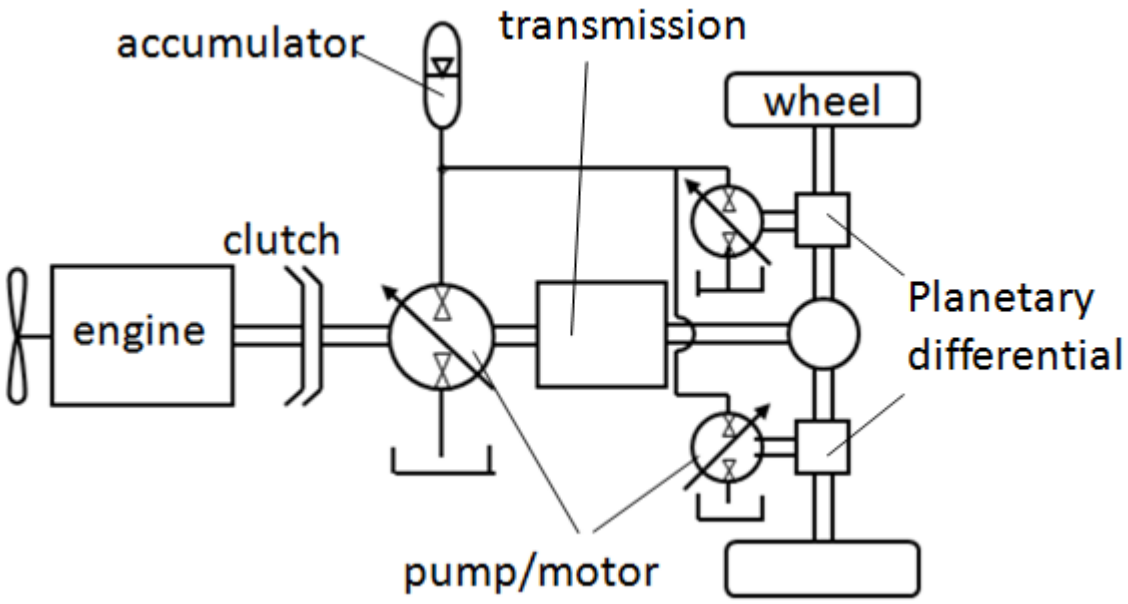


Figure 1.4: The power split hybrid architecture.

from wheel operation, full engine management is possible and the maximum engine efficiency can be achieved. Using the hydraulic unit at the wheel as a pump braking energy can be regenerated.

The power split architecture, chosen by the Test Bed 3 research group, combines the positive aspects of the parallel and series configuration. As seen in Figure 1.4 the engine in this drive train is coupled to the wheels through the mechanical carrier shaft. A hydraulic pump/motor is attached to the mechanical shaft to alter the engine operation in torque. Additional pump/motors combine the power from the engine with that of the hydraulic path through a planetary differential. The pump/motors at the output change the operation of the engine in speed. In this architecture the mechanical path can be used to transmit power from the engine efficiently, while the hydraulic path enables us to perform full engine management. The engine operation is decoupled from the wheel operation to allow for optimal operation. Energy can be recovered and stored in the accumulator by either hydraulic unit. This thesis attempts to verify and guide the choice of a power split vehicle.

With multiple power sources available the controls on hybrid vehicles are more complex than in conventional power trains. In conventional vehicles the power request is sent straight to the engine. In a hybrid vehicle the stored energy in the accumulator can be used to satisfy the power demand in addition to the combustion engine. A controls strategy is needed to specify the use of the stored energy, in order to achieve maximum overall system efficiency over a trip. In literature a significant amount of work can be found on control implementation on parallel or series hybrid vehicles. Little work has been done on power split hybrid vehicles due to their complexity. This thesis work focuses on the development of a strategy implementable on any hybrid configuration and aids in the developement of real-time controls on the HHPV vehicle in the CCEFP.

## 1.2 Literature review

This literature review highlights control strategies on hybrid vehicles in previous works. Energy management strategies proposed in the past can be seperated into two categories: Optimizations used in off-line simulation of the vehicle over a given drive cycle and algorithms that are implemented in real-time with no future knowledge of driving operations. In Section 1.2.1 algorithms used in off-line simulation will be discussed. Previous work on control algorithms that are implementable in real-time on hybrid vehicles will be shown in Section 1.2.2. In Section 1.2.3 literature on real-time implementation of such control algorithms will be discussed.

### 1.2.1 Controls strategies used in simulation

A majority of past work on controls in hybrid vehicles uses system models to simulate the vehicle operation in a quasi-static way. A known driving schedule can then be used to optimize the power train operation over the entire trip. This approach is often used to gain knowledge about the drive train configuration, its optimal operation, or best sizing of components. Various energy management strategies developed for off-line simulation are shown in [3] and include static optimization, numerical optimization methods like dynamic programming and analytic optimization such as the Lagrange Multiplier method. The mentioned approaches require a priori knowledge of the driving schedule and are therefore not implementable in real time. Due to the complexity of

the power split architecture previous work on this hybrid configuration has been mainly in off-line simulation. Zhu ([4]) has shown the results of using a four step method to design an appropriate energy management strategy for power split hybrid vehicles. With his approach he developed rule based and fuzzy rule based energy management algorithms to control the hybrid drive train. Using computer simulations he has shown the effectiveness of his approach.

Work showing a comparison of three control strategies on a power split hybrid has been done by Liu and Peng in 2006([5]) and 2008([6]). It was found that a equivalent consumption minimization strategy(ECMS) and a stochastic dynamic programming management strategy can achieve near optimum fuel economy. Using the knowledge of the entire drive cycle the dynamic programming approach specifies optimal fuel economy values for comparison. Research at Seoul National University ([7, 8]) is comparing the computational cost and fuel economy accuracy of dynamic programming versus the computation of an equivalent fuel consumption (EFC) factors. It has been shown that the EFC approach can compute similar fuel economy approximation in significantly less time. It is therefore more cost effective and should be used in off-line optimal simulation of the drive train over dynamic programming.

### 1.2.2 Controls strategy implementable in real time

While a considerate amount of literature can be found on real time control implementation in hybrid vehicles, the fraction discussing control strategies on power split hybrid vehicles is small. Various energy management algorithms have been shown to be implementable in real time to improve fuel economy in hybrid vehicles. Some can be found in [3, 9]. Here engine management strategies like rule-based control, equivalent consumption minimization strategies, predictive control and stochastic dynamic programming are discussed.

Algorithms shown to work effectively on power split hybrid vehicles are presented by Liu and Borhan. In his comparison([6]), Liu shows that stochastic dynamic programming and an ECMS approach can potentially achieve near optimal results and are implementable due to their causality. Borhan discusses a predictive energy management strategy in his work in [10]. It was found that a predictive control algorithm such as the receding horizon linear model predictive control can increase fuel economy when used

in real time control.

### 1.2.3 Implementation of control algorithms on real-time vehicle

Energy management algorithms presented in Section 1.2.2 do not require knowledge of future driving conditions and are therefore implementable in real time. Most work on real-time control shows supervisory energy management strategies, however, does not discuss system level control. For implementation purposes a control framework is needed to use the suggested algorithms. In 1997 Hubbard([11]) shows an approach of using a supervisory control scheme as well as a system level control in an electric hybrid bus to properly control the vehicle. In his work Hubbard proposes the implementation of a supervisory control scheme to handle engine management and the use of system level controllers to control the electric motors in the electric hybrid vehicle. Bathaee proposes a two level hierarchical control strategy in his work with a parallel hybrid vehicle in 2005([12]). As mentioned by him, in the controls design most complex systems require hierarchical approaches. In recent years work has been done at Wuhan University of Technology on optimal control of parallel electric hybrid vehicles. Researchers here propose a three level control strategy that seperates the control implementation into the organization level, the coordination level and the control level([13]). In this hierarchical control scheme the organization level uses an energy management strategy to ensure efficient operation of the powertrain. The coordination level consists of controllers specifying the strategy for individual modes of the power train. The control level contains engine, motor and battery controllers. An SAE technical paper published in 2006 by Pi Technology confirms the need for a framework for power and systems management in hybrid vehicles([14]). The need of a supervisory control unit becomes a necessity when working with a wide range of technologies. Pi Technology, working with hybrid technologies like fuel cells, battery systems and hydraulic based system, suggest the use of a Powertrain System Controls(PSC) that includes three distinct components and is responsible for the overall control of the powertrain. Seperate control systems for subsystems like the engine or hydraulic units are proposed in their strategy. Other work found on real-time implementation of energy management strategies often does not specify the system level control used.

## 1.3 Thesis goal

In most previous work hybrid energy management strategies have been investigated at a energy supervisory level only. For real-time control implementation in complex systems like hybrid vehicles a hierarchical control structure is needed to simplify the algorithm used. System level control is as important as the energy management strategy in real time control to achieve efficient system operation. The goal of this thesis is to present a framework that can be used to simplify the complex control structure of hybrid vehicles.

Control strategies in literature have been developed for simulation with the purpose of analyzing the drive train architecture or for real-time implementation to operate a hybrid vehicle efficiently. In the development of fuel efficient hybrid drive trains knowledge can be gained from drive train analysis that can then be used in the design and implementation of controls. The controls strategy proposed in this thesis guides off-line simulation work while using an implementable structure.

Literature often shows controls strategies specifically designed toward a vehicle architecture. Hybrid vehicles can be found in various configurations. The vehicles differ in alternative power sources, energy storage components but also in drive train configurations, like series, parallel or power split. This thesis aims at developing a general controls strategy that can be applied to the control design of any hybrid vehicle type. Hybrid drive trains are often complex to understand and therefore difficult to design and analyze. With the here defined hierarchical strategy drive train design is simplified into an easily solvable optimization problem. Analysis of the optimal operation of a hybrid vehicle becomes more organized. The goal here is to develop a strategy that can be used as a framework for hybrid vehicle analysis, drive train design and control development.

This thesis presents a control hierarchy together with examples of the use in simulation and implementation. The goal is to give the reader an idea of how the problem of controls design on a hybrid drive train can be approached.

## 1.4 Overview

In the following thesis two hydraulic hybrid vehicles are described in Chapter 2. Models for the vehicles are derived using their static and dynamic equations. A hierarchical

control strategy for hybrid vehicles is proposed in Chapter 3. The derivation of the strategy will be shown and three hierarchical levels will be discussed. The following two chapters show the use of such a strategy. In Chapter 4 the vehicle models are used together with the proposed control strategy in off-line simulation studies. Chapter 5 shows a real time control implementation approach on a hydraulic hybrid vehicle in power split configuration. Using the simplified control strategy a control algorithm is specified and test results are presented. In Chapter 6 a conclusion of this thesis work is presented and recommendations for future work in this area can be found. Matlab code that was used to perform simulations presented in this thesis can be found in Appendix A.

# Chapter 2

# System Modeling

The Test Bed 3 research group in the Center for Compact and Efficient Fluid Power at the University of Minnesota is currently working on two hydraulic hybrid vehicles. These are used in the Center to implement and test projects. Generation I, the Hydraulic Hybrid Passenger Vehicle (HHPV), is a hybrid vehicle in power split architecture with an input coupled drive train. Generation II consists of a Ford F150 Truck which was donated to the University by Ford Motor Company. The conventional transmission has been replaced with a hydro-static unit, that was developed by Folsom Technologies International. By adding valves and an accumulator to the vehicle it will be reconfigured into an output coupled power split hydraulic hybrid vehicle. In Chapter 2 models of the two vehicles will be derived by defining their static and dynamic equations. The modeling of engine and hydraulic components will be shown. These models will be used later in off-line simulations and real time implementation of a proposed control strategy.

## 2.1 Generation I: HHPV

In this section the Generation I vehicle will be introduced. The architecture of the vehicle will be described. The static equations of the drive train will be derived and the vehicle will be modeled using inertia dynamic relationships.

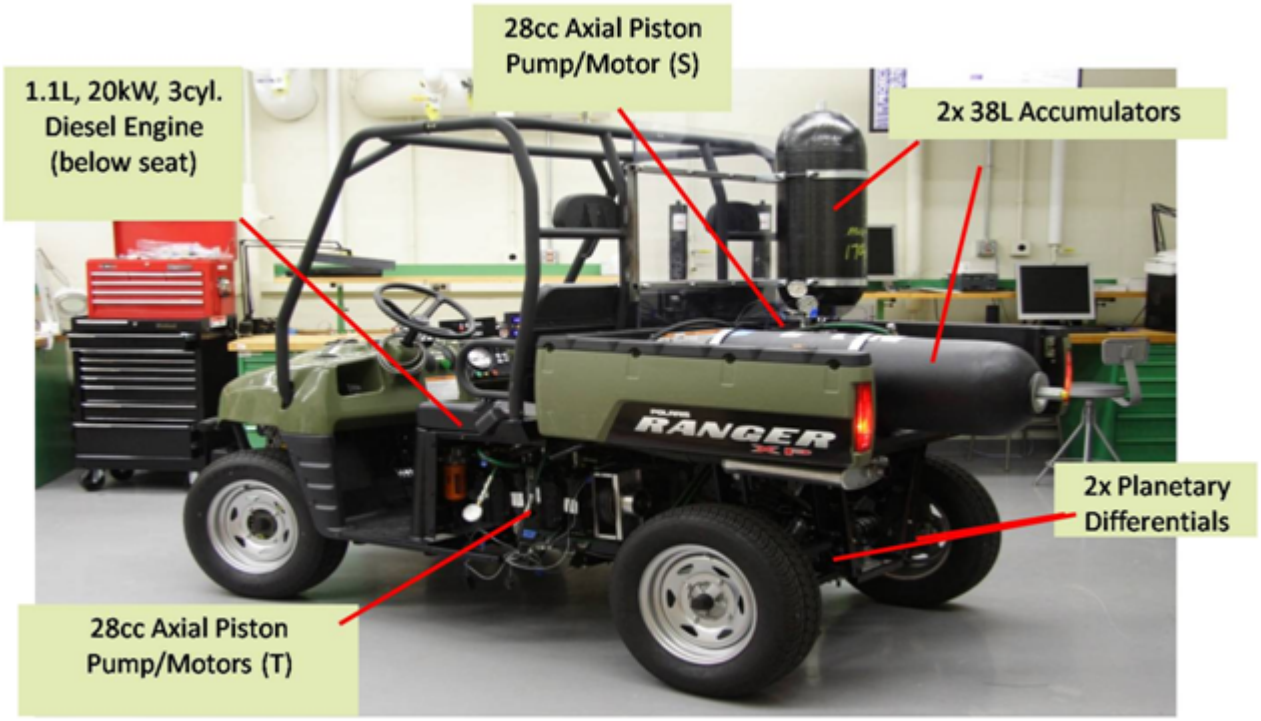


Figure 2.1: HHPV vehicle at the University of Minnesota.

### 2.1.1 The vehicle

The Gen 1 vehicle was built by reconfiguring the drive train of a commercially available Polaris Ranger vehicle as seen in Figure 2.1. The engine has been replaced by a small 1.1L Perkins 402C-11 3 cylinder diesel engine with a peak power of 19.5kW at 2500rpm. Sauer Danfoss swashplate axial piston pump/motors of the Series 42 were added to the vehicle. The vehicle was hybridized by attaching a high and low pressure 38 liter Eaton accumulator. In addition a 15L tank was added to the vehicle in order to store the hydraulic oil on board.

A drive train schematic can be seen in Figure 2.2. The front pump/motors are mechanically linked to the carrier shaft by a belt drive. When the clutch is engaged the engine speed is coupled to the pump/motor speed, which can subtract or add torque to the engine shaft. It is referred to as *torquer* and denoted by $T$. The power from the engine is split pre-transmission at the carrier shaft into the mechanical and the hydraulic

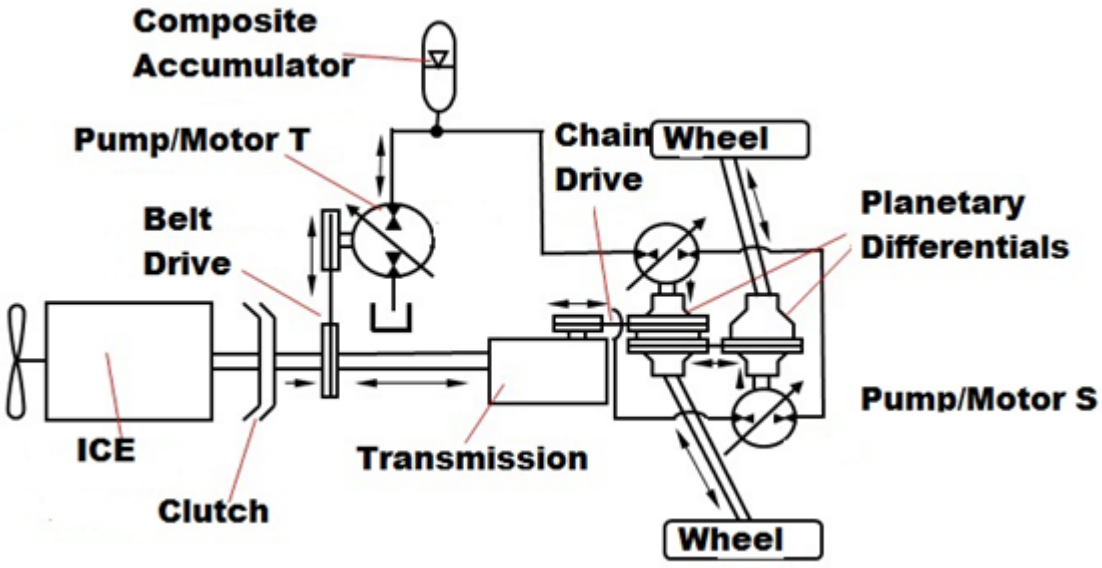


Figure 2.2: HHPV architecture.

path. At the wheels the power of the mechanical shaft and output from Pump/Motor (P/M)-S are combined by two planetary differentials. Due to the speed change of P/M-S the speed of the engine is decoupled from the wheel speed. These hydraulic units in the rear are therefore refered to as *speeders*.

### 2.1.2 Static equations

Utilizing the mechanical constraint of the planetary differential the speed and torque constraints of the drive train are given by

$$2\omega_c = \omega_{wL} + \omega_{SL}/R_S \tag{2.1}$$

$$2\omega_c = \omega_{wR} + \omega_{SR}/R_S \tag{2.2}$$

$$T_L := -R_S T_{SL} = -T_{wL} = T_{cL}/2 \tag{2.3}$$

where $\omega_c$ corresponds to the speed at the carrier input, $\omega_{wR/L}$ correspond to the right and left wheel speeds, and $\omega_{S,R/L}$ correspond to the right and left speeds of P/M-S's with the speed reduction $R_S$ between the axle of the differential and the pump/motor.

The torque at the shaft of P/M-S $T_{S,R/L}$, the torque at the shaft of the wheel $T_{w,R/L}$, and the torque at the carrier shaft $T_{c,R/L}$ are related by $T_{R/L}$ as seen in Equation 2.3. $GR_R$ is the total transmission ratio between the clutch and the differential. The speed reduction ratio $R_T$ relates the speed of the engine to the speed of P/M-T. Thus

$$(GR_R)\omega_c = \omega_{eng} = \omega_T/R_T \tag{2.4}$$

The values of the current reduction ratios in the drive train can be seen in Table 2.1.

Table 2.1: Speed Reduction Values

| **ratio notation** | **ratio** |
|---|---|
| $GR_R$ | 15.96 |
| $R_T$ | .676 |
| $R_S$ | 3.8 |

The static equations derived above model the input coupled power train of the Generation I vehicle. From the equations it can be seen that the speed of P/M-T is coupled to the engine speed while the torque of P/M-S is coupled to the commanded torque at the wheels. As seen in these equations, there are two degrees of freedom in speed but only one degree of freedom in torque at each differential. It is reflected in the static equations that the engine operation is fully decoupled from the wheel operating point, therefore full engine management is possible.

### 2.1.3 Inertia dynamics

To derive a dynamic model of the vehicle the inertia relationships are described including all major rotating parts. Due to the speed coupling of the engine and P/M-T the entire mechanical shaft can be modeled as one rotating group in two modes, engine declutched and engine clutched on. Therefore the inertia dynamic equations will be evaluated for the vehicle, for P/M-S and for the mechanical shaft. Considering longitudinal and yaw dynamics of the vehicle the following equations are derived for the rotating inertias:

$$\frac{1}{2}J_{veh}(\dot{\omega_{wR}} + \dot{\omega_{wL}}) \quad = \quad -(T_L + T_R) + D_{veh} \tag{2.5}$$

$$\frac{1}{2}J_{yaw}(\dot{\omega_{wR}} + \dot{\omega_{wL}}) = -(T_L - T_R) + D_{yaw} \quad (2.6)$$

$$J_S\dot{\omega_{SL}} = -T_L/R_S + u_{SL} \quad (2.7)$$

$$J_S\dot{\omega_{SR}} = -T_R/R_S + u_{SR} \quad (2.8)$$

$$J_{mech}\dot{\omega_c} = 2(T_L + T_R) + T_{mech} \quad (2.9)$$

where $T_L$ and $T_R$ are the internal torques as specified in Equation 2.3. The torque provided by the mechanical shaft, $T_{mech}$, is a combination of the scaled torques of the engine and P/M-T and can be evaluated by:

$$T_{mech} = \begin{cases} GR_R(T_{eng} + R_T u_T) & \text{if } u_{clutch} = 1 \\ GR_R R_T u_T & \text{if } u_{clutch} = 0 \end{cases} \quad (2.10)$$

where $u_{clutch}$ is a binary signal specifying the state of the clutch. If $u_{clutch} = 1$ the clutch is engaged and torque from the engine is transmitted to the drive shaft. When the clutch is disengaged, $u_{clutch} = 0$, and the engine torque does not contribute to the mechanical shaft torque. The inputs $u_T$ and $u_{S,L/R}$ are the torque of the P/M-T and P/M-Ss provided to the drive train. $u_{T/S}$ are functions of the pressure in the accumulator ($P$), speed of the hydraulic unit ($\omega$) and fractional displacement of the swashplate ($x$). The inertia of the vehicle as seen at the wheel is given by $J_{veh}$. $D_{veh}$ is a disturbance representing external forces like drag and rolling resistance of the vehicle or grade angle. The inertias of P/M-S and P/M-T are referred to as $J_S$ and $J_T$. Using the engine inertia, $J_{eng}$, and the inertia of P/M-T the inertia of the mechanical shaft at the differential can be calculated by:

$$J_{mech} = \begin{cases} (GR_R)^2(J_{eng} + R_T^2 J_T) & \text{if } u_{clutch} = 1 \\ (GR_R R_T)^2 J_T & \text{if } u_{clutch} = 0 \end{cases} \quad (2.11)$$

The engine inertia values are provided by the manufacturer, the values for the hydraulic pump/motors were experimentally identified and the vehicle inertia was theoretically calculated assuming a vehicle-weight of 1000kg. Inertia values for the engine, the pump/-motors and the vehicle can be seen in Table 2.2.

Due to the mechanical constraint of the planetary differential the inertia dynamic relationships derived in Equation 2.5-2.9 can be reduced by one degree of freedom. Considering the relationship $\omega_{veh} = (\omega_{wR} + \omega_{wL})/2$ of the longitudinal vehicle speed

Table 2.2: Inertia values

| **rotating part** | **inertia value** $[kgm^2]$ |
|---|---|
| $J_{eng}$ | .0975 |
| $J_T = J_S$ | .0018 |
| $J_{veh}$ | 65.36 |

the reduction process will be illustrated. Using Equation 2.1 and Equation 2.2 together with Equation 2.5-2.9 the following new relationships can be derived by eliminating $T_{L/R}$ and $\omega_{s,R/L}$:

$$\begin{pmatrix} J_{veh} + 2R_S^2 J_S & -4R_S^2 J_S \\ -4R_S^2 J_S & J_{mech} + 8R_S^2 J_S \end{pmatrix} \begin{pmatrix} \dot{\omega_{veh}} \\ \dot{\omega_c} \end{pmatrix} = \begin{pmatrix} -R_S(u_{SR} + u_{SL}) + D_{veh} \\ 2R_S(u_{SR} + u_{SL}) + T_{mech} \end{pmatrix} \tag{2.12}$$

The yaw dynamics can be reduced similarly assuming $\omega_{yaw} = (\omega_{wR} - \omega_{wL})/2$ . The yaw dynamics are not considered here, it is assumed that the vehicle operates symmetrically and $\omega_{yaw} = 0$.

The derived inertia relationships can be used to simulate the vehicle dynamics. The system can be represented using two states, the vehicle speed and the carrier speed. The speed of the pump/motors S can then be derived from the states using the mechanical constraints.

### 2.1.4 Power Analysis

The drive train equations derived above can be used to perform a power analysis on the Generation I hybrid architecture. In this power split hybrid drive train the power from the engine is split at the carrier shaft into the hydraulic path and the mechanical path.

In Figure 2.3 the power distribution can be seen. In this graph the engine map is displayed, with the engine speed on the x-axis and engine torque on the vertical axis. The blue circle shows the operating point when transmitting 100% of the power to the wheels through the mechanical branch. The light blue rectangle represents the power needed at the wheels to propel the vehicle at the desired rate. The engine operating point is shifted in torque by P/M-T, here seen in maroon, and in speed by P/M-S,

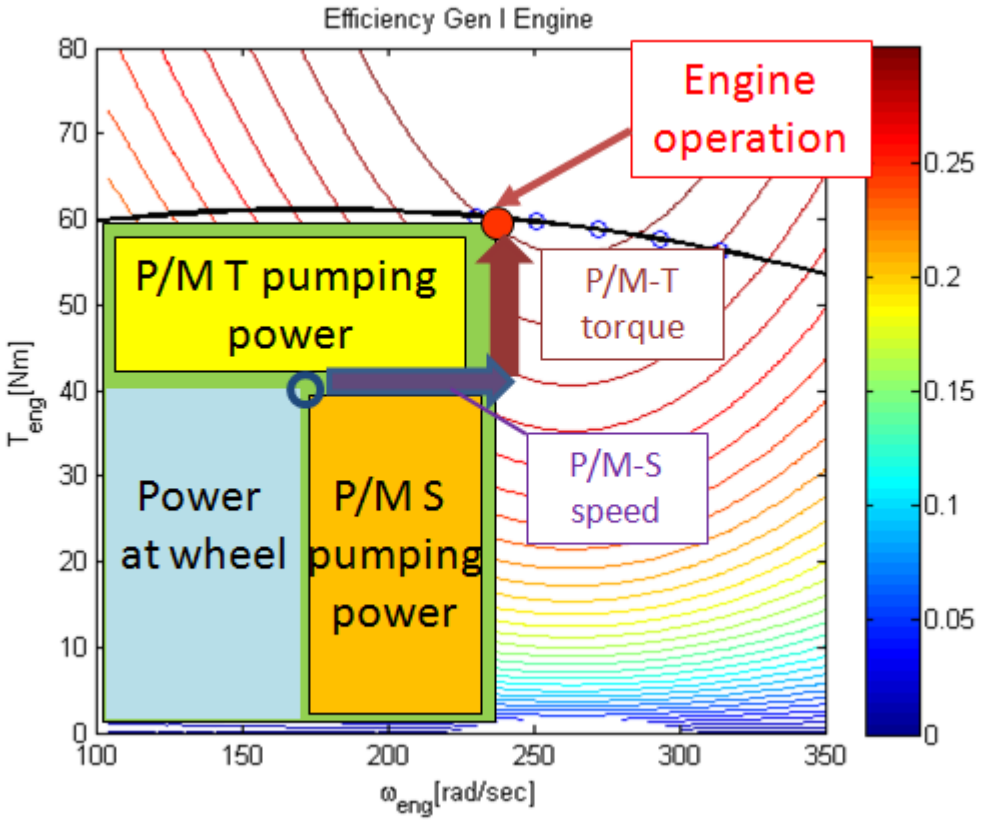


Figure 2.3: Gen I Power Analysis.

displayed in purple. Shifting the engine to a more optimal point results in an excess of power. The output power of the engine when shifting to the new operating point, specified in red, is illustrated by the green rectangle. Here displayed in yellow is the power provided by the hydraulic units. In this case this power is negative and therefore the hydraulic units are absorbing the excess engine power and storing the energy in the accumulator for later use. The pump/motors provide either negative power to absorb additional engine power or positive power to assist the engine to generate the required output power.

## 2.2 Generation II: Ford F 150

In this section the output coupled power split architecture of the Generation II vehicle will be described. The operation of the hydro static transmission unit will be explained. To model the vehicle, static relationships of the drive train will be derived and inertia dynamic equations will be stated. Restrictions on the operation of the hydraulic units in the hydro static unit will be discussed.

### 2.2.1 The vehicle

The vehicle is a Ford F150 truck as seen in Figure 2.5. Using a Folsom hydraulic transmission the vehicle will be reconfigured from the conventional drive train to a truck with hydro static transmission (configuration I). By adding valves, a low and a high pressure accumulator, it will be further developed to a hydraulic hybrid vehicle (configuration II). In Figure 2.4 the two configurations are illustrated.

In configuration I the hydraulic transmission is used to operate the engine at its most efficient operating point on a constant power curve that satisfies the demand of power at the wheel. In configuration II, adding energy storage makes the engine management more flexible. By using stored energy the engine can operate in a more optimal region independent of the power output. Lost energy through friction braking can now be regenerated in the high pressure accumulator. The main power source of the conventional F150 truck is a 4.6L 3 valve V8 gasoline engine with 292 maximum horsepower at 5700rpm and 430Nm maximum torque at 4000rpm. The differential at the rear splits the power between the two wheels with a final drive ratio of 3.31. Including

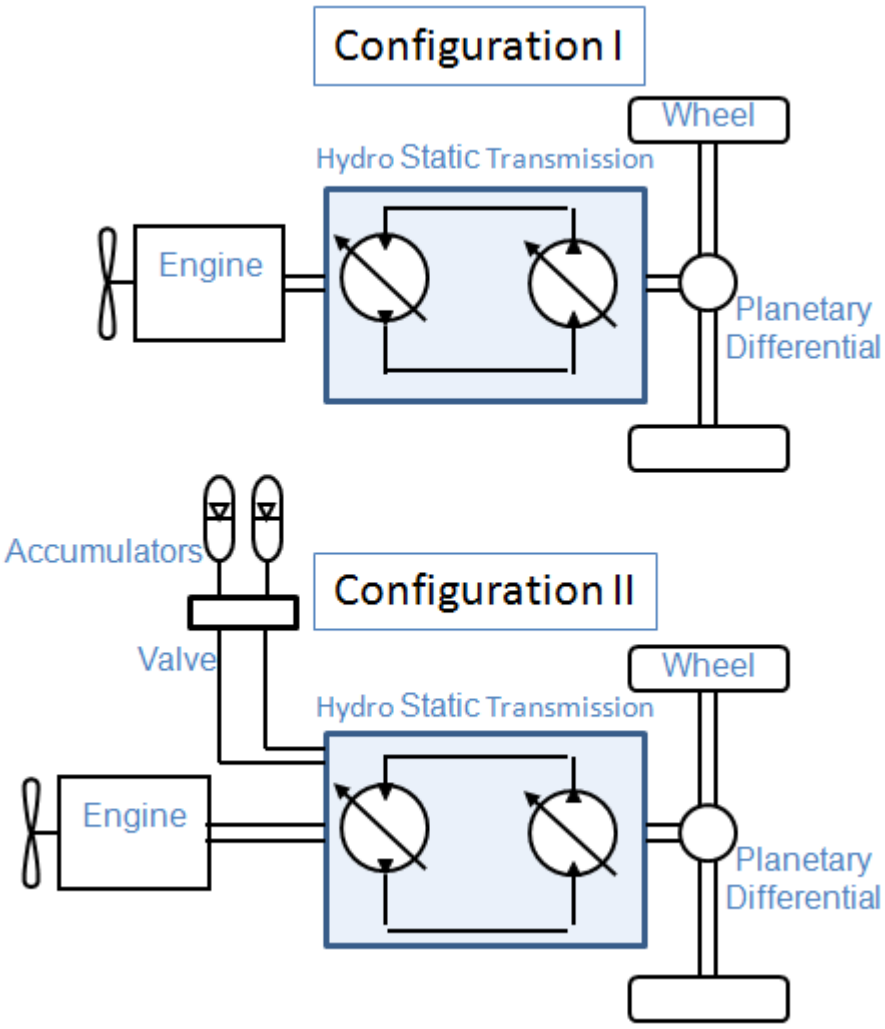


Figure 2.4: Configuration I versus Conifguration II.

Figure 2.5: Ford F150.

engine, drive train and all auxiliary losses the conventional F150 truck achieves a fuel economy of 17.9mpg in the city and 26.0mpg over the highway drive cycle.

### 2.2.2 The Hydro Static Transmission

The Folsom Hydro Static Unit ([15]) consists of two 222cc variable displacement bent axis pump/motors, three planetary gear sets, a clutch, two morse chains, and a variable displacement charge pump (Figure 2.6).

In the transmission the engine side is referred to as the input while the wheel side is considered the output side. The charge pump is located at the driveshaft on the input side. The input shaft is connected to the first planetary gear set at the planet carrier. The power from the engine is split between the sun gear and ring gear. The sun gear is connected through the second planetary gear set and a morse chain to the first 222cc hydraulic unit. The carrier of the second planetary is grounded by a clutch and therefore works as a simple gear ratio. The ring of the first planetary gear set transmits power to the output through a mechanical drive shaft. The third planetary gear set is mechanically linked to the output at its planet carrier. A clutch on the sun gear can enable or disable the transmission of torque through this gear set. Planetary gear

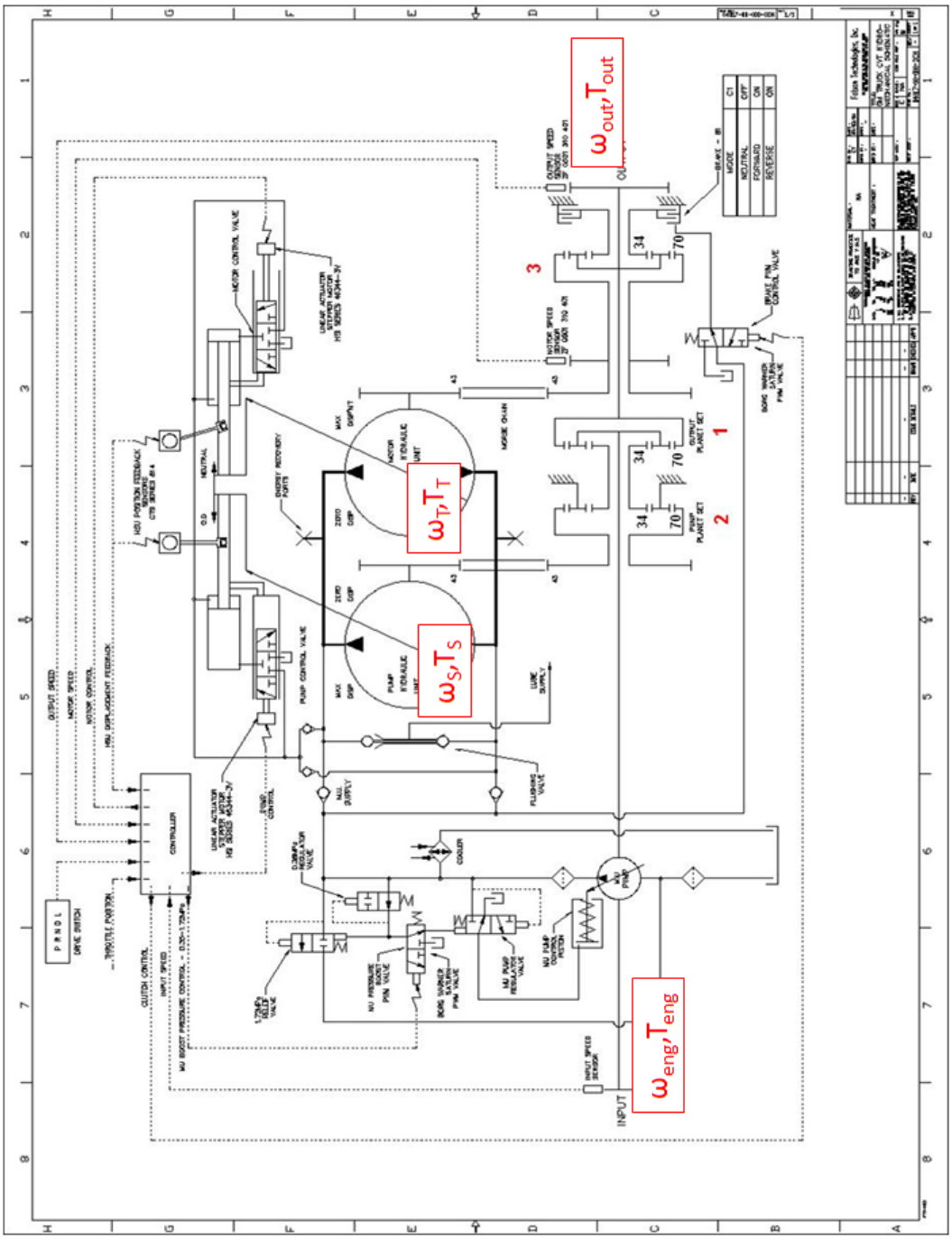


Figure 2.6: Hydro Static Transmission Schematic.

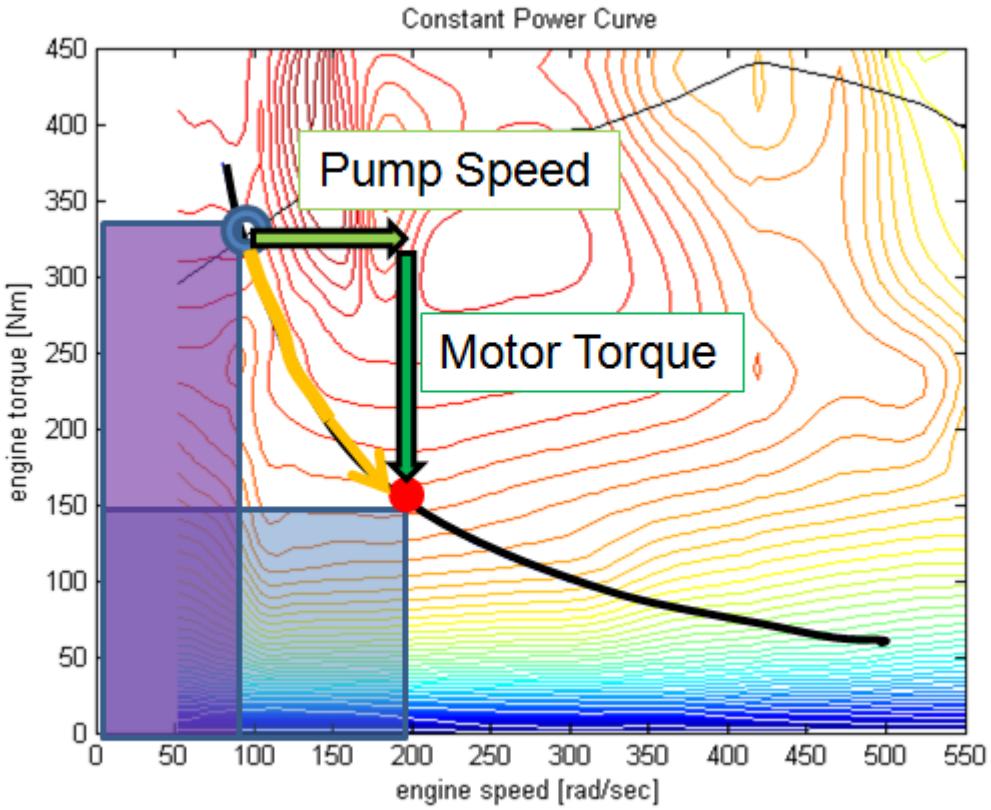


Figure 2.7: Engine shifting with the Hydro Static Transmission ( Config. I)

three is used to combine the power from the second hydraulic unit and the mechanical carrier. The hydraulic pump/motor is linked through a morse chain to the ring gear. When operating the vehicle in configuration I with a hydro static transmission the pump/motor at the engine is mainly operated as a pump and the hydraulic unit at the wheels is used as a hydraulic motor. The two units share their high and low pressure hydraulic line.

In Figure 2.7 shifting of the engine is illustrated. In a vehicle with hydro static transmission the engine operating point is shifted on a constant power curve to a more efficient region. As seen here, in this drive train the pump shifts the engine to a higher speed and the motor shifts the operation to a lower torque. Due to the power constraint

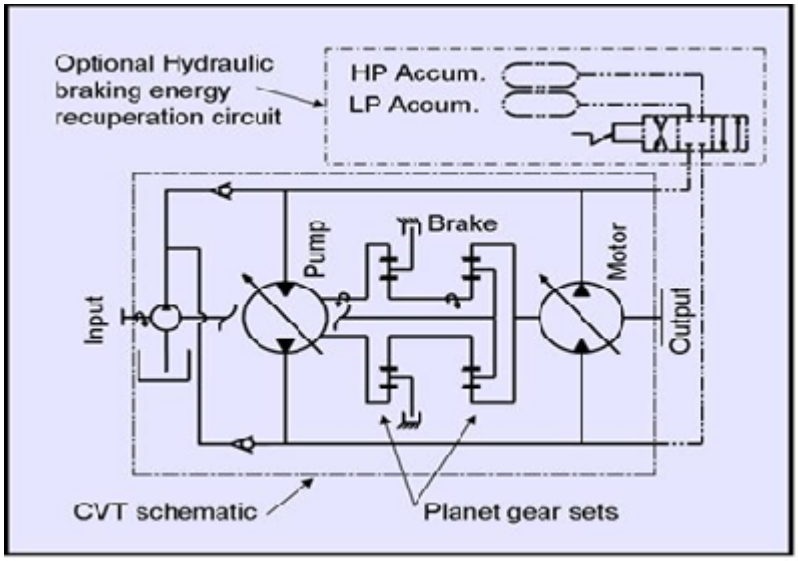


Figure 2.8: Hydro Static Transmission with Hybrid (Config. II).

the blue and purple areas under the curve are equal in size. The purple area represents the power provided by the engine when operating in mechanical only mode. The blue area shows the power provided by the engine after it was shifted into a more efficient operating region.

In order to hybridize the vehicle and achieve configuration II the transmission has two ports, one in the high pressure line and one in the low pressure one. These ports can be used to connect the hydraulic pump/motors to a high and low pressure accumulator. A directional valve is implemented between the hydro static unit and the accumulators such that the high and low pressure sides of the pump/motors can be interchanged (Figure 2.8). When operating the vehicle in configuration II both pump/motors can operate as a pump or as a motor at any time. This results in a shift of the engine operation with respect to its operating point in a conventional drive train. The hydraulic unit at the engine achieves a change in engine speed; It is therefore referred to as *speeder* and will be denoted S. The pump/motor at the wheel is often referred to as *torquer* (P/M-T) because it shifts the engine operation in torque.

In this hybrid drive train the speed of P/M-T is coupled to the wheel speed. Such an architecture if often referred to as *output-coupled power split* drive train.

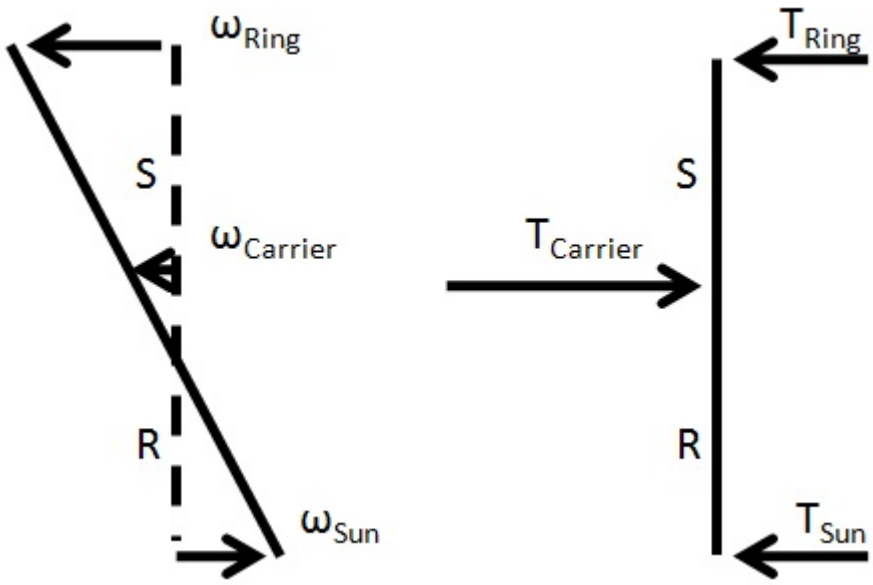


Figure 2.9: Lever diagram for planetary gear set.

### 2.2.3 Static equations

A planetary gear set can be modeled using its speed and torque constraints. The following equations are derived from the lever diagram in Figure 2.9 and show the relationship of speed and torque:

$$\omega_{sun}S + \omega_{ring}R = \omega_{carrier}(S+R) \tag{2.13}$$

$$T_{sun} = T_{carrier}\frac{S}{S+R} \tag{2.14}$$

$$T_{ring} = T_{carrier}\frac{R}{S+R} \tag{2.15}$$

$$T_{carrier} = T_{sun} + T_{ring} \tag{2.16}$$

where R is the radius of the ring gear and S is the radius of the sun gear. As seen in the static equations planetary gear sets have two degrees of freedom in speed but only one degree of freedom in the torque constraint. When grounding one of the gears with a clutch to zero speed the planetary works as a simple gear ratio, as in planetary set

2 in Figure 2.6. Each of the planetary sets in the hydraulic transmission consists of a ring gear with 70 teeth and a sun gear with 34 teeth. For simplicity the parameter $r = \frac{R+S}{S} = \frac{70+34}{34}$ is used in the derivation of the static equations. Using the notation seen in Figure 2.6 the static equations of the drive train are given by:

$$\begin{bmatrix} \omega_T \\ \omega_S \end{bmatrix} = \begin{bmatrix} R_1 & 0 \\ 1 & -R_1 \end{bmatrix} \begin{bmatrix} \omega_{out} \\ \omega_{eng} \end{bmatrix}$$

$$\begin{bmatrix} T_T \\ T_S \end{bmatrix} = \begin{bmatrix} -R_2 & -R_3 \\ 0 & R_2 \end{bmatrix} \begin{bmatrix} T_{out} \\ T_{eng} \end{bmatrix}$$

where $R_1 = \frac{r}{r-1}$, $R_2 = \frac{r-1}{r}$, and $R_3 = \frac{(r-1)(r-1)}{r^2}$.

It should be noted that in the equations above the torque excerted by the vehicle onto the road is negative and therefore

$$T_{drivecycle} = -T_{out} R_f \tag{2.17}$$

$$\omega_{out} = \omega_{drivecycle} R_f \tag{2.18}$$

where $R_f = 3.31$ is the final drive ratio. In configuation I of the Generation II vehicle all of the power provided to the wheel is coming from the combustion engine. With this power equality the relationship between the pump/motor operations and the engine and output power can be described by

$$\begin{bmatrix} \omega_T & \omega_S \end{bmatrix} \begin{bmatrix} T_T \\ T_S \end{bmatrix} = \begin{bmatrix} \omega_{out} \\ \omega_{eng} \end{bmatrix} \begin{bmatrix} T_{out} & T_{eng} \end{bmatrix}$$

Constraints of flow and pressure in the hydro static transmission will ensure that power balance. These constraints will be discussed in more depth in Section 4.2.1.

The static equations derived represent an output coupled hybrid drive train. The speed of P/M-T is coupled to the output speed while the torque of P/M-S is specified by the engine output torque. In order to transmit the engine torque P/M-T has to provide sufficient torque. The output torque is represented by a sum of the torque from the engine and the torque from P/M-T.

### 2.2.4 Inertia dynamics

The dynamic equations can be derived using the derived static relationships together with the kinetic energy and power constraints. In the following the inertia matrix $M$

and the torque matrix $\Gamma$ will be derived such that

$$[M] \begin{bmatrix} \dot{\omega_{out}} \\ \dot{\omega_{eng}} \end{bmatrix} = \Gamma \tag{2.19}$$

holds.

The kinetic energy in the system can be specified by

$$K_E = \frac{1}{2}(J_{veh}\omega_{out}^2 + J_{eng}\omega_{eng}^2 + J_S\omega_S^2 + J_T\omega_T^2) \tag{2.20}$$

which can then be simplified by applying the static relationships derived in Section 2.2.3, to

$$K_E = \frac{1}{2} \begin{bmatrix} \omega_{out} & \omega_{eng} \end{bmatrix} [M] \begin{bmatrix} \omega_{out} \\ \omega_{eng} \end{bmatrix}$$

The resulting relationships can then be used to derive the inertia matrix $M$. Similarly the power in the system is specified by

$$Power = \omega_{veh}T_{veh} + \omega_{eng}T_{eng} + \omega_S T_S + \omega_T T_T \tag{2.21}$$

which can be reduced to

$$Power = \begin{bmatrix} \omega_{out} & \omega_{eng} \end{bmatrix} \Gamma$$

by applying the static equations of the drive train. This relationship is used to derive the torque vector $\Gamma$.

Using this approach the resulting inertia dynamic relationships can be derived for the Generation II system to be

$$\begin{bmatrix} J_S + J_T R_1^2 + J_{veh} & -J_S R_1 \\ -J_S R_1 & J_S R_1^2 + J_{eng} \end{bmatrix} \begin{bmatrix} \dot{\omega_{out}} \\ \dot{\omega_{eng}} \end{bmatrix} = \begin{bmatrix} T_{out} + T_S + R_1 T_T \\ T_{eng} - R_1 T_S \end{bmatrix} \tag{2.22}$$

In order to model the drive train using the dynamic equations the inertias of the rotating parts have to be identified. A Pro-Engineer representation of the hydraulic transmission shows the rotating parts in Figure 2.10. Using the Pro-Engineer software the inertia values can be evaluated theoretically. The inertia values for components with major contributions to the dynamics of the system are shown in Table 2.3.

As expected the hydraulic pump/motors have the largest inertia but surprisingly the chains that connect the hydraulic units to the drive shaft are also a major contribution

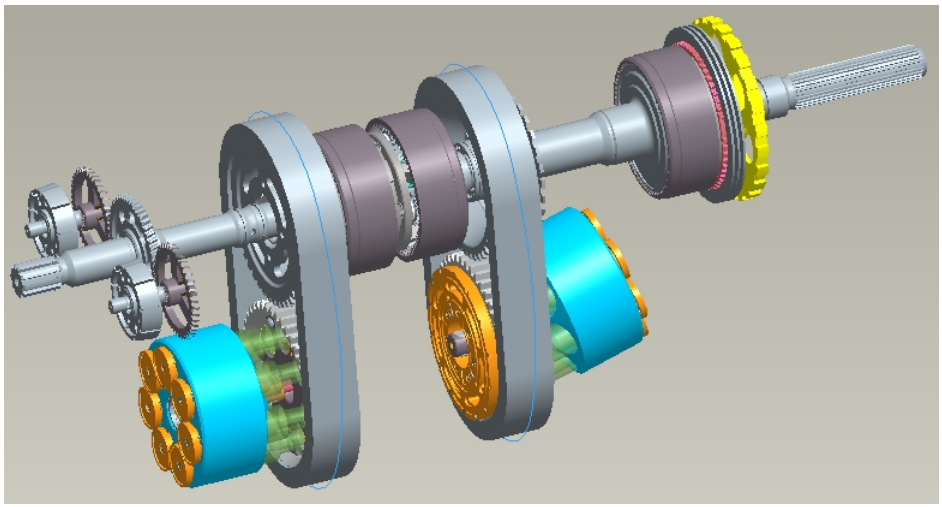

Figure 2.10: Rotating Parts of Hydro Static Transmission

to the inertia values. To implement these values in the dynamic equations they are summed at important points in the drive shaft: at the pump, the motor, the engine and the output shaft. The third planetary gear set in the drive shaft can be clutched or declutched, which changes the inertia values slightly. When clutched the P/M-T and the output shaft are mechanically coupled through the gear ratio in the planetary. In this mode the inertia of the output and P/M-T can be transferred to a common point and added. When the clutch is disengaged it is spinning freely. The inertia of the clutch then contributes to the output shaft. P/M-S can spin but does not contribute to the system. The values of inertia in the two modes can be seen in Table 2.4.

The inertia relationships can be used to dynamically simulate the Generation II vehicle with or without accumulator. The system is represented by two states, here the engine speed and the output speed. From these the speed of P/M-T and P/M-S can be derived using the static equations.

### 2.2.5 Restrictions of HSU

The hydro static unit was built with the intention to operate it as a CVT. In the configuration I vehicle, using the unit as a CVT, P/M-T is operated as a pump and P/M-S is operated as a motor. The advantage of a drive train with hydro static transmission

Table 2.3: Inertia Values of Rotating Parts

| **component** | **value**$[kg(mm)^2]$ |
|---|---|
| hydraulic pump motor | 19992 |
| morse chain | 33330 |
| ring gear | 2640 |
| sprocket | 6838 |
| shaft to ring | 184 |
| shaft to engine | 534 |
| charge pump | 203 |
| planet carrier | 1867 |
| output shaft | 2141 |

Table 2.4: inertia values in major categories

| **unit** | **mode 1** | **mode 2** |
|---|---|---|
| $J_S$ | 69638 | 69638 |
| $J_T$ | 67182 | 67182 |
| $J_{eng}$ | $J_{eng} + 2807$ | $J_{eng} + 2807$ |
| $J_{veh}$ | $J_{veh} + 6648$ | $J_{veh} + 8768$ |

is to shift the engine operating point along constant power into a more efficient region, but in contrast to a hybrid drive train the engine management has only one degree of freedom. The operating point of the combustion engine can be shifted in speed and torque, while the output power of the engine is fixed. From the static relationships of the drive train it can be seen that the torque of P/M-S is coupled to the engine and is therefore positive. To shift the engine to a more efficient operating point, P/M-S is pumping at negative speed and positive torque while P/M-T is motoring at positive speed, outputing positive torque. This operation is displayed in Figure 2.7.

Due to limited space in the Folsom Hydraulic Transmission the bent axis pump/motor operation in negative over center displacement ranges is restricted. P/M-S is built to

achieve a range in displacement from -.1 to 1, while P/M-T can only operate at positive displacement. The 10% over center displacement of P/M-S enables the configuration I vehicle to drive in reverse without additional gears or clutches in the transmission.

While the operation of the vehicle with CVT does not require negative displacements on both pump/motors in the hybridized vehicle engine management relies on the flexibility of the hydraulic units. In a hydrid vehicle in power split the pump/motors can both be used as pump or motor to regenerate energy operating at negative power or to propel the vehicle by adding power to the drive train. A major contribution to improve fuel economy in a hybrid vehicle is the engine management. Operation of each of the two hydraulic units as either pump or motor, resulting in four combinations, can shift the engine operating point to the most efficient spot for any wheel operation. With restrictions on the displacements in the Folsom transmission the flexbility of engine management is limited.

In Figure 2.11 the operation of the Generation II in configuration II can be seen. This graph shows an engine operating map in which the operating point of the engine in mechanical-only operation can be seen in blue and the shifted, more optimal engine operation is displayed in red. In this specific case the engine operating point to satisfy the wheel power request is in a low torque and low efficiency region. When shifting the engine operation to a higher torque and more efficient region the excess torque has to be absorbed by the hydraulic system. In this case an operation of P/M-T in the negative displacement range is necessary. The graph shows the pumping power of P/M-T in bright yellow and the pumping power of P/M-S in dark yellow. Due to this negative power operation of the hydraulic units the excess energy from the engine is stored in the accumulator and can be reused at a later time.

Since the pump/motor can not operate over center a directional valve is added between the hydro static unit and the high and low pressure accumulator. This can be seen in Figure 2.8. By swaping the high and low pressure lines the directional valve enables operation of P/M-T at full negative torque while P/M-S operates in the range of -1 to .1 fractional displacement. In Table 2.5 the achievable ranges of the pump/motors in the Folsom transmission are shown in comparison with ideal pump/motor operation in a hybrid vehicle.

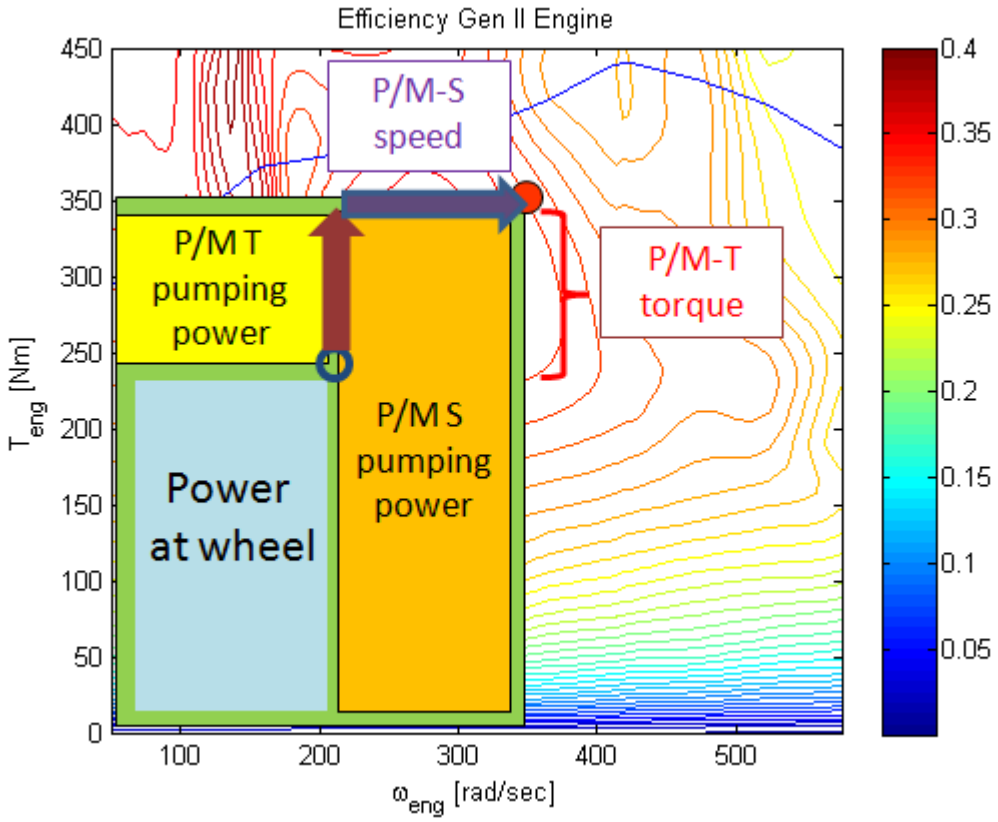


Figure 2.11: Hybrid operation Gen II.

Table 2.5: Range of Folsom Transmission Pump Motors versus Ideal Case

| **P/M** | **Folsom P/M range** | **directional valve position** | **Ideal P/M Range** |
|---|---|---|---|
| P/M-T | $-.1 \rightarrow 1$ | 1 | $-1 \rightarrow 1$ |
| P/M-S | $0 \rightarrow 1$ | 1 | $-1 \rightarrow 1$ |
| | OR | | OR |
| P/M-T | $-1 \rightarrow .1$ | 2 | $-1 \rightarrow 1$ |
| P/M-S | $-1 \rightarrow 0$ | 2 | $-1 \rightarrow 1$ |

These restrictions in pump/motor displacements have an effect on engine management of the power split hybrid. As seen in the derived static equations (Section 2.2.3) the torque of P/M-S is coupled to the torque of the engine and is always positive. To transmit the torque from the engine the torque provided by P/M-S has to be set to $T_S = R_2 T_{eng}$. If the torque provided by the engine exceeds the maximum torque capacity of P/M-S the torque will not be transmitted to the output shaft. In general, using 222cc pump/motors at full displacement should allow to operate the engine at any torque. Under ideal conditions a torque of up to about 480Nm at 2000psi can be transmitted. However if the engine management specifies the torque of P/M-T to be negative the directional valve is switched and P/M-S can only provide positive torque with up to a 10% positive displacement.

The maximum torque capacity of P/M-S then depends on the setting of the directional valve as well as on the pressure in the accumulator. For varying pressures Table 2.6 shows maximum torque values computed with an ideal pump model. Restricted areas in the engine management are shown in Figure 2.12 and happen in the ranges where P/M-T provides negative torque.

To better illustrate this concept an example will be given using Figure 2.12. Assuming the engine operating point in mechanical only operation, meaning P/M-S speed is zero and P/M-T torque is zero, is at 200rad/s and 130Nm. In the hydraulic vehicle fuel economy is increased by shifting the operating point to a more efficient region. If it is desired to shift the engine into quadrant one P/M-S is pumping at positive torque and

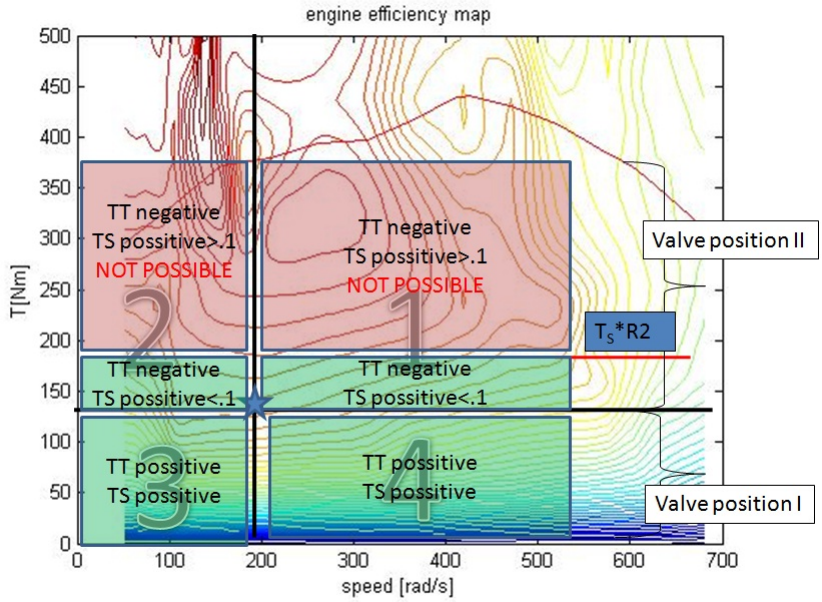


Figure 2.12: Restrictions on the engine operating point.

negative speed. P/M-T is pumping at positive speed and negative torque. For P/M-T to provide negative torque the directional valve has to be flipped into position 2. Since P/M-S can only operate at 10% displacement in the positive range the engine operation point can not be shifted higher than $T_{engmax} = 1/R2 * T_{Smax}$ in torque. $T_{Smax}$ values can be seen in Table 2.6 for varying pressures. When shifting the engine operating point into quadrant 2 P/M-S is pumping, operating at negative speed and positive torque. P/M-T is motoring at positive speed and negative torque. For this operation the directional valve is in position 2. Due to the restriction in displacement to only 10%, the maximum torque transmitted from the engine is restricted to the maximum torque P/M-S is capable. See values in Table 2.6. When shifting the engine into quadrant 3 and 4, P/M-T provides positive torque. In quadrant 4 P/M-T is pumping and P/M-S is motoring while in quadrant 3 both pump/motors are motoring. In both quadrants $T_S$ and $T_T$ are positive but the speed of P/M-S is negative in quadrant 4 and positive in quadrant 3. To operate in these quadrants the directional valve is set to possition 1 and there are no restrictions for operation within these quadrants.

Table 2.6: Restricted torque values

| **pressure** | $T_S[Nm]$ | $T_{eng} = R_2 T_S[Nm]$ |
|---|---|---|
| 500 psi | 12.18 | 16.16 |
| 1000 psi | 24.36 | 32.32 |
| 2000 psi | 48.72 | 64.65 |
| 3000 psi | 73.01 | 96.97 |

The values shown in Table 2.6 are an upper bound of maximum torque provided by P/M-S at 10% displacement. These values were computed assuming ideal pump/motors. Actual values can be calculated using a pump model with the relationship

$$T_S = \frac{PD.1}{2\pi} - torqueLoss$$

where $P$ is the pressure and $D$ is the maximum displacement of P/M-S. A maximum torque of $T_{eng} = -R_2 T_S$ can then be transmitted from the engine to the output shaft.

Comparing the optimal engine operating points of 350Nm to values in this table the significance of this restriction becomes obvious. The operation of the hybrid vehicle with restrictions and the impact of the restrictions in the hydro static transmission on fuel economy will be investigated in Section 4.2.3 in more depth.

## 2.3 Coordinate Transformation

On hybrid vehicles the fuel economy depends on the controls algorithm used in the drive train. Especially on power split vehicles the design and implementation of such an algorithm is often complex. From Equation inertiaeqGenI and inertiaeqGenII it can be seen that the carrier speed ($\omega_c$) and the wheel speed ($\omega_{out}$) are coupled in a power split vehicle configuration. For control purposes this is not optimal. To simplify control implementation the system can be decoupled into internal and external coordinates. The external coordinate is here represented by the wheel speed and referred to as output speed. Decomposing the system enables us to satisfy the driver input using the external coordinate while using the internal coordinate, $\omega_{int}$, to optimize the system operation. The desired torque at the wheels is specified by the driver and denoted $T_{out}$. Such

a decomposition will be shown here using the approach given by Lee in [16]. The transformation matrix $S$ can be represented by:

$$\begin{bmatrix} \omega_{out} \\ \omega_c \end{bmatrix} = \overbrace{\begin{bmatrix} 1 & 0 \\ a & 1 \end{bmatrix}}^{S} \begin{bmatrix} \omega_{out} \\ \omega_{int} \end{bmatrix}$$

The coefficient $a$ in S can be determined by

$$\left[S^T\right][M][S] = \begin{bmatrix} M_{ext} & 0 \\ 0 & M_{int} \end{bmatrix}$$

defining the internal coordinate to be orthogonal to the external coordinate.

Applying this transformation matrix $S$ to the inertia dynamic relationship in Equation 2.19 results in:

$$\left[S^T\right][M][S] \begin{bmatrix} \dot{\omega_{out}} \\ \dot{\omega_{int}} \end{bmatrix} = \left[S^T\right][\Gamma] \tag{2.23}$$

which is equivalent to

$$\begin{bmatrix} M_{ext} & 0 \\ 0 & M_{int} \end{bmatrix} \begin{bmatrix} \dot{\omega_{out}} \\ \dot{\omega_{int}} \end{bmatrix} = \begin{bmatrix} T_{out} \\ T_{int} \end{bmatrix} \tag{2.24}$$

In this formula $M$ refers to the inertia matrix derived in Sections 2.1.3 and 2.2.4.

For the Generation I vehicle the parameter $a$ was evaluated to

$$a = \frac{4R_S^2 J_S}{8R_S^2 J_S + J_{mech}} \tag{2.25}$$

and the internal speed can then be computed by

$$\omega_{int} = \omega_c - a\omega_{out} \tag{2.26}$$

The resulting decoupled dynamic relationships of the Generation I vehicle can be seen below.

$$M_{ext}\dot{\omega_{out}} = D_{veh} + R_S(u_{SR} + u_{SL})(1 - 2a) + aT_{mech} \tag{2.27}$$

$$M_{int}\dot{\omega_{int}} = 2R_S(u_{SR} + u_{SL}) + T_{mech} \tag{2.28}$$

Using the new coordinates $\omega_{int}$, $\omega_{ext}$ the controls logic can ensure that the desired wheel speed is satisfied by using the external coordinates. The internal coordinates can

Table 2.7: Decomposed Coordinate Parameter for Generation I

| **parameter** | **equation** |
|---|---|
| $a$ | $\frac{2R_S^2 J_S}{8R_S^2 J_S + J_{mech}}$ |
| $M_{ext}$ | $J_{veh} + \frac{a}{2} J_{mech}$ |
| $M_{int}$ | $J_{mech} + 2R_S^2 J_S$ |
| $T_{out}$ | $D_{veh} - R_S(u_{SR} + u_{SL})(1 - 2a) + aT_{mech}$ |
| $T_{int}$ | $2R_S(u_{SR} + u_{SL}) + T_{mech}$ |

Table 2.8: Decomposed Coordinate Parameter for Generation II

| **parameter** | **equation** |
|---|---|
| $a$ | $\frac{J_S R1}{J_S R1^2 + J_{eng}}$ |
| $M_{ext}$ | $J_S + J_T R1^2 + J_{veh} + a(-2J_S R1 + aJ_S R1^2 + aJ_{eng})$ |
| $M_{int}$ | $J_S R1^2 + J_{eng}$ |
| $T_{out}$ | $D_{veh} + T_S + R1T_T + a(T_{eng} - R1T_S)$ |
| $T_{int}$ | $T_{eng} - R1T_S$ |

be used for the purspose of optimizing fuel economy only. The above tranformation will be used together with the derived inertia dynamic relationships for Generation I and Generation II. The equations for $a$, $M_{ext}$, $M_{int}$, $T_{ext}$ and $T_{int}$ that follow from this procedure for the two specified vehicles can be seen in Table 2.7 and Table 2.8.

It can be seen that the values of the internal inertia, $M_{int}$, depends on the inertia of the carrier shaft $J_{mech}$ and on the inertia of P/M-S in Generation I, whereas in Generation II it depends on the engine inertia and the P/M-S inertia only. Similarly the internal torque $T_{int}$ in the Generation I vehicle is computed by the pump/motor S torques and the mechanically transmitted torque, while in Generation II it is composed of the engine torque and pump/motor S torque. Computing the values of the internal inertia $M_{int}$, the internal torque $T_{int}$, the external inertia $M_{ext}$, and the external torque $T_{ext}$ a control strategy can be derived to control $\omega_{int}$ to the optimal value for engine and pump/motor operation. The decomposition can be useful to simplify the

implementation of a control strategy on a vehicle in real time.

## 2.4 Internal Combustion Engine Modeling

The efficiency of the conversion between chemical energy in the liquid fuel to mechanical energy in the internal combustion engine is not constant over its operating speed and torque range. A major contribution to the fuel economy improvement in hybrid vehicles is due to the operation of the engine at its *sweet spot*, meaning the most efficient region. Minimizing the losses in the engine is necessary to ensures maximum fuel economy. Therefore it is important for the analysis of hybrid drive trains to model the engine accurately. One approach to do so is to use the Willans line model described in [17, 18]. This method is mainly used for combustion ignition engines and uses the friction power in the engine to determine the losses. The method uses a small sample of operating points to determine three parameters $T_0$, $T_1$ and $T_2$. These parameters are used to determine the loss in the engine for any operating point, as seen in Equation 2.29.

$$Loss_{eng} = T_1\omega_{eng} + T_2\omega_{eng}^2 + T_3\omega_{eng}^3 \tag{2.29}$$

The efficiency, $\eta$, and fuel consumed can then be computed using the following relationship:

$$\eta_{eng} = \frac{T_{eng}\omega_{eng}}{T_{eng}\omega_{eng} + Loss_{eng}} \tag{2.30}$$

$$fuel = T_{eng}\omega_{eng} + Loss_{eng}/LHV \tag{2.31}$$

$$\tag{2.32}$$

where $LHV$ represents the lower heating value. For diesel fuel a value of $LHV = 43MJ/kg$ can be used. The fuel consumed is given in kg.

The Willans line method was used to model the Generation I diesel engine. A data set of fuel values for 5 operating points that was provided by the manufacturer was used to determine $T_0$, $T_1$ and $T_2$. The resulting efficiency contour together with the 5 data points can be seen in the contour plot in Figure 2.13. where the maximum torque is specified by the black contour line. The engine is at idle at 100rad/sec and can not be operated below.

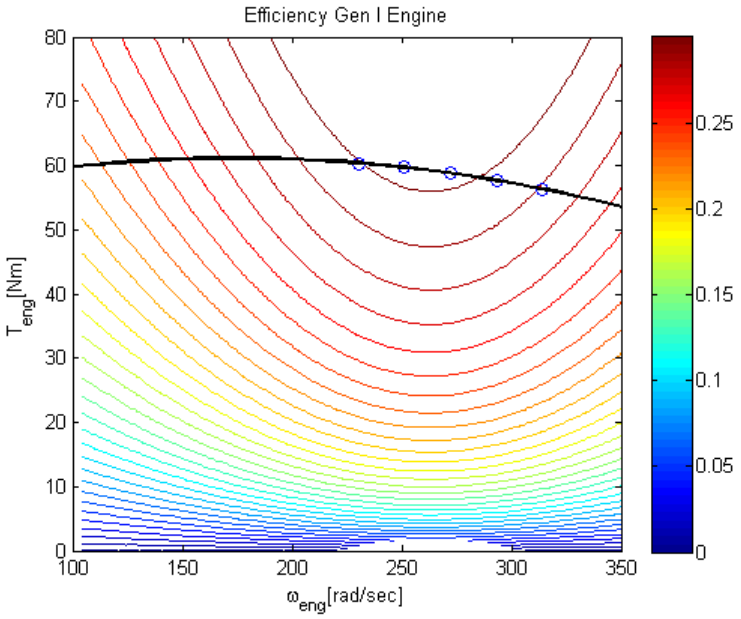


Figure 2.13: Efficiency Contour of the 1.1l Perkins Engine.

Whenever a larger set of engine operating data is provided to model the engine a simpler approach can be taken. The data can be organized in an array with two dimensions, namely operating speed and operating torque. This array can then be used to interpolate over for any operating point. Being given a significant set of data points by Ford for the 4.6L gasoline engine this approach was chosen. The efficiency map together with the maximum torque curve can be seen in Figure 2.14. The relationship from Equations 2.29- 2.31 can be used with a lower heating value of $LHV = 42.5MJ/kg$ for gasoline.

It has to be noted at this point that the engine model derived from the data set provided by Ford was found to be non-realistic. The efficiency of a gasoline engine is not expected to exceed 35%, while in this model a peak efficiency of 38% can be found at maximum torque at 140rad/sec. A new engine model with a peak efficiency of 35% was recently provided by Ford. Since a change in engine efficiency mapping will not alter the trends presented in this thesis it will not be used in the scope of this work.

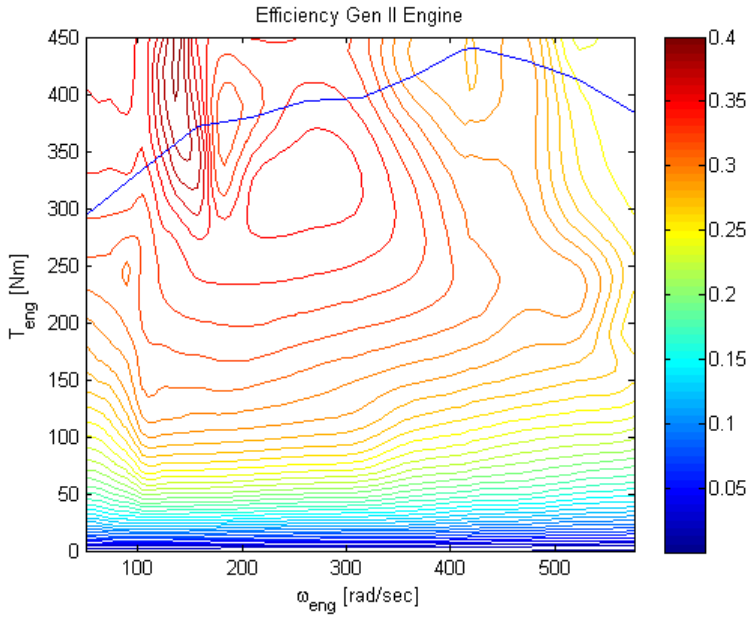


Figure 2.14: Efficiency Contour of the 4.6l Ford Engine.

The derived engine models are used in simulating the vehicles and in the controls development.

## 2.5 Hydraulic Component Modeling

With the goal of operating a hybrid drive train at its optimal operation the losses in all major components in the system should be considered. Therefore a model of the hydraulic components is needed to determine the losses in the hydraulic pump/motors. The efficiency of pump/motor operation depends on the operating speed, the displacement and the pressure difference between the high pressure and low pressure line, and therefore the state of charge in the accumulator. Developing simple models with the data available temperature dependency is not included in the modeling. In this section a dynamic model of the accumulator will be provided and loss models for various pump/motors will be discussed.

### 2.5.1 Accumulator Model

Gas charged accumulators are often modeled using the ideal gas law. If the temperature in the accumulator is assumed to be constant over the charging and discharging process the isothermal relationship can be used where

$$P_1 V_1 = P_2 V_2 \tag{2.33}$$

. In many hydraulic applications there is only little or no heat transfer between the accumulator and the environment ([19]). A more accurate way to model the hydraulic energy storage can be derived by assuming that the process is adiabatic. When no heat is transferred the following constraint holds:

$$P_1 V_1^k = P_2 V_2^k \tag{2.34}$$

where $k$ is the specific heat constant and holds the value $k = 1.4$ for diatomic gases like nitrogen and hydrogen. In this thesis we will assume an adiabatic process. The pressure in the accumulator can then be given by:

$$P_{acc} = P_p \left( \frac{V_p}{V_p - V_{acc}} \right)^k \tag{2.35}$$

where $P_p$ is the pre-charged pressure and $V_p$ refers to the pre-charged volume. The volume in the accumulator can be retrieved by integrating over the flow.

$$\dot{V_{acc}} = Q_{acc} \tag{2.36}$$

Assuming the initial pressure in the accumulator is known the initial value of $V_{acc}$ is given by:

$$V_{acc,ini} = V_p - \left( \frac{P_p V_p^k}{P_0} \right)^{1/k} \tag{2.37}$$

where $P_0$ is the initial pressure. $Q_{acc}$ can take on positive or negative values dependent on pumping or motoring operation of the P/Ms. $Q_{acc}$ is a function of the pressure difference in the hydraulic line, the speed of the P/Ms and the displacements. It is evaluated by:

$$Q_{acc}(P, \omega_T, \omega_S, x_T, x_S) = Q_T(P, \omega_T, x_T) + Q_S(P, \omega_S, x_S) \tag{2.38}$$

In the Generation I vehicle $Q_S$ is the sum of flows of $P/M_{SR}$ and $P/M_{SL}$.

### 2.5.2 Hydraulic Pump/Motors

The fuel economy in hydraulic hybrid vehicles does not only vary with the efficiency of the internal combustion engine but also with the efficiency of the hydraulic units. Various ways to model hydraulic pump/motor are discussed in [20], [21] and [22]. Given the resources and data available for the Generation I and Generation II pump/motors different approaches were taken to model the hydraulic units. These are described in the next two sections.

#### Generation I

Given the manufacturer data of the S42 hydraulic units a mathematical spline model was used to identify a polynomial that describes the mechanical and volumetric efficiencies of the pump/motors. This model is simple to use in simulation of the drive train and can easily be scaled in order to project performances of the drive train including more efficient hydraulic components. The efficiency map for a S42 unit operating at a pressure of 3000psi can be seen in Figure2.15

For real-time implementation a more accurate model for specific pump units used in Generation I was evaluated. A pump stand was built and pump/motor testing was performed to retrieve efficiency data ([21]). To develope a model that fits the data the Dorey model ([22]) was used to approach the problem. Finally parameters were added to describe the experimental data more accurately with the model. The relationship of speed and displacement to operating efficiency at a pressure of 3000psi can be seen in Figure 2.16.

Both model approaches were used to create look up tables that can be used in simulation and implementation. In the following the model using the manufacturer data will be used in simulation while the model derived using pump stand data will be used in implementation to control the system.

#### Generation II

To model the hydraulic components in the Folsom Hydro Static Transmission a physical model was used. Folsom developed a detailed model for the bent hydraulic pump/motors that includes mechanical losses such as friction between components and volumetric

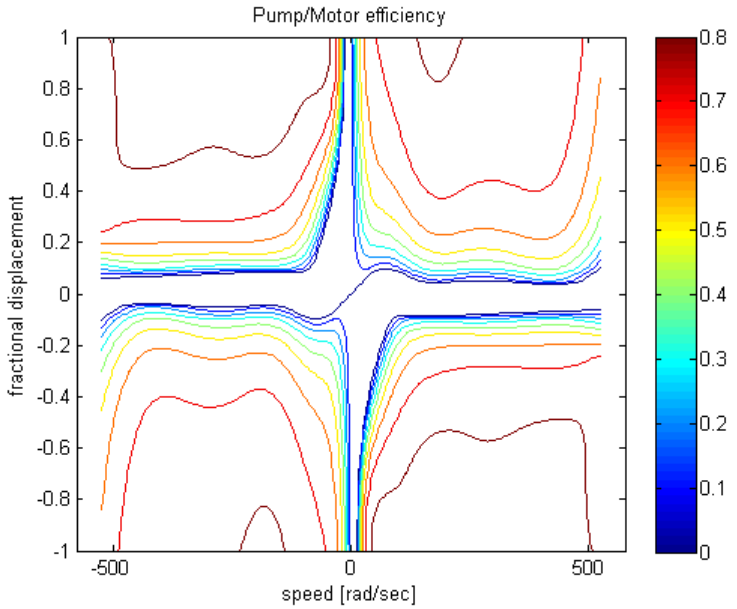


Figure 2.15: Efficiency Contour of S42 Swashplate Pump/Motors at 3000psi.

losses like leakage and compressibility. The rather complex physical model was used to create a three dimensional look up table that simplifies the use of the efficiency model in simulation and implementation. Torque and flow were stored as functions of displacement, speed and pressure. Displacement was stored as a function of torque, speed and pressure. Including mechanical and volumetric losses the pump/motor efficiency can be plotted and seen in Figure 2.17.

## 2.6 Conclusion

A model of the Generation I input coupled hybrid drive train has been derived. Inertia dynamic relationships together with engine and hydraulic component models can be used to simulate the drive train dynamics and to design controls for the vehicle. The Generation II output coupled drive train has been modeled. This vehicle uses a hydro static transmission in connection with an accumulator to achieve a hydraulic power split

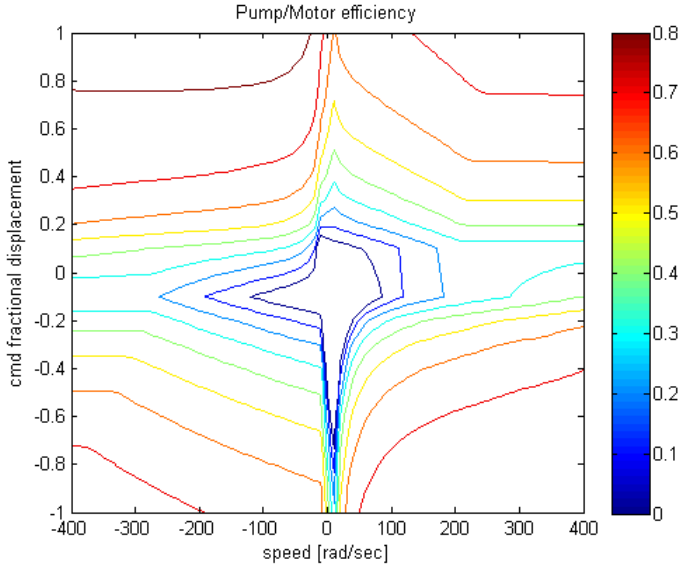


Figure 2.16: Experimentally Derived Efficiency Contour of S42 Swashplate Pump/Motors at 3000psi.

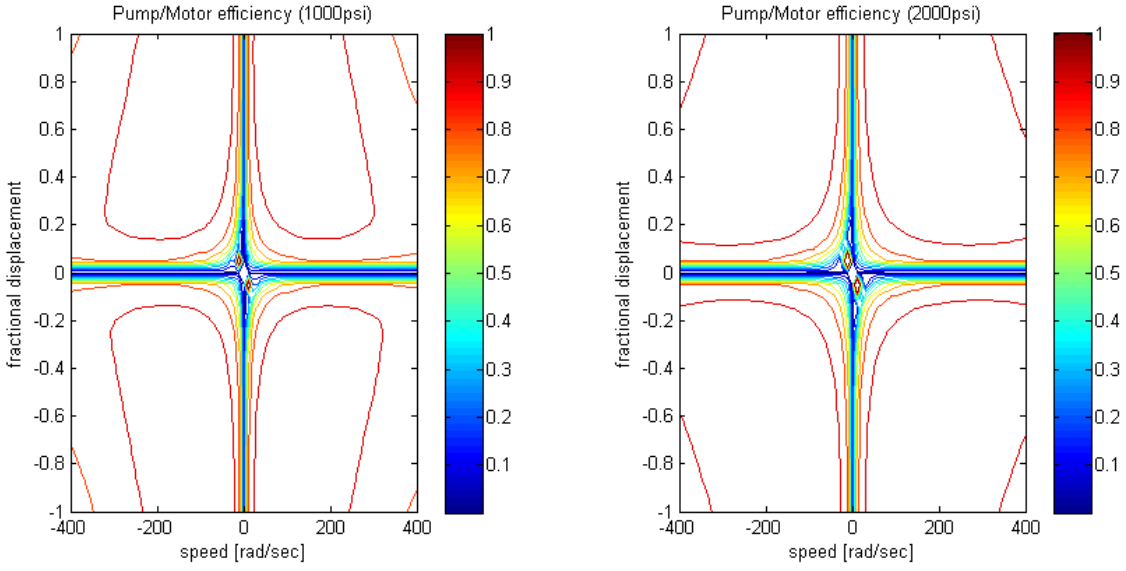


Figure 2.17: Efficiency Contour of Bent Axis Pump/Motors at 1000psi and 2000psi.

drive train. The derived equations can be used to analyze the drive train operation and simluation the vehicle.

# Chapter 3

# A Control Hierarchy for Hybrid vehicles

Hybrid vehicles have high potential in increasing fuel consumption in passenger vehicles. By recovering energy while braking, the drive train achieves a major increase in fuel economy. To further increase fuel economy the drive train has to be operated such that it optimizes its operation over a desired driving schedule. Dynamic programming or other optimization strategies have been used ([3]) to solve this problem. But since all operating points have to be considered the evaluation of the optimum in this way is very expensive. In this chapter a strategy will be introduced that simplifies the optimization process and reduces the complexity of the control for implementation purposes.

As seen in Figure 3.1, the strategy is hierachical and consists of three levels that are referred to as low, mid and high level control. The three levels interact through their inputs and outputs, here shown as arrows. The accumulator pressure, the vehicle speed and the commanded wheel torque by the driver are inputs to the control strategy. In real time the pressure is measured as the difference of the high pressure and low pressure accumulator. The vehicle speed can be retrieved from the encoders at the wheels and the desired vehicle torque is a translation of the pedal input by the driver.

In the high level control an energy management strategy is utilized to specify the power required from accumulator given the state of charge and the power required by the vehicle. The mid level control optimizes the drive train operation while satisfying

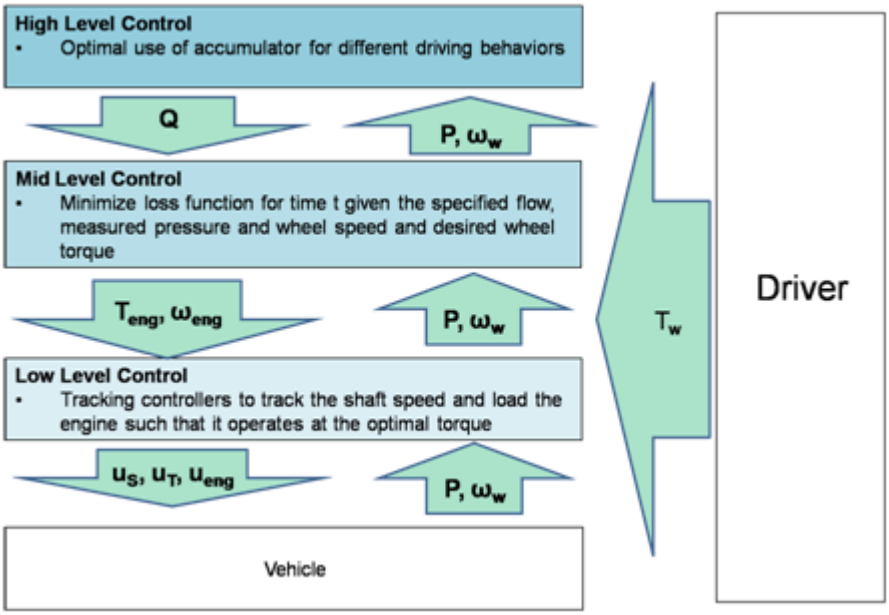


Figure 3.1: Architecture of Control Strategy.

the power demand specifications from the high level control. The low level controller is needed in real time implementation to ensure that the components operate at the specified speed and torque. In the next sections the strategy will be validated and the three levels will be discussed in more detail.

## 3.1 Derivation of Strategy

### 3.1.1 A Quasi-Static Analysis

In this quasi-static analysis it is assumed that the internal torque, derived in Section 2.3, is set to zero. Assuming a given drive cycle for off-line simulation or a driver command in real-time implementation it can be assumed that the vehicle speed and desired wheel torque is known. In the following the process is illustrated using the static equations from the Generation I vehicle. Using a similar approach the same results can be achieved using other hybrid architectures like Generation II. For simplification it is assumed that both P/M-S are operated at the same displacement and therefore $u_S = u_{SL} = u_{SR}$.

Using the equations in Table 2.7 and the assumption that $T_{int} = 0$ the static equations for the torque can be rewritten to

$$T_{mech} = T_{out}/2 \tag{3.1}$$

$$u_S = -T_{out}/R_S \tag{3.2}$$

where $T_{mech}$ is given by Equation 2.10 as a sum of $T_{eng}$ and $T_T$. From these equations it can be seen that by choosing the operating point of the engine ($\omega_{eng}$,$T_{eng}$) and specifying the wheel speed and torque ($\omega_{out}$,$T_{out}$) the operating points of the two pump/motors can be determined uniquely using Equation 2.1 and Equation 2.2.

Note here that operating the drive train most efficiently is equivalent to minimizing the losses in the system over the driving period. In this analysis the losses in the engine, P/M-T, and P/M-S, are included. Losses in transmission, differential and clutch can be added in the same fashion but will not be considered here. The instantaneous loss function of the system can then be specified by:

$$\begin{aligned} Loss_t(T_{eng}, \omega_{eng}, T_{out}, \omega_{out}, P) &= Loss_{eng}(T_{eng}, \omega_{eng}) + Loss_{P/M-T}(x_T, \omega_T, P) \\ &\quad +2Loss_{P/M-S}(x_S, \omega_S, P) \end{aligned} \tag{3.3}$$

where $x_S$, $x_T$, the displacements of the pump/motors and $\omega_T$, $\omega_S$, the speeds of the hydraulic components, can be determined from the engine operating point and the vehicle operation.

It is obvious that minimizing this loss function at each instance of the drive cycle would maximize system efficiency. Assuming free accumulator power the engine would then never be turned on since the losses in the hydraulic units is less than in the internal combustion engine. But since the state of charge in the accumulator can not be used without consequences this aspect has to be included in the simulation.

### 3.1.2 Power Train Optimization

As discussed in Section 2.3 the vehicle operation is specified by either the drive cycle or a the driver request. For a given set ($\omega_{out}$,$T_{out}$) and known accumulator pressure $P$ choosing the engine operation ($\omega_{eng}$,$T_{eng}$) results on two consequences. These are

1. The flow from the accumulator ($Q_{acc}$) changes.

2. The losses in the system, given by Equation 3.3 vary.

The power from the accumulator can be evaluted by $Pow_{acc} = PQ_{acc}$. For a known pressure the flow from the accumulator then specifies the power.

The energy capacity of the accumulator restricts the accumulator power. Therefore the accumulator power can not be evaluated seperately for every instance in time but rather as a function of time over an entire drive cycle. On the other hand, since total loss is always to be minimized it can be done at every instance as long as the constraints are satisfied. We therefore formulate a static optimization problem, where the losses are minimized given the accumulator power at time $t$. The solution to the problem can be given by:

$$Loss^*(\omega_{out}, T_{out}, P, \overline{Q_{acc}}) = \min_{\omega_{eng}, T_{eng}} Loss_{total}(\omega_{eng}, T_{eng}, \omega_{out}, T_{out}, P) \tag{3.4}$$

subject to $Q_{acc}$.

It has been shown that the controls problem can be seperated into two steps. First finding the accumulator power for $t$ in a drive cycle and second, minimizing the losses in the system at time $t$ for a give accumulator power $Pow_{acc}$. To seperate the problem of finding the optimal accumulator use over a cycle and evaluating the minimum loss function a hierarchical controls startegy is porposed. The control strategy specifies the accumulator power optimization in the high level. The solution to the static minimization problem is found in the mid level control. This approach will be explained in detail in the next sections.

## 3.2 High Level Control

In the high level control an energy management strategy is implemented. Inputs like the vehicle speed, desired wheel torque and accumulator pressure are used to decide how the accumulator should be utilized at any instance in time to optimize the operation of the system over the entire driving period. This problem has been investigated by many researchers and a variety of strategies have been proposed. Some simple solutions that have been proposed inlcude rule based algorithms using heuristic knowledge in a finite-state mashine [9]. Another approach used in Eatons Hydraulic Launch Assist (HLA) system [23] is to regenerate energy when stopping and re-using the energy when the

vehicle is accelerated. The torque of the internal combustion engine is low at low speed while alternative components often can produce high torque at low speed. Therefore the hydraulic pump/motors are used to accelerate the vehicle up to a chosen speed. Similar control strategies formulize boolean or fuzzy rules [24]. More complex strategies include Lagrange optimization ([25, 26], dynamic programming ([27, 28], equivalent consumption minimization strategies(ECMS) ([29, 30]) and stochatic dynamic programming ([31]).

There are advantages and disadvantages to each of these. Lagrange optimization and the dynamic programming approach can only be implemented in simulation with a given driving schedule. Knowledge of future vehicle operation is needed to implement these solutions. It is therefore not feasable in real-time. The advantage of these approaches is that the real optimum is determined and is therefore often used to evaluate upper bounds for performances of different architectures and components. ECMS and stochastic dynamic programming on the other hand can be implemented in real-time but do not achieve optimal fuel economy as seen in [6]. By seperating the energy management from the drive train optimization the control strategy proposed in this thesis reduces the complexity of the vehicle control. As seen in Section 3.1.2 only a single output ($Pow_{acc}$) is needed from the high level control.

## 3.3 Mid Level Control

As mentioned in Section 3.1.2 the shift of the engine operating points results in a change of accumulator power and instantaneous losses in the system. Given the desired accumulator power, $Pow_{acc}$, the mid level specifies the optimum operation of the system to result in the minimum losses in the entire drive train. To better understand this process an example is used to illustrate it. To reduce the complexity of the problem the pressure is assumed to be constant at 3000psi. It is assumed that at time $t$ vehicle speed $\omega_{out}$ and desired wheel torque $T_{out}$ are given. As seen in Section 3.1.1 choosing the engine operation ($T_{eng}$, $\omega_{eng}$) specifies the operation of the pump/motors to satisfy the requested vehicle performance ($\omega_{out}$, $T_{out}$). This results in a change of losses in the system and a change in power drawn from the accumulator. Figure 3.2 shows two engine maps. The left graph shows a contour plot of power coming from the accumulator for

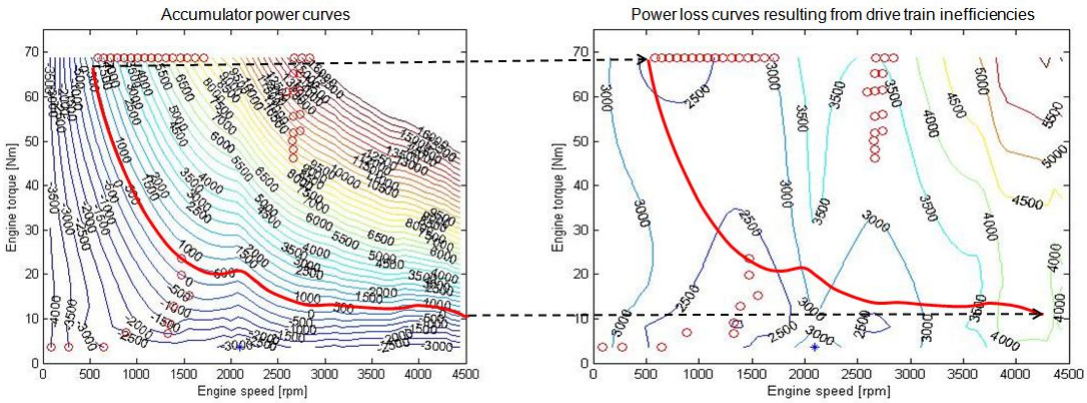


Figure 3.2: Accumulator Power and System Losses for Varying Engine Operating Points.

varying engine operating points. The accumulator power curves seen here result from varying pump/motor operations which get specified by $\omega_{out}$, $T_{out}$, $\omega_{eng}$, $T_{eng}$ together with the static equations in Section 2.1.2. The right graph shows a contour of the total losses in the system for varying engine operations. As seen the losses in the system, which include engine and pump/motor loss, vary with the change of the engine operating point.

We assume the high level control specifies an accumulator power $Pow_{acc} = 500Watt$. Then the engine has to operate on the 500Watt contour line in the left graph of Figure 3.2. With this constraint the mid level control then finds the operating point with the least losses for the entire system. This point is given by the minimum of the loss contour in the second graph of Figure 3.2 on the red line. The engine would have to operate at about 1500rpm and 25Nm in order to minimize the instantaneous loss.

Using this procedure minimum operation values can be computed for varying wheel speeds, wheel torques, accumulator pressures and accumulator power. This 4 dimensional function can be computed off line, stored and then used in real time implementation. This will reduce the computation cost of the control in the vehicle in real-time implementations.

## 3.4 Low Level Control

In the low level control feedback controllers are designed to ensure that components will operate at specified points. This level becomes important when the control strategy is implemented in real time. When simulating the vehicle with control algorithms it can be assumed that the engine operates at the desired speed and torque, and the pump/motors follow torque requests specified by the mid level control. The inputs from a logic unit to the vehicle are usually throttle command to the engine, and displacement commands to the hydraulic pump/motors. In contrast to this the input from the mid level specifies the speed of components as well as torque outputs of components. The torque required by P/M-S and P/M-T can be translated into a displacement command by using the pump models discussed in Section 2.5.2, where torque is a function of displacement, speed and pressure. Operating components at a desired speed is achieved by developing feedback controllers. In this procedure the error between the reference speed and the actual speed is used to specify the input to the system which then reduces the tracking error. In the engine the torque is commanded through the throttle input.

## 3.5 Conclusion

A three level control strategy has been proposed. This strategy simplifies controls implementation on hybrids in off-line simulation as well as real-time implementation. It has been shown that the optimization problem of a hybrid vehicle operation can be seperated in two levels, where the high level computes the optimal energy storage use for a given time. The mid level can be computed off-line and specifies minimium loss vehicle operation for a given vehicle speed, vehicle torque, accumulator pressure and accumulator power requested by the high level. In the lowest level tracking controllers are designed. In the next chapters the use of this strategy will be demonstrated.

# Chapter 4

# Off-line Applications

The EPA urban and EPA highway drive cycles are common drive cycles used in the United States to predict the efficiency of passenger vehicles. In this section it will be shown how the control strategy developed in Chapter 3 can be used to predict the efficiency of hybrid vehicles over such a cycle. In simulation the lowest level in the controls hierarchy can be omitted. The mid level control is represented by a precomputed look up table which specifies the best operation of the drive cycle for a given vehicle speed, wheel torque, pressure and accumulator power. In the high level control an optimization strategy is used to find the best energy efficient operation of the vehicle over the entire cycle. In this chapter the high level control is simulated using the Lagrange Multiplier Method. The cost function to be minimized can be defined by

$$J = \sum_{t=0}^{T} Loss(\omega_{out}(t), T_{out}(t), \omega_{eng}(t), T_{eng}(t), P(t), Q_{acc}(t)) \tag{4.1}$$

where $T$ is the final time in the drive cycle. The cost function should be minimzed over a given driving schedule given the constraint

$$\sum_{t=0}^{T} Q_{acc}(t) = 0 \tag{4.2}$$

The pressure $P(t)$ can be evaluated using Equation 2.5.1.

Using Lagrange Optimization Methodology ([32]) the optimization of a cost function with respect to a equality constraint is simplified to a single unconstrained cost function

that can be solved. Such a function can be defined by

$$\max_{\lambda} \min_{\omega_{eng},T_{eng},Q_{acc}} J = \sum_{t=0}^{T} Loss(\omega_{out}(t), T_{out}(t), \omega_{eng}(t), T_{eng}(t), P(t), Q_{acc}(t)) + \lambda \sum_{t=0}^{T} Q_{acc}(t) \quad (4.3)$$

This function is then used to find a *sattle point* $(x^*, \lambda^*)$ such that $J(x^*, \lambda) \leq J(x^*, \lambda^*) \leq J(x, \lambda^*)$ for all $(x^*, \lambda)$ and $(x, \lambda^*)$ sufficiently close to $(x^*, \lambda^*)$([32]). $x$ refers to the vector of variables to minimize over, here $\omega_{eng}$, $T_{eng}$ and $Q_{acc}$.

Using this concept the optimization is simplified to just one single variable $\lambda$. Using this optimization method the following chapter will show applications of the developed control strategy in off-line simulations on the Generation I and Generation II vehicle. First, fuel consumption of the Generation I vehicle will be investigated. Studies will be performed to investigate the impact of component sizing, operation of the drive train and hydraulic efficiency on fuel consumption. The results will be shown in Section 4.1. In addition, for various hydraulic efficiencies, a comparison between parallel, series and power-split hybird configurations will be presented. In Section 4.2 the potentials of implementing a hydro static transmission or hybridization of the Ford F150 will be analyzed. The effect of pump/motor restrictions in the Folsom hydro static unit on engine management and fuel consumption will be discussed.

## 4.1 Gen I: Case Studies

Due to the changing pressure in the accumulator a detailed study should be performed using varying pressures, here a constant pressure of 3000psi is assumed to simplify the calculation and reduce the computational cost of the optimization. Using the strategy described above a baseline number was computed. The hydraulic hybrid vehicle in its current configuration, as specified in Section 2.1, is projected to achieve a fuel economy of 49.8mpg over the EPA urban driving schedule. Auxiliary losses and penalties for turning the engine on and off are not included in these calculations. To get an idea of the maximum range of improvement it is useful to compute an upper bound in fuel economy. This number is evaluated assuming the engine is operated off, at zero losses, or on at its optimal operation. The Perkings engine used in this vehicle has a maximum

efficiency of 31%. All the kinetic energy is assumed to be regenerated while braking and the pump/motors are assumed to be 100% efficient. With these assumptions the upper bound fuel economy can be calculated to be 113mpg for the urban drive cycle.

### 4.1.1 Study 1: Sizing Hybrid Vehicles

The Generation I vehicle currently in use at the University of Minnesota is a first approach in the process of building a fuel efficient fluid power power-train. By analysing the performance of the drive train knowledge was gained about the operation of a power split configuration. Applying this knowledge the drive train can be redesigned. Simulating the current vehicle versus a resized vehicle has shown fuel economy improvements of 8%.

The current vehicle hydraulic components sizes and gear ratios are given in 2.1.2. To resize the drive train most efficiently the following approach can be taken: First, the desired vehicle performance has to be specified. In this study a 0 to 60mph acceleration will not be considered. The drive train will be sized such that it satisfies the requirements of the EPA urban and EPA highway drive cycle. The drive cycle requirements in speed and torque can be seen in Figure 4.1. In addition the engine and pump/motor components are assumed to operate as specified in the models derived in the Sections 2.4 and 2.5.

Sizing of the transmission ratio is done by assuming the engine's *sweet spot* is mapped to the low speed centroid of the drive cycle operating points. As seen from Figure 4.1 this point is specified to 34rad/sec. The most efficient operating point of the engine can be found from Figure 2.13 and is assumed to be 60Nm at 260rad/sec. In this study the engine is not replaced. If a smaller more efficient engine is available downsizing of the engine can improve fuel economy further. Ratio $R_T$ is set to unity since the operating speed of P/M-T is optimized at 260rad/sec as well. To specify ratio $R_S$ it is assumed that the maximum speed of P/M-S is at 400rad/sec. With the engine operating at its optimal point the speed operation of P/M-S is found to be less than 34rad/sec at all times in the drive cycle. With the ratio $R_S$ the maximum speed of the hydraulic unit is mapped to this largest necessary speed. All ratios in the drive train are specified using the described method and can be seen in Table 4.1. The resulting transmission ratio for the carrier shaft is 15.3, and the ratio between P/M-S and the differential becomes

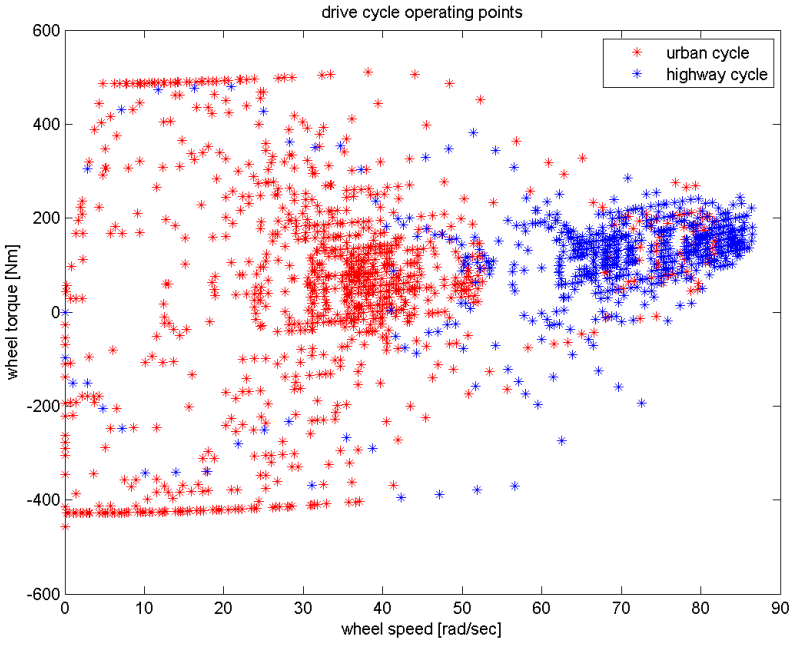


Figure 4.1: EPA urban and highway drive cycle operating points

12. It should be noted here that a ratio of value 12 is not feasable in implementation,

Table 4.1: Ratio Values

| **ratio notation** | **ratio** |
|---|---|
| $GR_R$ | 15.3 |
| $R_T$ | 1 |
| $R_S$ | 12 |

but will be simulated in order to show the fuel economy improvement for an optimaly sized drive train.

To size the hydraulic P/Ms the static equations in Section 2.1.2 should be considered. P/M-S is sized such that it can provide the required torque to the wheels. P/M-T is sized such that torque at low speed can be provided by the pump/motor only, while the engine is turned off. The optimal sizes were found to be 21cc for P/M-T and 14cc for P/M-S.

Using this configuration fuel economy increases from 49.8mpg to 53.9mpg for the UDDS urban drive cycle. This increase in fuel economy is due to a shift in operation in the pump/motors into a more efficient operating region. This change can be seen in Figure 4.2. The first two graphs show the operation of the hydraulic unit in the vehicle in its current sized drive train. It can be seen that the pump/motors operate close to the y-axis of the plot, in the low speed region. Therefore the average efficiency over the drive cycle is low. In graphs three and four the operation of the hydraulic units in the resized vehicle can be seen. The operation of the pump/motors is shifted into a higher speed region and is therefore more efficient.

To increase the fuel consumption further a mechanical gear can be added to the simulated drive train. Mapping the high speed centroid of operating points of the urban cycle to the engine optimal speed this ratio was found to be 6.75. This addition to the drive train improves fuel economy by 11%.

A summary of the results of this study can be seen in Figure 4.3. For the Generation I vehicle it can be assumed that fuel economy increases from a baseline of 49.8mpg to

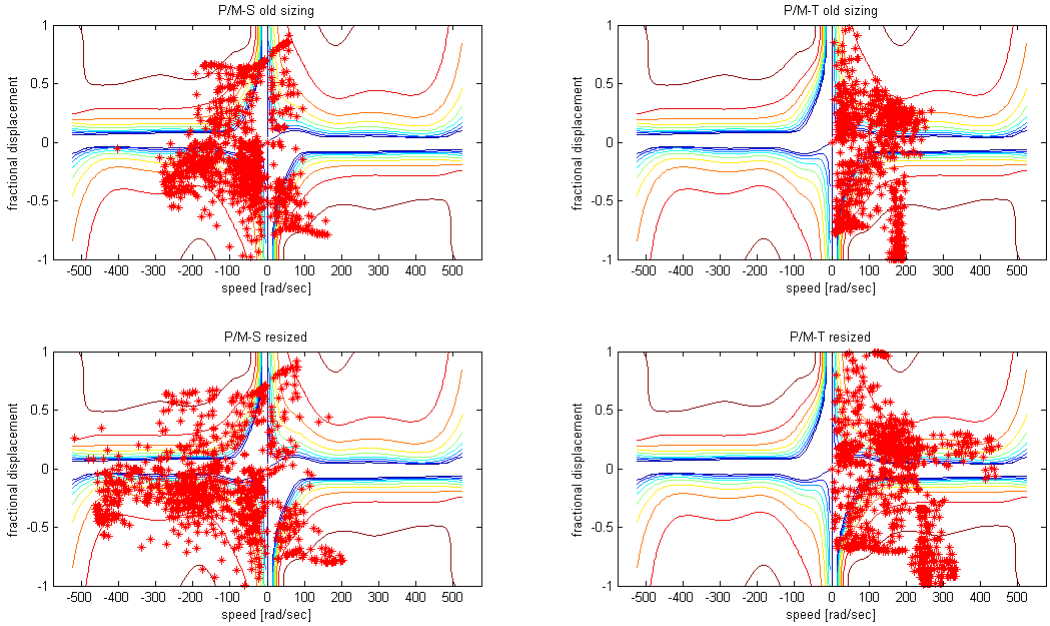


Figure 4.2: operation of pump/motor efficiency in old sized vehicle versus resized vehicle

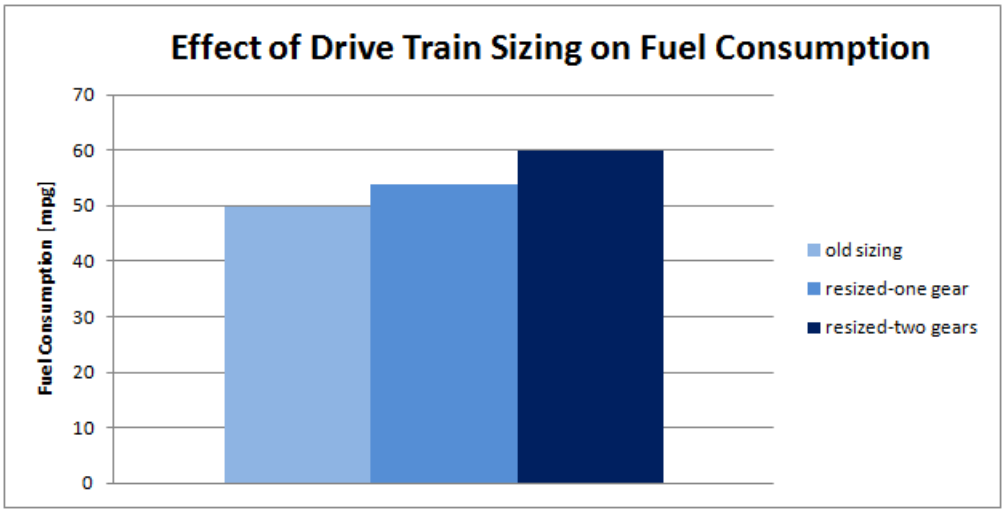


Figure 4.3: Fuel consumption for vehicle with old sizing and resized vehicle with one and two mechanical gear.

53.9mpg due to more optimal sizing. The addition of a second mechanical gear brings fuel economy to 59.8mpg.

### 4.1.2 Study 2: Operation Of The Power Split Hybrid

A power split hybrid vehicle is expected to improve fuel economy due to the flexibility in engine management. This implies that fuel economy strongly depends on the control of the drive train. In this study a modal operation of a power split hybrid drive train is suggested. Considering a normal power split operation with engine on/off option as mode 1, a parallel operation mode 2 and a series-like mode 3 operation the drive train can be operated most efficiently.

A schematic of the drive train for each mode can be seen in Figure 4.4. In mode 1 both hydraulic units are operated to shift the engine operating point. The engine can be turned off while the power train is driven by the hydraulic units only. The total losses in the system consist of the losses in the engine as well as losses in each pump/motor unit.

Due to the nature of the differential in the Generation I architecture the P/M-S has to provide a specific torque in order to transmit the engine torque. This results in losses in the hydraulic unit even if it is operated at zero speed, not shifting the engine operating point. In mode 2, to reduce the losses in such an operation it is assumed that a mechanical lock up of P/M-S is possible. One way to do this is to add a clutch to ground at the P/M-S shaft. The valves to the high pressure line can be closed which results in zero losses at P/M-S. This mode is called parallel-mode because the lock up reduces the power-split configuration to a drive train in parallel hybrid configuration. The engine can then provide power to the wheels while P/M-T can be used to alter the engine operating point in torque.

In mode 3 it is assumed that the entire drive shaft is locked mechanically. In this operation the only component contributing to the overall system losses is P/M-S. By disconnecting the high pressure line from P/M-T and turning the engine off the losses in these components are eliminated. This mode is similar to a series operation in the way that all power provided to the wheels is transmitted through the hydraulic path.

In Figure 4.5 the results of implementing a modal operation can be seen. The results on the left half of the graph are computed assuming the optimally sized Generation I

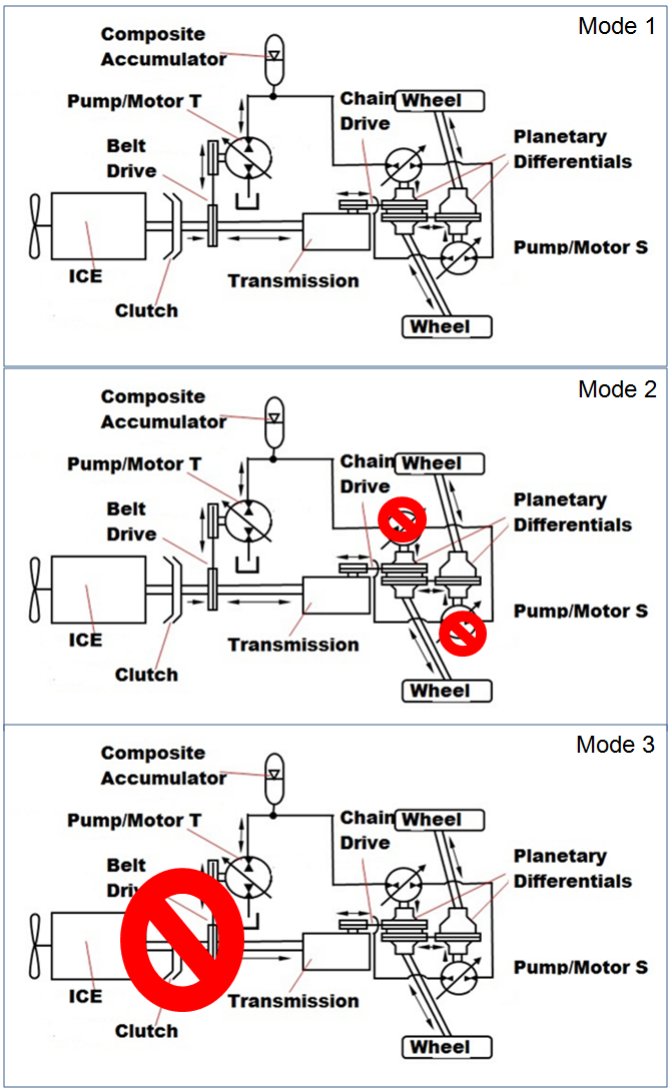


Figure 4.4: Lock up of components in modal operation.

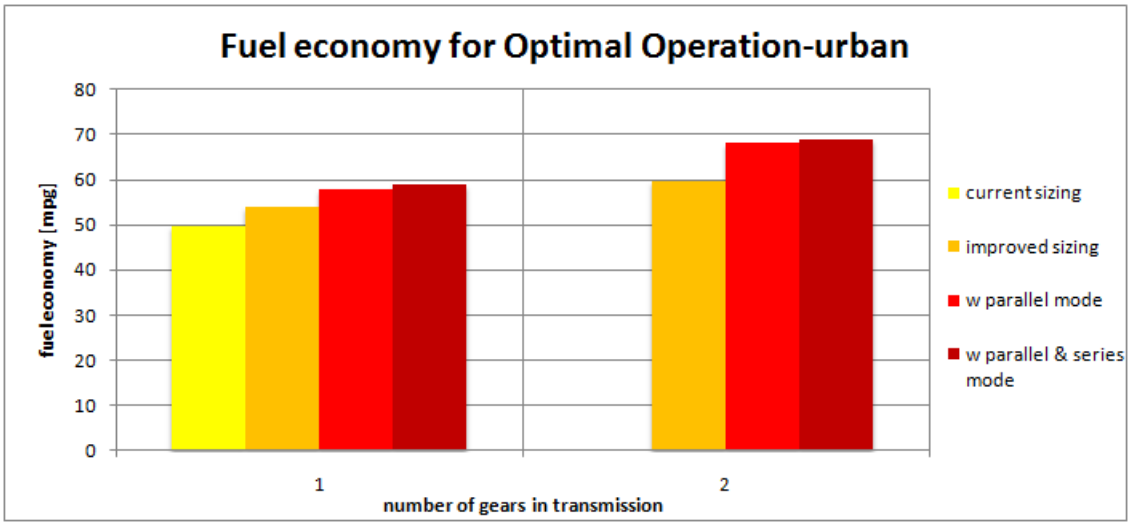


Figure 4.5: Fuel consumption improvements for modal operation in a power split vehicle over the urban drive cycle.

vehicle with one mechanical gear. In the right graph the numbers for the Generation I vehicle are shown with a two gear mechanical transmission. It can be seen that with respect to the baseline operation of the power split vehicle fuel economy increases by up to 16%. Basic operation of a power-split vehicle can achieve a fuel economy of 53.9mpg for a single gear power split configuration and 59.8mpg for the two gear power split drive train in the resized Generation I hybrid configuration. Adding the option of operating in modes 2 or 3 increases fuel consumption to 59.0mpg for a single gear and 68.1mpg for two mechanical gears.

To understand the operation of this input coupled power split architecture the use of each mode in the drive cycle has to be investigated. Figure 4.6 shows the wheel speed over the EPA urban driving schedule. In this graph the mode of operation of the vehicle has been specified a colors. The points plotted in red show the operation in mode 1, blue shows the operation in mode 2 and points plotted in green represent vehicle operation in mode 3.

From Figure 4.6 it can be seen that in low speed acceleration and deceleration the

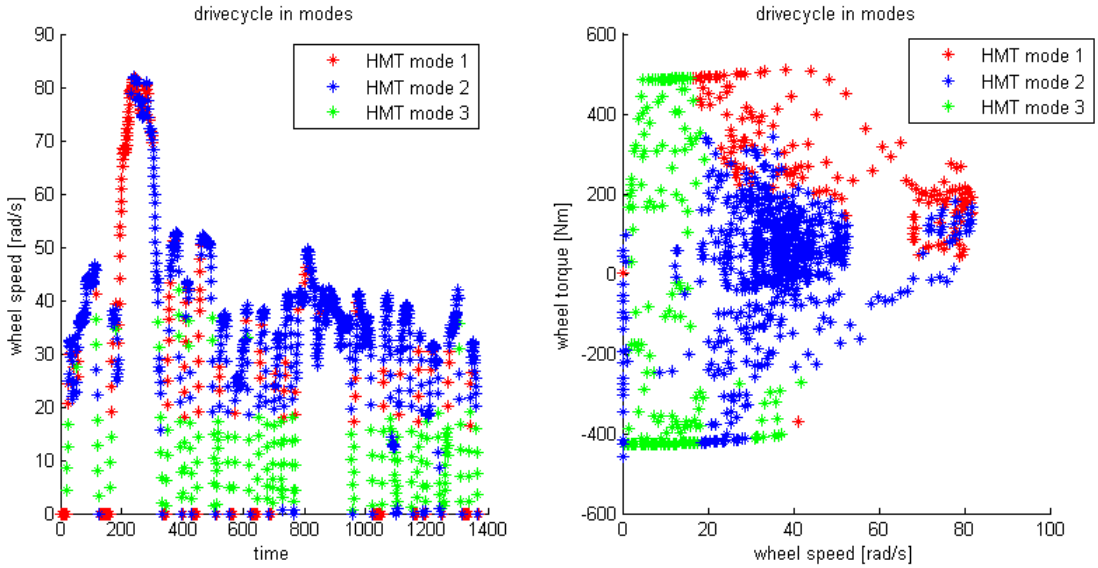


Figure 4.6: Modal operation over EPA urban driving schedule.

drive train operates most efficiently in series mode. Higher speed accelerations are usually performed in mode 1, operating the engine and both pump/motors as a normal power split. Cruising and high speed deceleration is chosen by the optimization to be performed in mode 2, where the drive train operates as a parallel hybrid. An operation in series mode at low speed and parallel mode in high speed in a power split hybrid has previously been suggested by Rizoulis ([33]) in 2001. In his SAE technical paper simulation results are used to show that the nature of the configuration of the power split drive train makes modal operation optimal. These findings can be usefull when developing engine management strategies. A rule based algorithm could be developed dependent on these finding.

Computing the fuel economy values for the vehicle over a highway driving schedule it has been found that the gain due to modal operation is not as significant. In highway driving the vehicle speed operates in a smaller range and large acceleration or deceleration maneuvers are unusual. It can be seen from Figure 4.7 that the improvement in a one gear Generation I vehicle with modal operation versus a vehicle without a modal strategy is only about 1mpg for a single gear vehicle and about 2mpg for a vehicle with

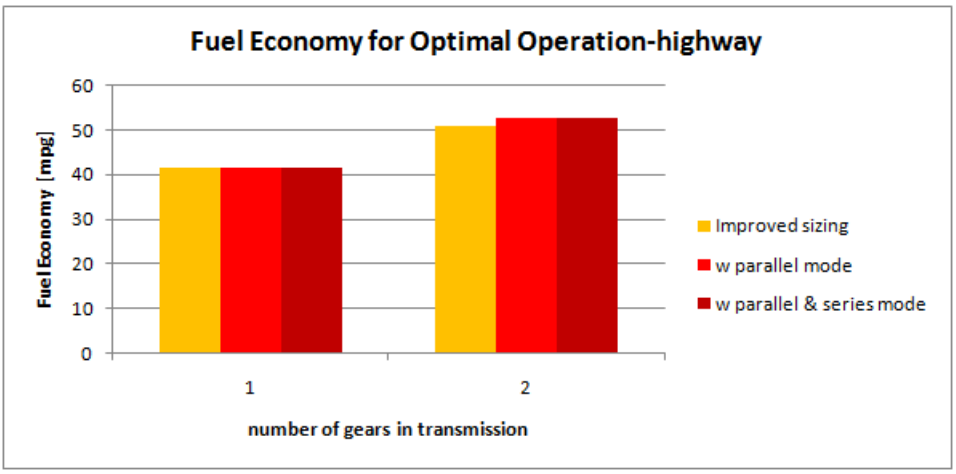


Figure 4.7: Fuel consumption improvements for modal operation in a power split vehicle over the highway drive cycle.

two gear transmission.

By plotting the drive cycle in the operated modes the reason for this small improvement becomes obvious. It can be seen from Figure 4.8 that for a majority of times the vehicles optimal operation is in normal HMT mode. Modes 2 and 3 are used rarely, mostly for start up acceleration and final braking. This is due to the fact that in highway driving the engine speed in conventional drive trains is already close to optimal. Therefore the operation of the engine does not have to be shifted significantly.

Using modal operation further sizing studies have shown that when the drive train in the power split vehicle is sized using a mathematical optimization fuel economy for this architecture can improve even further. Assuming modal operation in sizing the gear ratios and hydraulic pump/motors, sizes can be specified such that the drive train can achieve the drive cycle in any of the three modes. However the vehicle might not be able to satisfy the torque and speed requests of the drive cycle in power split mode at all times.

It has been shown that modal operation of a power split hybrid can improve fuel economy. A fuel economy increase of up to 16% can be achieved for the urban driving schedule. It has been found that modal operation does not have a significant impact on fuel economy in highway driving.

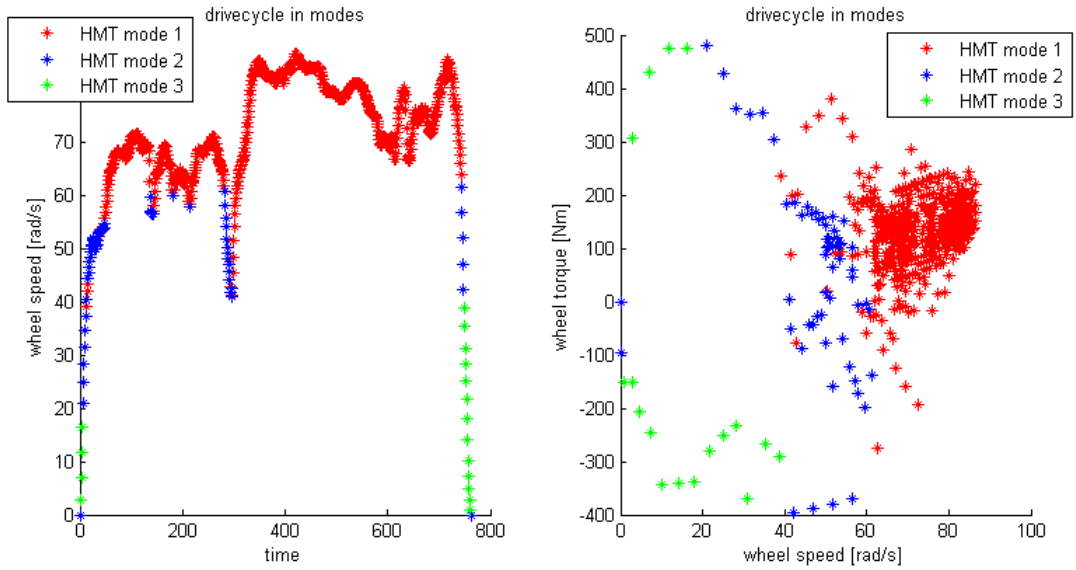


Figure 4.8: Modal operation over EPA highway driving schedule.

### 4.1.3 Study 3: Efficiency Of Hydraulic Components

Over the past years the technology of hydraulic pump/motors has improved. More efficient hydraulic units have been designed and pump/motors that can run in high efficiency regions over wide operating ranges are now available on the market. Even though this is the case high efficiency hydraulic units are often costly. Therefore the effect of changes in efficiency of the hydraulic components in the vehicle on overall system performance has to be investigated.

In this study the pump model described in Section 2.5.2 is used to vary hydraulic efficiency and to determine its impact on fuel efficiency of the vehicle. Using a loss factor the model enables us to simulate similar pump/motors with different efficiencies. Implementing the hierarchical controls strategy with a Lagrange optimization method the fuel economy is evaluated for the vehicle. For this computation the idealy sized Generation I vehicle is used assuming optimal operation in modes. Since a portion of the power to the wheels is transmitted through the hydraulic line it is expected that system performance changes with varying hydraulic component efficiency.

Due to varying operating points of the pump/motors throughout the drive cycle

the efficiency of the hydraulic units changes. To compare fuel economy dependent on hydraulic efficiency the average efficiency of both hydraulic units is computed. This includes volumetric efficiency as well as mechanical efficiency. The average efficiency can be computed by

$$\eta_{avghydraulic} = \frac{Power_{hyd_{out}}}{Power_{hyd_{in}}} \tag{4.4}$$

where $Power_{hyd_{out}}$ is the sum of the positive products of $T_S\omega_S$ and $T_T\omega_T$ and $Power_{hyd_{in}}$ is the sum of the negative products of $T_S\omega_S$ and $T_T\omega_T$.

In a power split vehicle the engine operating point is moved to its optimal using the hydraulic pump/motors. In this study it has been found that with increasing efficiency of hydraulic components the power transmitted through the hydraulic path grows. This was to be expected since the optimization chooses the most efficient path to deliver the requested power to the wheels. In Table 4.2 this trend can be observed. Using

Table 4.2: Impacts of Increased Hydraulic Efficiency

| **Pump Model Loss Factor [%]** | **Avg. Hydraulic Efficiency [%]** | **Avg. Engine Efficiency [%]** | **Power through Hydraulic Path [%]** | **Fuel Economy [mpg]** |
|---|---|---|---|---|
| 100 | 52 | 30 | 47 | 69.0 |
| 50 | 72 | 31 | 56 | 83.3 |
| 20 | 88 | 31 | 65 | 101.1 |

a loss factor of 100% in the hydraulic pump/motors the engine is operated at 30% efficiency. The engine is therefore not operated at its optimal at all times in the drive cycle. Only 47% of the power to the wheel is transmitted through the hydraulic path. This operation leads to a fuel economy of 69.0mpg. By scaling the losses a higher average hydraulic efficiency is achieved, simulating better pump/motors. Operating the hydraulic units at an average efficiency of 72% the engine mean efficiency is pushed to 31% and the hydraulic path now transmits 56% of the power to the wheel. Fuel economy then increases to 83.3mpg. With Pump/Motors that are 80% less lossy the

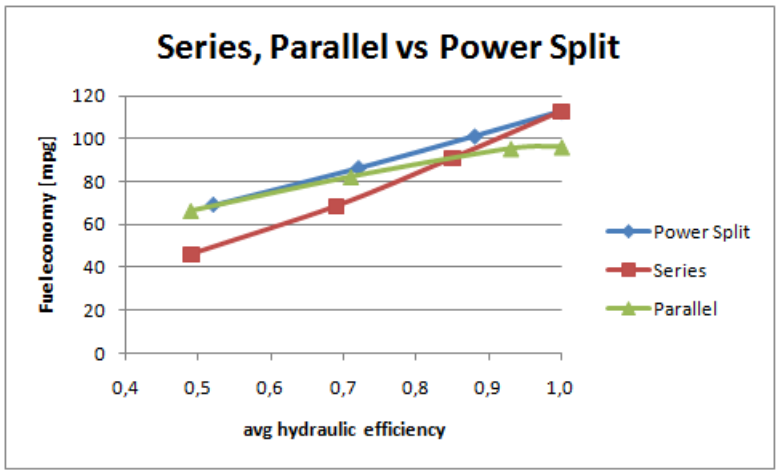


Figure 4.9: Hydraulic component efficiency versus fuel consumption.

fuel economy can potentialy be increased to 101.1mpg. In this case 65% of the power to the wheel is transmitted through the hydraulic line.

The relationship between fuel economy and hydraulic efficiency is approximated in Figure 4.9. In blue the results of this study can be seen. As mentioned fuel economy strongly depends on hydraulic efficiency. With the original pump/motor units a fuel economy of 69.0mpg can be achieved. Assuming more efficient pump/motors the fuel consumption decreases. With an average hydraulic efficiency of .72 fuel consumption improves to 86mpg while with a hydraulic efficiency of .88, 101 mpg can theoretically be achieved. Ideal hydraulic components with 100% efficiency for all operating points could potentialy achieve 113mpg over the EPA urban driving schedule With these numbers in mind the investment high efficient hydraulic pump/motors should be considered when designing a hydraulic hybrid vehicle.

### 4.1.4 Study 4: A Comparison Of Architectures

In the CCEFP the Test Bed 3 group is investigating potentials of hydraulic hybrid drive trains to improve fuel consumption. There are three main configurations of hybrid drive trains, the parallel, series and power split configuration. To achieve a set goal in fuel consumption and performance the approach taken by the Test Bed 3 group is to use

a drive train in power split configuration. It is anticipated that a power split hybrid architecture achieves higher fuel consumption than a parallel or series hybrid due to its flexibility to transmit power. Using the proposed three level control strategy a study was performed to examine fuel consumption of the three hybrid architectures in comparison. As seen in Section 4.1.3 fuel economy in hydraulic hybrid vehicles is dependent on the efficiency of the hydraulic components. Therefore the fuel economy of hybrid architectures will be discussed for varying hydraulic efficiency.

In a parallel hybrid vehicle all power is transmitted through the efficient mechanical shaft. The pump/motor attached to the carrier can shift the engine operating point only in torque. Therefore engine management is limited. While the engine is declutched the pump/motor can exert a negative torque to the drive shaft and slow the wheel down without applying friction brakes. In this configuration fuel economy is increased by turning the engine off, performing engine management and most importantly recovering braking energy.

In a series architecture all power to the wheels is transmitted through the hydraulic path. Depending on the quality of hydraulic components this path can be very inefficient. The engine operation is decoupled from the power desired at the wheels and can thus operate at its most efficient point. For a sufficiently large energy storage the engine is turned on and off at its optimal point to charge the accumulator such that the desired power at the wheels can be provided by the pump/motor. In comparison to a conventional vehicle this drive train reduces fuel usage by full engine management and by recovering braking energy.

A power split drive train combines the positive aspect of both these architectures. In this configuration fuel consumption is increased by performing full engine management, turning the engine off and by regenerative braking. The mechanical shaft can be used for efficient power transmission while the hydraulic path enables us to shift the engine operating point in speed and torque. From these facts it is expected that fuel economy in a hybrid vehicle in series configuration depends strongly on hydraulic efficiency whereas in a parallel architecture the relationship is weak.

In this study fuel economy values were computed for an optimaly sized parallel, series and power split hybrid vehicle. The sizing in the power split is as described in Section 4.1.1. The same method was used for the parallel sizing. The engine optimal region was

mapped to the two centroids of the urban drive cycle to specify the transmission ratios. The ratio between P/M-T was kept at unity. This approach results in equal ratios and pump/motor size in this drive train as specified for the parallel part of the power split configuration.

The series architecture used in this comparison was sized such that the pump can absorb the engine torque and the motor can provide the requested torque to the wheels. The ratio between the engine and the pump was found by maping the engine optimal speed to the most efficient speed operation of the hydraulic unit. The size of the pump was then calculated assuming an ideal pump model such that the pump's maximum negative torque is slightly higher than the maximum torque of the engine at this speed. The gear ratio between the hydraulic motor and the wheel was chosen such that the maximum wheel speed in the drive cycle is transferred to the motor maximum speed. The size of the motor is then specified by the torque required by the drive cycle.

All sizing of the hydraulic components was done assuming a pressure of 3000psi and an ideal hydraulic model. In each case the vehicle simulated was the Generation I vehicle. Ratios and hydraulic pump/motors were sized such that it was optimal for the architecture to perform the EPA urban cycle. The gear ratios and pump/motor sizes used in the simulation can be seen in Table 4.3. With a high range in speed in the EPA urban driving schedule it is not possible for the parallel configuration to perform the cycle with only one mechanical gear in the transmission. To make a fair comparison a two gear transmission was assumed for simulation of the parallel and power split case.

Table 4.3: Drive train ratios and pump/motor sizes for parallel, series and power split architecture

| **configuration** | $R_{trans}$ | $R_T$ | $R_S$ | **P/M-T** | **P/M-S** |
|---|---|---|---|---|---|
| Parallel | [15.36.75] | 1 | - | 21cc | - |
| Series | - | 1.4 | 6.34 | 21cc | 27cc |
| Power split | [15.36.75] | 1 | 12 | 21cc | 14cc |

The results of the study can be seen in Figure 4.9. It is shown that the power split configuration is superior to the other two hybrid architectures over a wide range

of hydraulic efficiency. Considering the operation of the power split architecture this is expected. Operating the power split architecture in modes enables it to operate in either parallel mode, series mode or in power split. Therefore at any point in the drive cycle the efficiency of this configuration is at least as good as the parallel or series architecture.

For an average hydraulic efficiency of 52% the vehicle in power split configuration achieves a fuel economy of 69mpg while the parallel hybrid vehicle achieves 66mpg for a hydraulic efficiency of 49% and a series configuration is projected to get 46mpg for an average efficiency of 49%. If hydraulic efficiency increases to 88% the vehicle in power split configuration can achieve a fuel economy of 101mpg, while the parallel architecture only achieves 95mpg for a hydraulic efficiency of 93% and the series configuration achieves 91mpg for a hydraulic efficiency of 85%.

The series architecture shows a large improvement in fuel economy when increasing hydraulic efficiency, while the fuel consumption of the parallel architecture does not improve as significantly. For low efficiency hydraulic components the parallel and power split configurations achieve higher fuel economy than the series architecture. In low efficiency ranges the power split operates mostly in parallel mode to reduce the losses in the hydraulic path and therefore achieves a fuel economy close to the parallel architecture. Using very efficient hydraulic components the engine is mostly operated at its optimal and the normal HMT mode and series mode are used more often in the power split architecture. Thus using efficient hydraulic units the fuel economy of the power split is similar to that of a series configuration.

It has been shown that for any hybrid architecture fuel economy depends on hydraulic efficiency. Because all the power is transmitted through the hydraulic path in the series architecture its dependency is very strong, while the parallel and power split architecture can achieve good fuel economy even with lower efficiency hydraulic components. It has been shown that the power split architecture performs as good or better than a parallel or series hybrid vehicle for the entire range in hydraulic efficiency.

## 4.2 Gen II: Case Studies

Heavy vehicles like pick-up trucks are known for their low fuel economy. Still in the United States people prefer driving large vehicles which enable them to be flexible in space and makes them feel saver in traffic. To reduce greenhouse gases it is therefore critical to improve efficiency of such vehicles.

The advantages of adding an accumulator to store regenerated energy from braking will be examined by this research. A simulation of the F150 vehicle including all losses in the drive train as well as auxiliary losses has been built by Ford previously. According to this model a conventional F150 achieves 17.9mpg in city driving and 26.0mpg over the highway drive cycle. This model will serve as a baseline in the studies performed here. In the following section the three model controls strategy will be used with the Lagrange optimization approach to discuss the performance of a Ford F150 vehicle with hydro static transmission. Then a potential fuel economy increase will be studied for the hybridized truck. Finally, in Section 4.1.2, the impact of pump/motor restrictions on engine management, and therefore fuel consumption, will be investigated.

### 4.2.1 Study 1: Fuel Economy of a Ford F150 with Hydro Static Transmission

In the conventional drive train all power going to the wheel is provided by the internal combustion engine and transmitted through the mechanical drive shaft. A gear box enables the engine to power the wheel over a wide range in torque and speed. Usually the mechanical transmission has a discrete number of gears with fixed ratios. Choosing any of these the engine is shifted to its most optimal operation possible. A hydro static transmission is often called a continously variable transmission because it can be used to continously change the transmission ratio to shift the engine to its most efficient operating point. Since there is no alternative energy source available on the vehicle all the power transmitted to the wheel has to be provided by the engine. Therefore, assuming an ideal transmission, in a vehicle with hydro static transmission the engine operation can be shifted on a constant power curve in the engine operating map. This can be seen in Figure 4.10, where the blue curve shows a constant power curve of 30000Watts.

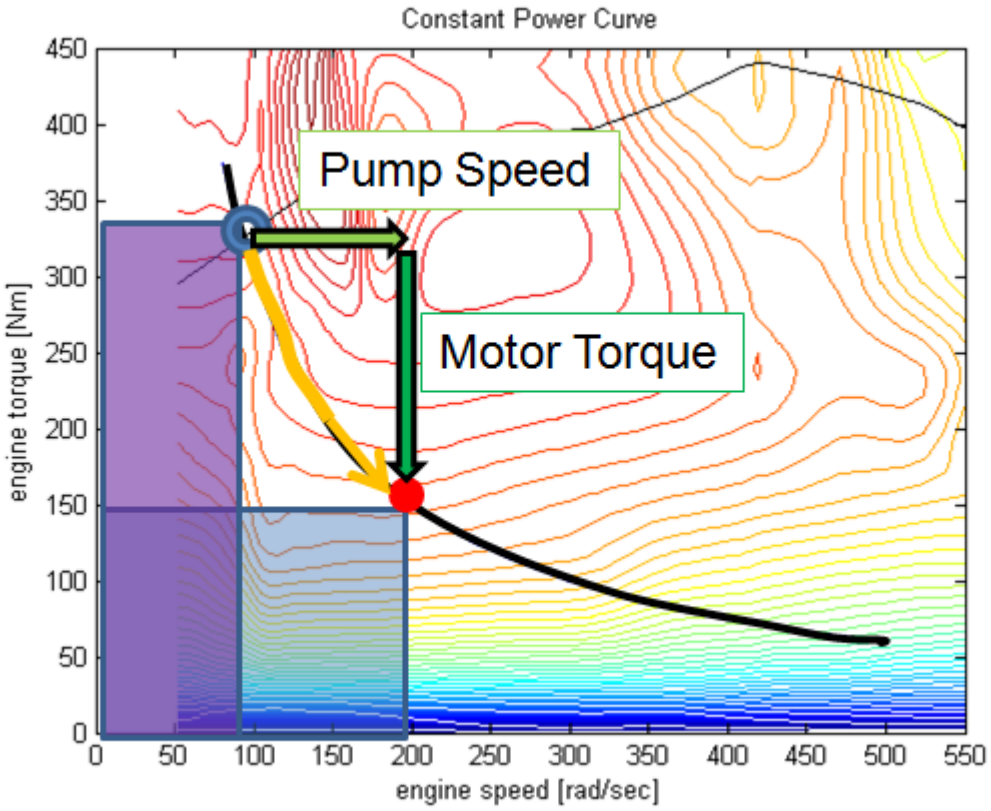


Figure 4.10: Constant power curve shifting of the Engine.

In a vehicle with hydro static transmission the engine operation can be shifted to any point on the constant power contour. To optimize instantaneous fuel consumption the engine operation of least losses on this contour should be found. Implementing the Folsom Hydro Static Transmission in a Ford F150 enables us to apply this concept to reduce fuel consumption. Assuming ideal transmission efficiency an upper bound in fuel economy can be computed for this vehicle configuration by finding the most efficient engine operation for output powers over the drive cycle. With a hydro static transmission the F150 vehicle was found to at most achieve 30.1mpg over the EPA urban drive cycle and 31.0mpg over the EPA highway driving schedule.

To get a more accurate approximation of the performance of this vehicle the efficiency of the transmission should be included. Shifting the engine results in varying operation of the hydraulic pump/motors in the hydro static transmission. To improve fuel economy the losses in the overall system have to be considered. Therefore the loss function of the system is defined to be:

$$J_{loss} = Loss_{engine}(T_{eng}, \omega_{eng}) + Loss_{P/M-S}(x_S, \omega_S, P) + Loss_{P/M-T}(x_T, \omega_T, P) \quad (4.5)$$

Without an accumulator storage system attached to the hydraulic high and low pressure lines the power from the pump has to equal power going into the motor minus the losses in the hydraulic components. Therefore the following constraints hold:

$$Q_S P = -Q_T P \quad (4.6)$$

$$Q_S = \omega_S x_S = -\omega_T x_T = -Q_T \quad (4.7)$$

With these equations and the efficiency contours of the engine and pump/motors the optimization can be solved step by step over the drive cycle. Including hydraulic pump/motor efficiencies and losses in the engine the Generation II vehicle was simulated with a hydro static transmission. It was found that a fuel consumption of 28.2mpg can be achieved over the EPA urban cycle and 28.3mpg over the EPA highway drive schedule. The power provided by the engine together with the power required at the wheel over the urban drive cycle can be seen in Figure 4.11. Here the engine speed and torque can be seen in the first two graphs. In the third graph we can see the power needed at the wheels in blue and the power provided by the engine in green. As expected the power provided by the engine is slightly higher than the output power of the vehicle.

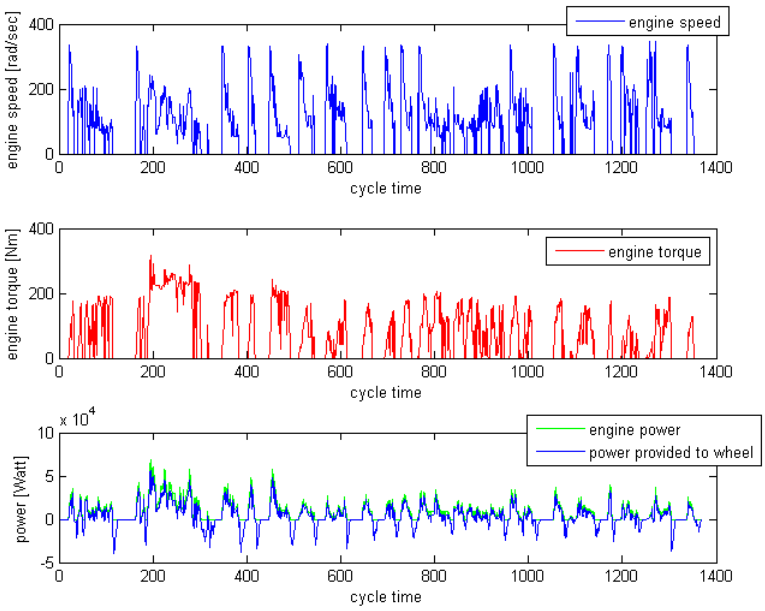


Figure 4.11: Operation of engine over the urban cycle. Engine output power versus power provided to wheel.

This is due to the losses in the hydro static transmission. Negative power required at the wheels is provided by friction braking in this configuration which results in a loss of this energy.

Since optimal engine management is not possible the engine operation point is not moved to its most efficient point. The engine operation for the urban drive cycle can be seen in Figure 4.12. The mean engine efficiency over the cycle is .13, which is low because the power provided by the engine is coupled to the power requested at the wheel. Operation can not freely be chosen.

It has been shown that a continuously variable transmission can improve fuel economy by up to 57% of the fuel consumption of a conventional drive train vehicle, but unlike in a hybrid drive train full engine management is not possible.

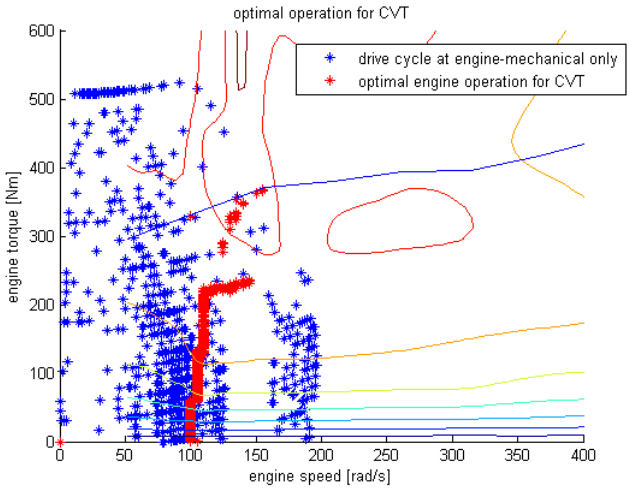


Figure 4.12: Operation of engine over the urban cycle plotted in the engine efficiency map.

### 4.2.2 Study 2: Fuel Economy in a hybridized F150

The hydro static transmission built by Folsom Technologies International has been designed such that the common high pressure and low pressure line in the transmission can be attached to a high and low pressure accumulator. Assuming that both pump/-motors have full functionality in pumping and motoring the engine operating point can be moved in speed and torque within the limits of the hydraulic components. Therefore the engine can be turned on at its optimal operating point or turned off to reduce losses. The power needed at the wheel can now be provided by the engine or the accumulator storage. Therefore

$$Power_{out} = Power_{eng} + Power_{acc} - Power_{loss} \tag{4.8}$$

holds. With ideal hydaulic components an upper bound fuel economy can be computed assuming that all negative power in the drive cycle is regenerated, stored and reused. The engine then only has to provide

$$Power_{eng} = \Sigma Power_{cycle} \tag{4.9}$$

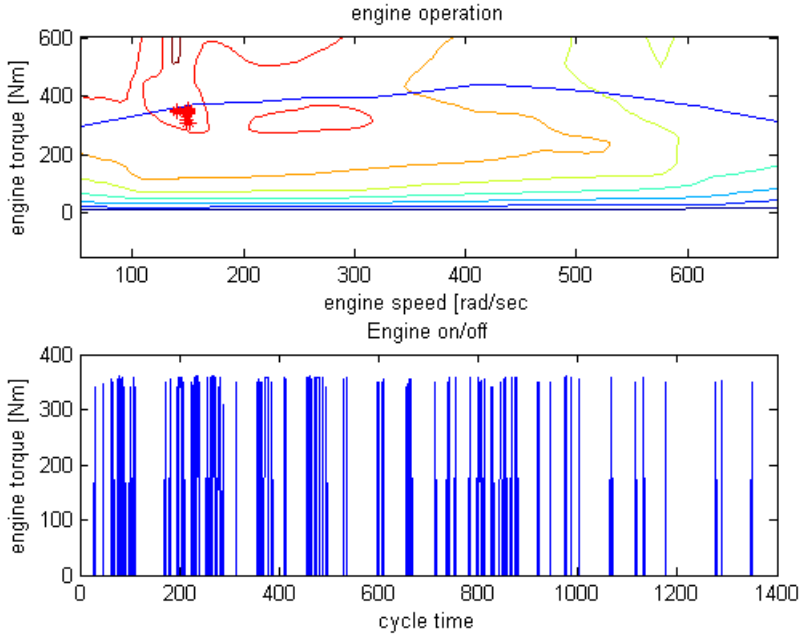


Figure 4.13: Operation of engine in hybridized F150 over urban drive cycle.

for discrete cycle time intervals. It was found that a Ford F150 vehicle in power split hybrid configuration with ideal hydraulic components can achieve 58.6mpg over the urban drive cycle and 39.3mpg in highway driving. Including pump/motor losses an approximation of the fuel consumption was calculated assuming a constant pressure of 2000psi over the drive cycle. Using Lagrange Optimization with the derived three level control strategy the fuel consumption has been evaluated for the EPA urban drive cycle and the EPA highway driving schedule.

The vehicle achieves 50.2mpg over the urban cycle and 37.8mpg over the highway drive cycle. For both cases the engine is operated close to its optimum over both cycles. Over the urban cycle an average engine efficiency of 37.8% is achieved while the engine is run at an average efficiency of 37.5% over the highway drive cycle. In Figure 4.13 the operation of the engine, and in Figure 4.14 the operation of the hydraulic pump/motors are plotted in a displacement-speed dependent efficiency map.

In the first graph it is shown that the engine operates in its most efficient region

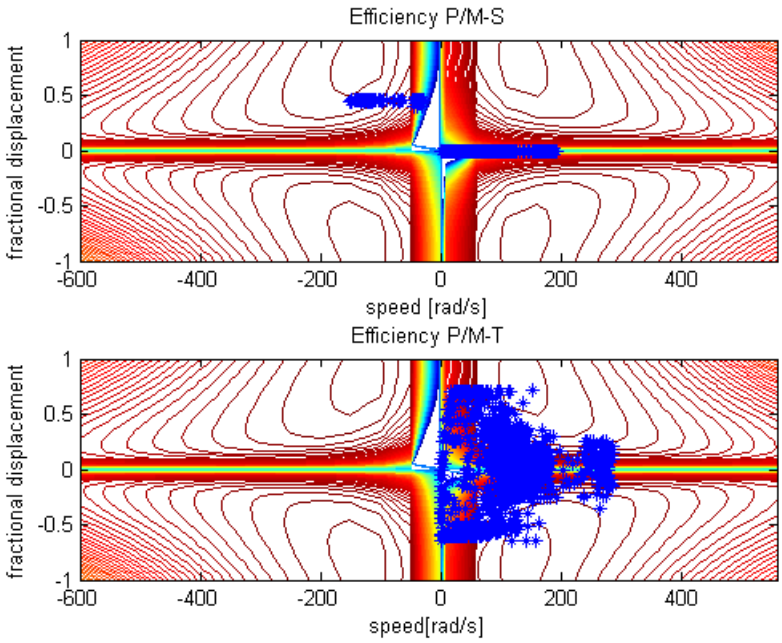


Figure 4.14: Operation of pump/motors in hybridized F150 over urban drive cycle.

only. The average engine efficiency is close to its optimum. P/M-S is coupled to the engine in torque and is therefore operating at a constant torque or off. This is shown in the first graph in Figure 4.14. The speed of the pump/motor ranges which results in a shift of the engine to its optimum. In the second graph P/M-T operation is shown. P/M-T is coupled in speed to the output and therefore operates in the possitive speed range at all times. The torque of P/M-T shifts the engine in torque to its optimum. P/M-T provides the negative torque to the wheels when needed for braking.

In the second graph in Figure 4.13 the engine torque can be seen. The engine is frequently turned on and off. To investigate why this is happening the instantaneous loss function

$$Loss_{inst} = Loss(\omega_{out}(t), T_{out}(t), \omega_{eng}(t), T_{eng}(t), P(t), Q_{acc}(t) + \lambda^* Q_{acc}(t) \qquad (4.10)$$

was plotted for the drive cycle. It is expected that the loss functions for the engine off and engine on operation in periods of frequent switching are close in value. In Figure 4.15 the loss function can be seen for a short period in the urban drive cycle. In this period the engine is switched on for one time sample and then turned off. As can be seen in the graph the losses in engine on versus engine off at frequent switching periods are similar. To prevent frequent engine switching from happening a penalty for turning the engine on and off should be added to the optimization.

In Figure 4.16 the operation of the engine over the EPA highway cycle can be seen. Similarly to what has been seen in the urban driving schedule the engine mainly operates at its most efficiency point. In the highway cycle less stop and go is performed over the drive cycle. Therefore less energy is recovered due to braking and the engine has to be turned on more often. In the second graph in Figure 4.16 it is shown that the frequency of turning the engine on and off has increased. In future more detailed simulations this can be prevented by adding a penalty for enigne on/off operation to the optimization. In Figure 4.17 the pump/motor operation over the highway drive cycle can be seen. Here P/M-S is displayed in the first graph and the operation of P/M-T is seen in the second graph.

It has been shown that hybridizing an F150 truck with a hydro static transmission can significantly increase fuel economy over the urban drive cycle as well as for highway driving. To compute more accurate approximations the pressure in the accumulator

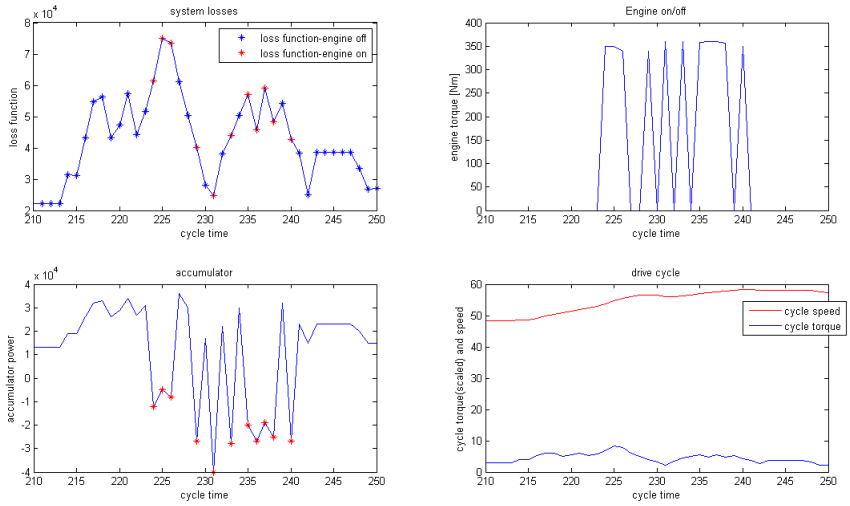


Figure 4.15: Period of optimized hybrid operation over urban drive cycle. Loss function in engine on vs engine off mode

should be varied and a penalty for turning the engine on and off should be added to the simulation.

### 4.2.3 Analysis of Pump/Motor Restrictions

The hydro static unit was designed to function as a hydro static transmission. In operation as a CVT, shifting the engine operating point on a constant power curve, the hydraulic unit S mostly operates as a pump. It is spining at negative speed and exerting positive torque onto the planetary ring gear. Pump/motor T is used as a motor, adding positive torque to the output shaft while spinning at positive speed. With this the engine is always shifted to lower torque and higher speed, which results in a more efficient operation. However in a hybrid vehicle, to be able to perform full engine management, the hydraulic units should be operable in all four quadrants, possitive and negative speed as well as possitive and negative torque. In Section 4.2.1 the fuel economy of the hybridized Generation II vehicle was analyzed. However, potential restrictions in the drive train were not considered when computing fuel economy. In this section the restrictions and their effect on the engine management and fuel consumption will

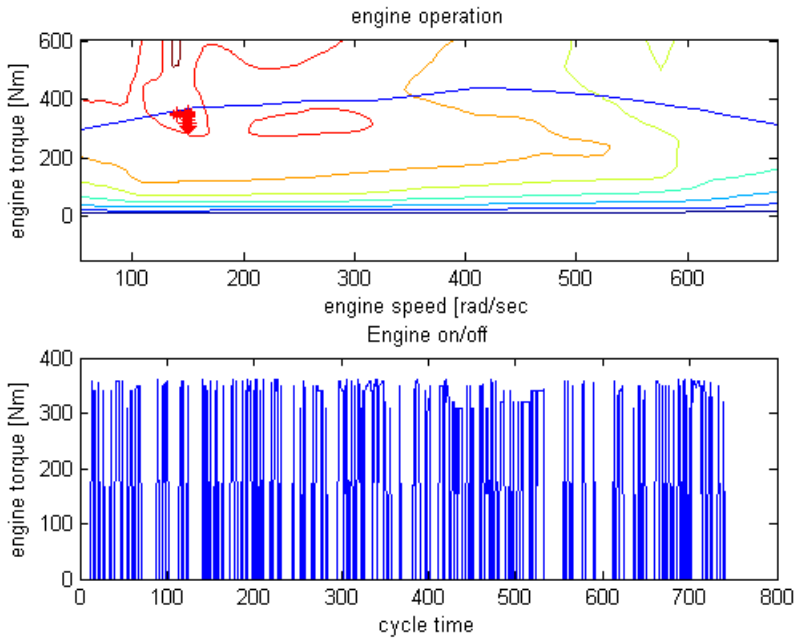


Figure 4.16: Operation of engine in hybridized F150 over highway drive cycle.

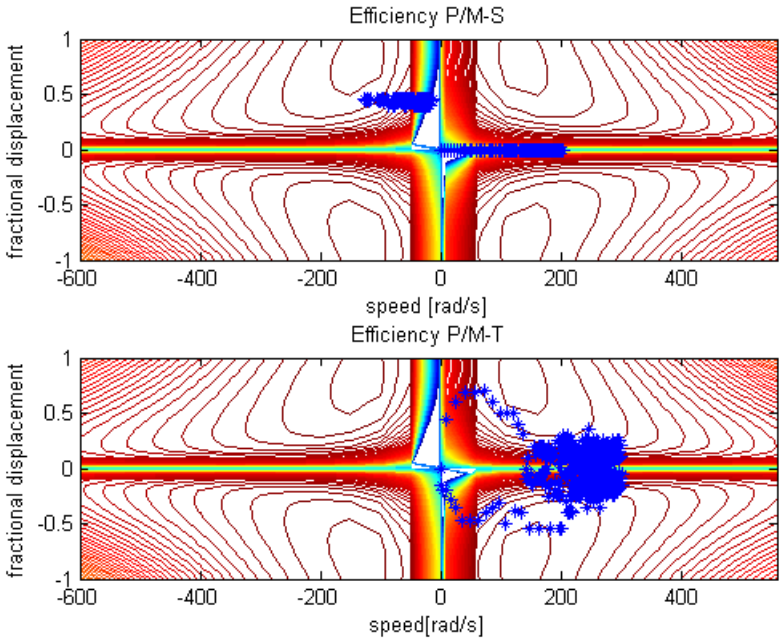


Figure 4.17: Operation of engine in hybridized F150 over highway drive cycle.

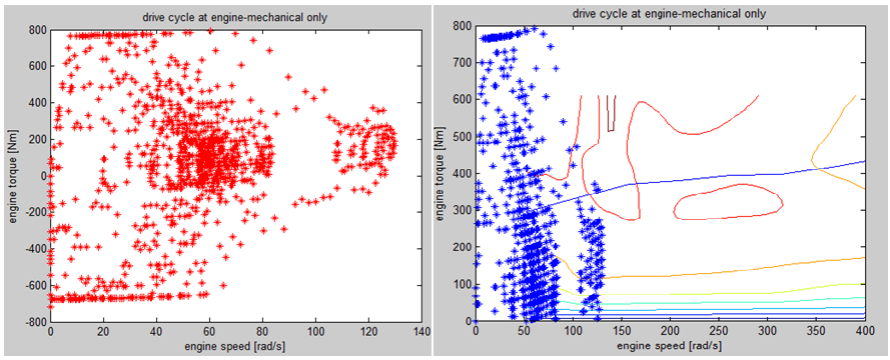


Figure 4.18: Drive cycle in mechanical only operation for Ford F150 with HSU.

be investigated.

The hydraulic pump/motor units are, as specified in Section 2.2.5, restricted in their displacement. While P/M-S can go 10% over center, P/M-T can not operate in the negative displacement range. Therefore a directional valve has been implemented. With this valve the displacement ranges can be seen in Table 2.5.

In a hybrid vehicle the engine is shifted to a more optimal operating point by using the torque from P/M-T to shift the engine operating point in torque and by using the speed of P/M-S to shift the engine operating point in speed. In Section 2.2.5 a four quadrant chart was plotted showing the restricted areas in the Ford Folsom configuration. To understand the meaning of this chart the engine operation in mechanical only mode over the EPA urban drive cycle was plotted in Figure 4.18. Mechanical only operation implies that no torque is added to the output by P/M-T and P/M-S operates at zero speed. In the graph it is seen that all drive cycle operating points are mapped to the low speed region, at speed lower than 130 rad/sec while the torque ranges up to 800Nm.

The most efficient operating point of this engine is at 350Nm while spinning at 150rad/sec. To shift the drive cycle operating points into the more efficient region speed has to be added by P/M-S. Since the torque in P/M-S is coupled to the engine, it will always operate at positive torque. Therefore, to shift the drive cycle operating points to the engine optimal, P/M-S is pumping at positive torque and negative speed. Shifting points of high torque to the engine optimal requests P/M-T to be motoring

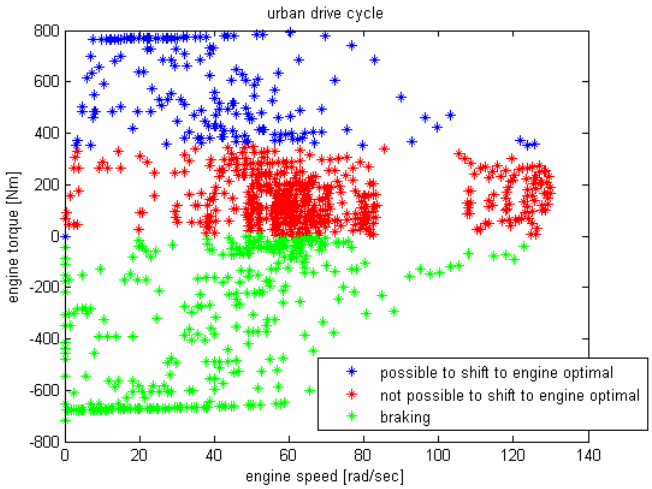


Figure 4.19: Drive cycle points that are able to be shifted to engine optimal.

at positive torque and positive speed. To shift low torque points P/M-T has to be pumping at negative torque. Negative torque from P/M-T can only be achieved if the directional valve is flipped into position 2, which then results in P/M-S being limited to 10% positive displacement. To understand the effect of this limitation the urban drive cycle is plotted in color in Figure 4.19. Operating points in blue can be shifted to the engine optimal. Points represented in green are points where negative torque is required at the wheel. Therefore the vehicle is braking and all the power is regenerated using P/M-T only. Points plotted in red are points that can not be shifted to the engine optimal operating points.

It is shown that if the engine optimal point is at 350Nm all drive cycle points resulting in mechanical only points lower than 350Nm can not be shifted to a 350Nm torque level in the engine operation. This graph is computed assuming a 2000psi pressure difference between the high and low pressure accumulator. But it has been observed that changing the pressure does not effect the patter of Figure 4.19. An engine torque of 350Nm can simply not be transmitted unless the pressure difference is increased to 9800psi, which is practically not feasable. Although the engine can not be shifted to its optimal, increasing the pressure does increase the maximum power possible to be transmitted from the engine. In Table 2.6 upper bound values for engine torque for

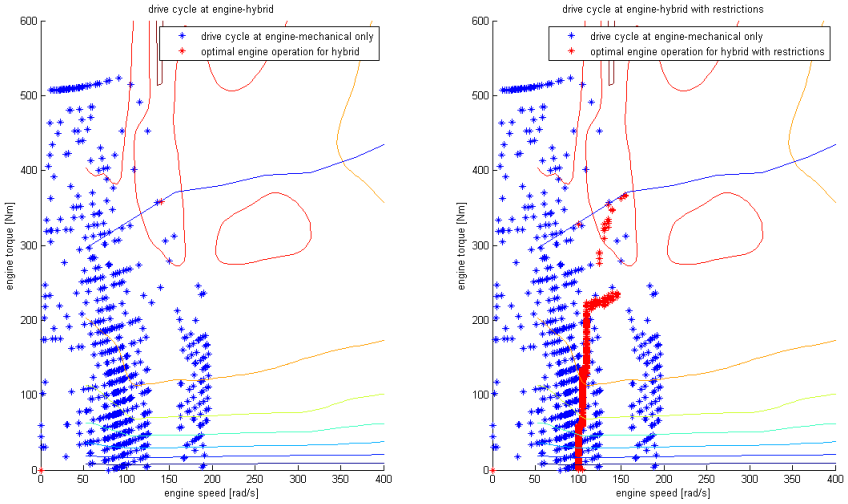


Figure 4.20: Urban drive cycle operating points optimaly shifted hybrid vs hybrid with restrictions.

varying pressures can be found.

Assuming optimal engine management and ideal pump/motor efficiencies the optimal operating point possible for each point in the drive cycle can be plotted. In Figure 4.20 the optimal engine operations can be found for a non-restricted power split hybrid vehicle versus a drive train with restrictions. In a hybrid drive train without restrictions it is possible at any time where possitive power is provided to the wheel to operate the engine at its most efficient point. The average engine efficiency is therefore at 38%. This can be observed in the left graph. Whereas in the right graph we can see the optimal operation of the engine in a hybrid architecture with the displacement restrictions in the hydro static transmission unit. Many engine operating points can not be shifted to its optimal. Therefore the average engine efficiency over the drive cycle drops to 32%.

As shown restrictions in hydraulic units effect the engine management and therefore have to be taken into consideration when developing real time control for the vehicle. It is expected that restrictions in the pump/motor displacement have an impact on fuel economy. To understand the penalty in fuel economy due to such a restrictions preliminary fuel economy values were computed for the Generation II drive train. The

| fuel economy[mpg] | | city | hway |
|---|---|---|---|
| F150 conventional (baseline) | | 17.9 | 26 |
| upper bound(includes only engine loss) | | | |
| | HSU | 30.1 | 31 |
| | HSU with accumulator | 58.6 | 39.3 |
| using tranmission model | | | |
| | HSU* | 28.2 | 28.3 |
| | HSU with accumulator | 50.2 | 37.8 |
| | HSU with accumulator w restrictions+ | 49.8 | 34.8 |

Figure 4.21: Fuel economy values for F150 Generation II vehicle.

values can be seen in Figure 4.21 and are calculated using the proposed three level controls startegy with a Lagrange optimization strategy. First upper bound values were computed for the case of a hydro static transmission as well as for the hybridized case. Then the pump/motor model was used to include engine and hydraulic unit losses in the simulation. It can be seen that over the urban drive cycle the fuel economy for a hybridized vehicle increases from 28.2mpg to 50.2mpg. For highway driving an increase in fuel economy of 32% is expected. In the last column results for the hybridized vehicle with restrictions can be seen.

Unexpectedly, the values for the restricted hybrid do not differ much from the performance of a hybrid with full engine management. For the EPA urban cycle almost no change in fuel consumption is seen and only a 3mpg drop in fuel consumption is observed for the highway driving schedule. Investigating the reasons for these results it was found that the nature of the optimization reduces the impact of the restrictions of the hydro static transmission. With the knowledge of the entire drive cycle operation in advance the optimization chooses the engine to be turned off at those operating points where the drive train can not shift the engine to its most efficient point. Therefore the impact of the restrictions is not represented in these fuel consumption values. In real-time implementation of an engine management strategy on the vehicle this would not be the case. Using the knowledge gained from this analysis the restrictions should be investigated in more depth with respect to real time controls to fully understand its impact on fuel consumption.

## 4.3 Conclusion

It has been shown that a three level controls strategy can be used in off-line simulation in a simple way to perform studies to understand and analyze hybrid drive train architectures. The Generation I vehicle was used as an example to show that fuel economy in a power split configuration can be improved by optimaly sizing the drive train to its performance specifications. Gained knowledge about the hybrid architecture can be used to define control laws. It has been shown that the operation of the drive train is critical to improve fuel economy. Using the power split architecture in modal operation can achieve maximum system efficiency. For any hybrid architecture fuel consumption is dependent on hydraulic pump/motor efficiency. With this it has been found that the power split hybrid configuration performs as good or better as the series and parallel hybrid drive train for all ranges of hydraulic component efficiency. Therefore while power split configurations involve more complex real-time control for optimal operation, this drive train has the highest potential in improving fuel consumption.

Using the Generation II vehicle it has been shown that using a hydro static transmission can decrease fuel consumption in comparison to the use of a conventional vehicle. Hybridizing the vehicle by adding an energy storage component to it can improve fuel economy further. An analysis of pump/motor restrictions in the hydro static transmission have been shown to restrict the engine management, though no significant effects on the amount of fuel consumed over a drive cycle has been seen in off-line optimization. Due to its effect on the controls of the hybrid vehicle it is expected that fuel economy declines. To fully understand the impact of restrictions in the hydraulic units on fuel economy further studies are needed to investigate real-time implementable algorithms.

# Chapter 5

# Real Time Implementation

Hybrid vehicles are used to reduce fuel consumption and CO2 emissions in passenger vehicles. The fuel used is reduced by operating the engine in a more efficient region, by capturing energy using regenerative braking and by turning the engine off. In comparison to a conventional vehicle, where the input from the driver is transferred to the engine as a power demand, the drive train operation in a hybrid vehicle is more flexible. To optimally operate the drive train and to specify the inputs to various power sources, a controls unit is needed. Using the proposed three level control strategy in a user interface, controls has been implemented in real time and tested on the Generation I vehicle at the University of Minnesota. In this chapter the control algorithms will be discussed. In the first section each level of the hierarchical controls strategy will be shown. A major part of real time implementation is the design of feedback controllers. Therefore the emphasis of this chapter will be on control design in the low level. In the second part the user interface that enables the driver to operate the vehicle similarly as a conventional passenger vehicle, accelerating with the *gas* pedal and slowing the vehicle down by applying the brake, will be discussed.

## 5.1 Controls

Using the proposed controls strategy the implementation of control algorithms is seperated into three parts. This simplifies this often complex process. Each level in this hierarchical structure uses the vehicle speed, torque requirement at the wheel and the

state of charge in the energy storage as inputs. The vehicle speed is retrieved from encoders attached to each wheel axle of the differentials in the rear of the vehicle. Pressure sensors at the low and high pressure accumulators are used to calculate the pressure difference, which represents the state of charge in a hydraulic hybrid vehicle. The torque required at the wheels is specified by the driver and is defined by the position of the accelerator pedal. Therefore all three values are assumed to be known in the following sections. In Section 2.3 a tranformation has been shown that seperates the internal and external coordinates. In the development of control algorithms for the Generation I vehicle this tranformation will be used. The external coordinate, $T_{ext}$, will be used to satisfy the driver request while the internal coordinate, $\omega_{int}$ can be used to optimize the drive train operation. All inertia values for the Generation I vehicle have been derived in [34]. It has been shown that the following approximations can be assumed.

$$T_{ext} = -R_S T_S \tag{5.1}$$

$$\omega_{int} = \omega_c \tag{5.2}$$

For controls purposes it can be assumed that the internal speed is represented by the speed of the mechanical carrier, while the external torque can be specified by the torque exerted from P/M-S. In the following this relationship will be used in the development of the three level controls strategy.

### 5.1.1 High Level Control

In the highest level of controls an energy management strategy is designed. Some algorithms developed in this area have been shown in Section 3.2. In this first implementation of this strategy a simple rule based high level algorithm has been implemented. Using the state of charge in the energy storage as the only input the controls algorithm operates in two modes, engine on and engine off. The engine is turned on when the pressure difference between the high and low pressure accumulator drops below a lower bound. Then, while the engine is running, P/M-T is operated as a pump and thereby charges the accumulator. The engine is turned off once the upper treshold in pressure is reached. This strategy is often referred to as engine on/off strategy.

In the CCEFP, project 1A.1 is working on an energy management strategy which uses stochastic dynamic programming to determine the optimal operation of the power

split vehicle. This strategy is developed such that it can be used in real time. It only uses past knowledge of the vehicle operation and a probability distribution of likely future vehicle operations. In future work this high level startegy will be implemented on the Test Bed 3 vehicle to measure the improvement in fuel economy of the use of such an optimal algorithm.

### 5.1.2 Mid Level Control

The mid level control determines the drive train operation that accumulates the least losses in the system. For a given wheel speed, wheel torque and a, by the high level specified, accumulator power the operation of each component is specified such that the losses in the overall system are minimized. A look up table, representing this level, can be created off-line as shown in Section 3.3. Due to restrictions of the CPU in the vehicle a look up table as used in simulation was found to not be suitable for real time implementation on this vehicle. To reduce storage size of the mid-level control, it was simplified for implementation purposes.

From simulation results it has been seen that the engine is mostly operated at its *sweet spot*, at constant speed and torque, when turned on. A simple mid level control strategy therefore specifies the optimal engine operating point in engine on mode. The engine is then operated at 2500rpm. To achieve a constant load on the engine P/M-T is operated in pumping mode. The displacement of P/M-T is changed such that the engine torque in Equation 2.10 stays constant for varying torques of P/M-S.

In engine off mode, the hydraulic pump/motor at the carrier shaft provides the requested torque and can only be varied in speed. From optimization results it has been seen that the speed of P/M-T changes in the range of 70rad/sec to 180rad/sec. For an interval in the urban drive cycle where the engine is mostly turned off P/M-T speed can be seen in Figure 5.1. The graph shows P/M-T speed in the first plot, the wheel speed in the second plot and P/M-S speed in the third plot. As seen P/M-S and P/M-T are coupled by Equation 2.2 such that the wheelspeed specified by the drive cycle is achieved. To achieve maximum efficiency the speeds of P/M-T and P/M-S are varied.

In Figure 5.2 an operation of P/M-T at constant speed is assumed. In this graph P/M-T speed can be found in the first plot, P/M-S speed is seen in the second plot,

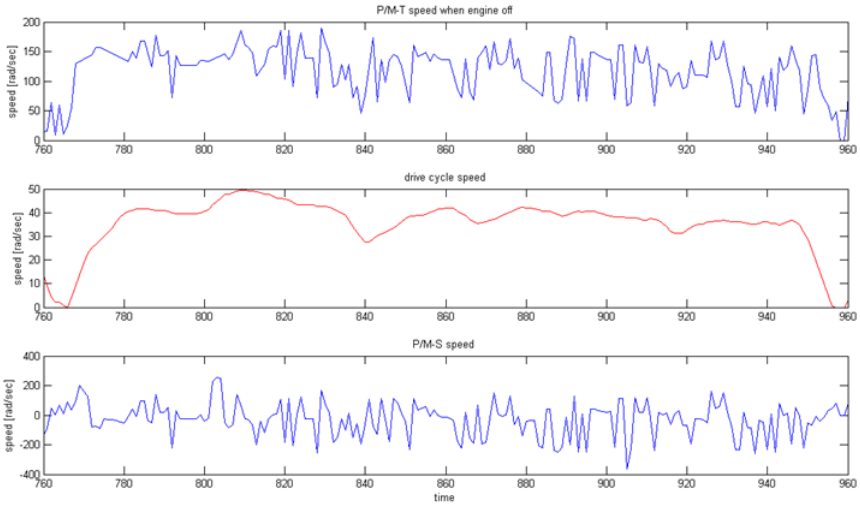


Figure 5.1: Operation of P/M-T in engine off mode

accumulator flow is shown in the third plot and overall system losses are shown in the last plot. In blue the optimized component operation can be seen, while in red we can see the operation of P/M-T and P/M-S while the speed of P/M-T is kept constant. To compute these values an ideal pump/model is assumed to achieve the same accumulator flow before and after the speed adjustment.

It was found that when operating P/M-T at constant speed and therefore only varying P/M-S speed the losses in the overall system do not change significantly. The losses in the hydraulic units using constant P/M-T speed versus changing P/M-T speed is an order in magnitude smaller than the value of the losses. With respect to the losses in the internal combustion engine the losses occuring in the hydraulic units are smaller by one order of magnitude. Therefore the impact of a speed change in the pump motors does not have a significant impact on overall fuel economy. In simulation a drop in fuel economy from 59.8mpg to 59.3mpg was seen using the two gear resized power split configuration without modal operation over the urban drive cycle. This is a decrease in fuel economy of about 1%.

With these findings a first approach taken in real time implementation of this control strategy specifies a constant operating point in engine on mode and a constant carrier

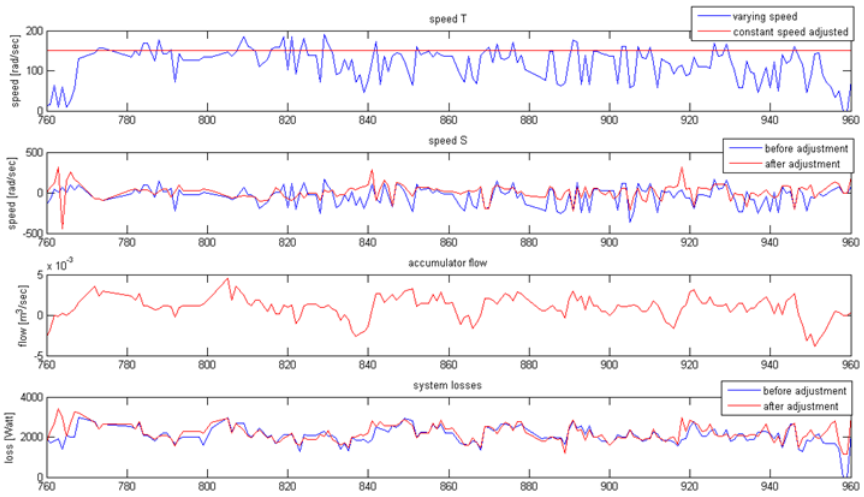


Figure 5.2: Operation of P/M-T in engine off mode. Varying P/M-T speed versus constant P/M-T speed

speed in engine off mode in the mid level control.

### 5.1.3 Low Level Control

A low level control layer is an important part of real time implementation of this proposed strategy. This level ensures that components are operating at the specified speed and torque. To design feedback controllers the approach described by Sim in [34] was used. Following this design, tracking controllers were designed in two modes. In mode 1, referred to as engine mode, the clutch on the engine shaft is engaged and torque from the engine is transmitted to the drive train. In mode 2, called hydraulic mode, the clutch is disengaged, the engine is turned off, and all power to the carrier shaft is provided by P/M-T. Using Sims initial design but improving the feedback controller performances, algorithms were designed in each mode. Engine Mode control and Hydraulic Mode control will be described in the following sections. Then a switching logic to enable bumpless transfer between the two modes will be described.

**Engine Mode**

Operating the drive train most efficiently it has been seen from simulation that the engine is operated at its most efficient region only. An engine controller should therefore be designed to force engine operation to its *sweet spot*. In the Generation I vehicle a Perkings Diesel Engine with mechanical governor system is used. The mechanical feedback control of the governor should have simplified the regulation of the engine speed. But as shown in [34] the performance of the mechanical governor is not sufficient to regulate the engine at a constant speed. Therefore a proportional-intergral controller was designed. The controller can be described by the following transfer function

$$G_C = \frac{Kps + Ki}{s} \tag{5.3}$$

where

$$Kp = 7.180757 \times 10^{-4} \tag{5.4}$$

$$Ki = 1.436151 \times 10^{-2} \tag{5.5}$$

This control algorithm together with a reference feedforward term was found to be suitable for engine tracking. The performance of the controller can be seen in Figure 5.3.

The engine speed can be seen in the first plot. As shown the engine tracks very well following a constant reference of first 180rad/sec and later 200rad/sec. With a step input the rise time is 3sec which is sufficient for the application in a hybrid vehicle. Seen in the second graph, at time $t = 210sec$ a displacement is applied on P/M-T to simulate a disturbance on the engine control. As shown disturbance is rejected and the engine speed remains constant. In the third graph the pressure difference between the high and low pressure accumulator can be seen. Due to pumping by P/M-T the energy storage is charged.

To operate the engine at a constant load a torque is applied by P/M-T. For a known torque on the differential the engine torque in Equation 2.10 can be balanced to a constant value. With the developed algorithms the combustion engine is operated at its most efficient region when the drive train is operating in engine mode.

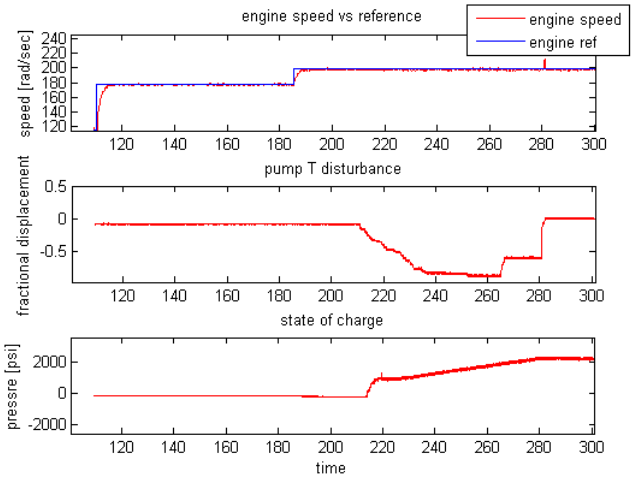


Figure 5.3: Performance of Engine Feedback Control with Disturbance

### Hydraulic Mode

In hydraulic mode the engine is declutched and P/M-T is providing the necessary torque to the carrier shaft. This reduces the freedom of control in the drive train by one degree. Using Equation 2.3 it can be seen that with the specification of the drive torque at the wheels the torque requirements of P/M-S and P/M-T are fixed. Only the speed of the two pump/motors can be varied. A feedback controller is needed to gain control over the speed profile of P/M-T. The previously implemented algorithm consisted of a proportional integral control with integral windup and a reference feed forward term. It has been found that for the purpose of implementation of this control structure the control performance of such a controller was not sufficient. Tracking was not guaranteed for various vehicle operations. The system was therefore re-identified. An observer estimating the states of the system was designed and implemented in a state feedback loop.

To identify the dynamic response of the carrier shaft to a torque input of P/M-T a closed loop system identification approach is used. A block diagram of the set up can be seen in Figure 5.4.

Given the torque input the displacement can be found using an inversion of the pump

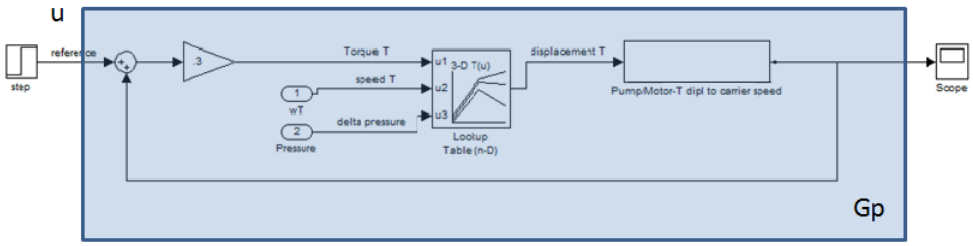


Figure 5.4: Schematic of System Identification Approach

model ([21]) described in Section 2.5.2, where $x_T$ is a function of $T_T$, $\omega_T$, and pressure. A proportional gain of 0.3 was used in the feedback loop. Applying step inputs to the proportional feedback loop the response of the system was found. Assuming as second order system the least squares estimation method was used to identify the transfer function. The closed loop transfer function of the system was found to be

$$G_p = \frac{54.43}{s^2 + 5.022s + 50.44} \tag{5.6}$$

The performance of the model versus the experimental response can be seen in Figure 5.5 where two step input responses are shown. Here the step inputs are normalized and therefore shifted to zero speed. To avoid having static friction affect the identification the step inputs were applied to the pump/motor while it was already in motion.

It is shown that the transfer function approximates the response of the plant well. A small delay can be seen in the plant, which might be due to swashplate dynamics. While the experimental data shows some oscillation in steady state the model does not imitate this behavior. It is assumed that the oscillation is due to noise and can therefore be omitted in the model. To simplify the design the controller was developed such that it can be wrapped around the identified closed loop system.

Using the identified plant model an observer is designed in state space form using a Kalman estimator. The second order single input single output system can be represented using two states by

$$\dot{x} = Ax + B(u + x_d) \tag{5.7}$$

$$y = Cx \tag{5.8}$$

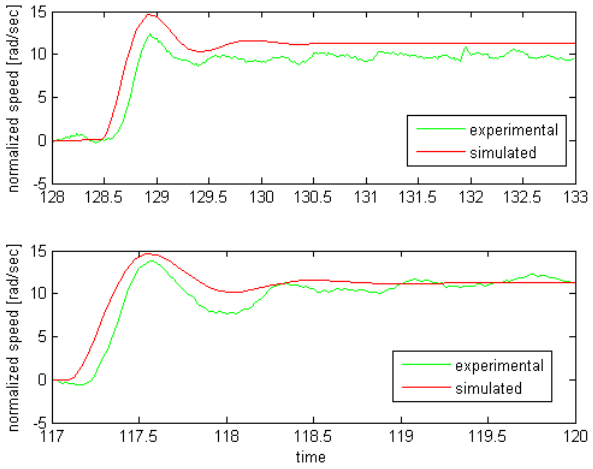


Figure 5.5: Identified P/M-T Tranfer Function validated

with

$$A = \begin{bmatrix} -5.0220 & -50.4300 \\ 1 & 0 \end{bmatrix}$$

$$B = \begin{bmatrix} 1 \\ 0 \end{bmatrix}$$

$$C = \begin{bmatrix} 0 & 54.43 \end{bmatrix}$$

To improve disturbance rejection a disturbance state was added to the observer to estimate a constant disturbance. Applying the internal model prinicple the disturbance can be modeled in state space as

$$\dot{x_d} = 0 \tag{5.9}$$

Assuming the disturbance enters the system prior to the plant with the input $u$, the resulting augmented controller can be represented in state space form by:

$$\begin{bmatrix} \dot{x} \\ \dot{x_d} \end{bmatrix} = A^* \begin{bmatrix} x \\ x_d \end{bmatrix} + B^* u \tag{5.10}$$

$$y = C^* \begin{bmatrix} x \\ x_d \end{bmatrix} \tag{5.11}$$

where

$$A^* = \begin{bmatrix} -5.0220 & -50.4300 & 1 \\ 1 & 0 & 0 \\ 0 & 0 & 0 \end{bmatrix}$$

$$B^* = \begin{bmatrix} 1 \\ 0 \\ 0 \end{bmatrix}$$

$$C^* = \begin{bmatrix} 0 & 54.43 & 0 \end{bmatrix}$$

Using this model and the measured speed of P/M-T to estimate the three states of the system a Kalman linear optimal filter was designed. Assuming the process noise and the white noise are normally distributed with 0 mean and covariance Q and R respectively the Matlab command *lqr* was used to find the observer gain that minimizes the estimation error between the estimated state $\hat{x}$ and the actual state $x$. The values of Q and R where found by experiment to be

$$Q = \begin{bmatrix} 5 & 0 & 0 \\ 0 & 1 & 0 \\ 0 & 0 & 70 \end{bmatrix}, R = 0.3$$

With a resulting observer gain of

$$L = \begin{bmatrix} 2.47 \\ 1.85 \\ 15.28 \end{bmatrix}$$

the observer can then be written in state space form:

$$\begin{bmatrix} \dot{x} \\ \dot{x_d} \end{bmatrix} = A_{obs} \begin{bmatrix} x \\ x_d \end{bmatrix} + B_{obs} \begin{bmatrix} u \\ y \end{bmatrix} \tag{5.12}$$

$$y = C_{obs} \begin{bmatrix} x \\ x_d \end{bmatrix} \tag{5.13}$$

where

$$A_{obs} = \begin{bmatrix} -5.02 & -184.72 & 1 \\ 1 & -100.72 & 0 \\ 0 & -831.43 & 0 \end{bmatrix}$$

$$B_{obs} = \begin{bmatrix} 1 & 2.47 \\ 0 & 1.85 \\ 0 & 15.28 \end{bmatrix}$$

$$C_{obs} = \begin{bmatrix} 1 & 0 & 0 \\ 0 & 1 & 0 \\ 0 & 0 & 1 \end{bmatrix}$$

with $x_1$ and $x_2$ being the two states of the plant and $x_d$ representing the disturbance. The input to the observer consists of the input to the plant, here the P/M-T torque specification, and the output of the plant, here the speed of P/M-T.

In the design of the state feedback control a least squares regulator approach was chosen to place the poles of the system. The least squares regulator strategy aims to drive the initial state of the system to the smallest possible value with the least effort in controls. This is achieved by minimizing the following cost function:

$$J = \int_{t_o}^{t_f} x^T Q^* x + u^T R^* u \, dt \tag{5.14}$$

For $t_f \to \infty$ the optimal solution can be found by solving the Continous Time Dynamic Riccati Equation (CTDRE) ([35]) and can be used in a feedback control law. Tests have shown that values for optimal control performance are

$$Q^* = \begin{bmatrix} 0 & 0 \\ 0 & 10 \end{bmatrix}, R^* = 1.$$

The resulting feedback gain can be computed using the matlab command *lqr*:

$$K = \begin{bmatrix} 0.0197 \\ 0.0990 \end{bmatrix}$$

The input to the system is then defined by

$$u = -Kx \tag{5.15}$$

With the designed observer state feedback the closed loop system results in

$$\dot{x} = A_{cl}x + B_{cl}(u) \tag{5.16}$$

$$y = C_{cl}x \tag{5.17}$$

where

$$A_{cl} = \begin{bmatrix} -5.022 & -50.44 & 0 & .00203 & .0001983 \\ 1 & 0 & 0 & 0 & 0 \\ 0 & 0 & -5.022 & -411 & 1 \\ 0 & 0 & 1 & -174.2 & 0 \\ 1 & 0 & 0 & -2108 & 0 \end{bmatrix}$$

$$B_{cl} = \begin{bmatrix} 1 \\ 0 \\ 0 \\ 0 \\ 0 \end{bmatrix}$$

$$C_{cl} = \begin{bmatrix} 0 & 54.43 & 0 & 0 & 0 \end{bmatrix}$$

with closed loop poles at

$$Poles = \begin{bmatrix} -2.51 + .0664i \\ -2.51 - .0664i \\ -171.81 \\ -4.92 \\ -2.49 \end{bmatrix} rad/sec$$

The vector $x$ here consists of 5 states, two states of the plant, two observer states and a disturbance state approximated using the observer.

Since the LQR regulates the system to zero speed the reference input has to be introduced into the system for it to track a desired reference speed. Three methods to do so are described in [36] in Chapter 7. The autonomous estimator approach was chosen, such that the state estimator equation is independent of the reference. The reference can then be introduced into the control loop by multiplying it with a proportional gain, here referred to as $\bar{N}$. Knowing the state feedback gain $K$, $\bar{N}$ can be computed by

$$\bar{N} = N_u + KN_x \tag{5.18}$$

where $N_u$ and $N_x$ can be calculated by

$$\begin{bmatrix} N_x \\ N_u \end{bmatrix} = \begin{bmatrix} \mathbf{A} & \mathbf{B} \\ \mathbf{C} & D \end{bmatrix}^{-1} \begin{bmatrix} \mathbf{0} \\ 1 \end{bmatrix}$$

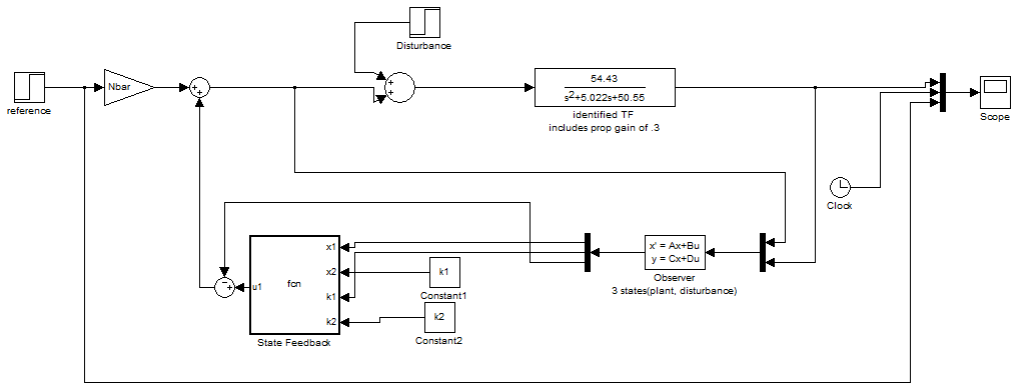


Figure 5.6: Block Diagram Schematic of Observer State Feedback Controller

In Figure 5.6 a block diagram schematic of the controller can be seen.

The performance of the developed observer state feedback control algorithm can be seen in Figure 5.7. In the first graph the pump/motor speed with the reference speed is shown. In the second graph the input to the pump/motor, which is computed with the pump model as a function of torque, speed and pressure, can be seen. With decreasing pressure, shown in the third graph, the displacement is increased for a constant desired torque. It is shown that tracking is achieved with the designed algorithm. The steady state value is reached within 1sec of applying a step input.

From Figure 5.7 it seems that the performance of the controller is sufficient for constant speed control. However testing the controller on disturbance rejection it is found that the tracking in presence of disturbances from P/M-S is not satisfactory. Since the displacement input of P/M-S is known, the pump model shown in Section 2.5.2 can be used to approximate the torque, generated by P/M-S, onto the mechanical shaft. Integrating a feed forward control of P/M-S torque into the hydraulic mode control loop a constant feed forward gain was found to give sufficient performance. In Figure 5.8 the results of this addition to the control system can be observed. In the left column the response of the system without feed forward gain can be seen. The first row of graphs displayes the speed of the carrier, the second row shows the pump/motor

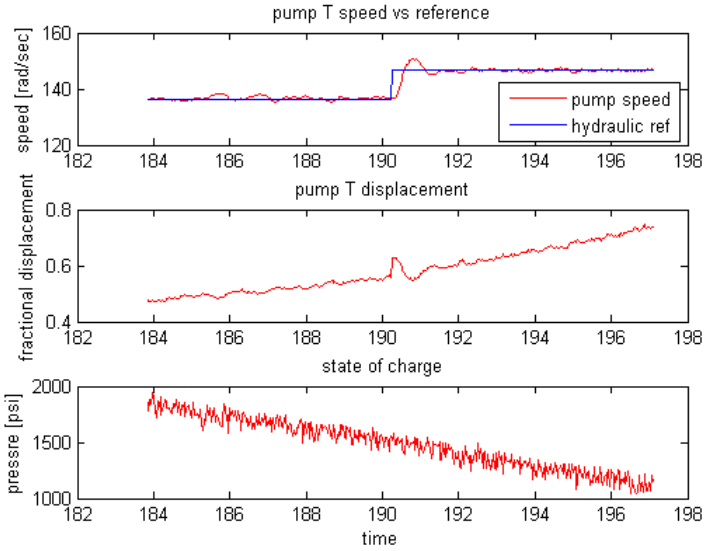


Figure 5.7: Performance of Observer State Feedback Controller

displacements of P/M-T in red and P/M-S in blue. The last row of graphs shows the pressure difference between the high and low pressure lines. In the top left graph it can be seen that without a feedforward term the speed changes when a disturbance is applied. In the top right graph it can be seen that this speed change is minimal for a system with feed forward control.

After implementation of the observer state feedback control the closed loop system was re-identified using step changes of the reference. The transfer function modeling the system was found to be

$$G_{closed} = \frac{34.84}{s^2 + 4.717s + 34.27} \tag{5.19}$$

The simulated system versus the experimental dynamic response can be seen in Figure 5.9.

An inverse of the transfer function together with a filter of degree two was used to design a reference feed forward. The performance of the control system with and without reference feed forward can be seen in Figure 5.10. In this plot the left graphs show operation of the system without reference feed forward and in the right graphs the

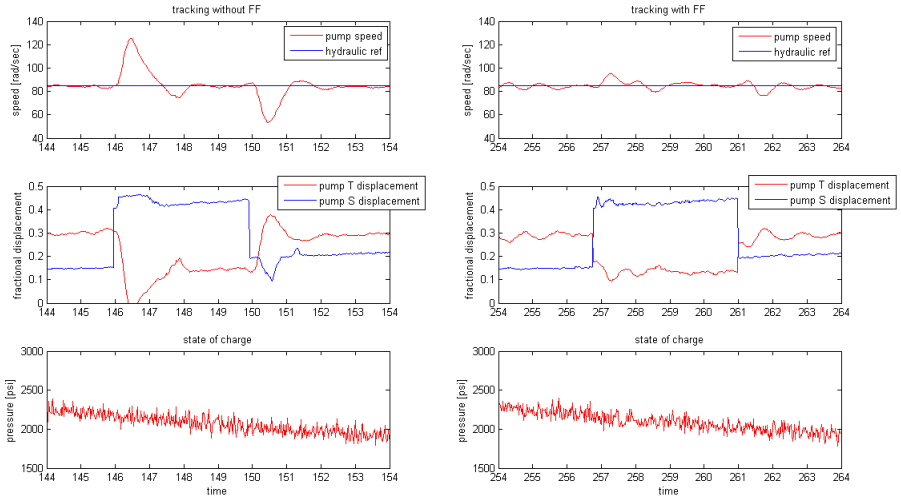


Figure 5.8: Response of plant without FF versus with FF

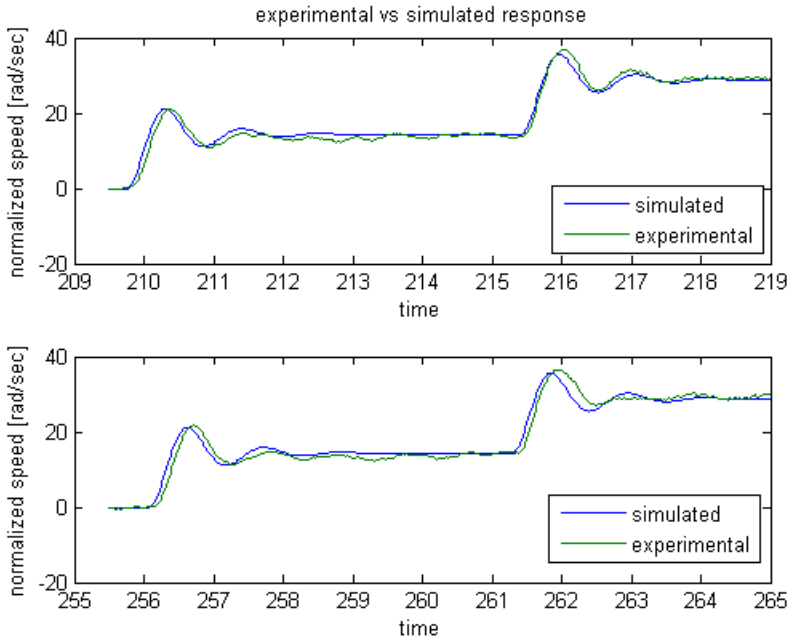


Figure 5.9: Simulated versus experimental closed loop control system response

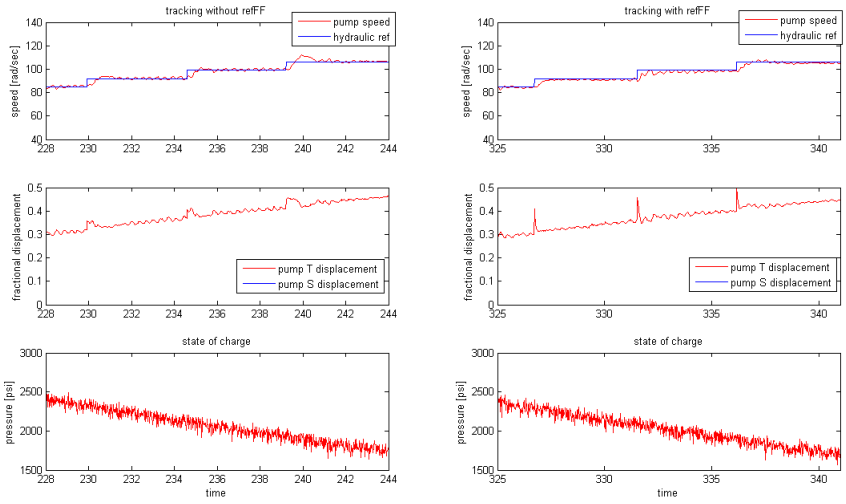


Figure 5.10: Response of plant without reference FF versus with reference FF

reference feed forward was implemented in the control system. The speed of P/M-T is shown in the first row, pump/motor displacement can be seen in the second row and the state of charge in the accumulator is shown in the third row of graphs. It is shown that in the system with reference feed forward overshoot and rise time is reduced.

As shown a controller has been designed for hydraulic mode tracking. It has been shown that satisfying performance in tracking a desired carrier speed is achieved as well as disturbance rejection of an input torque from P/M-S.

### Mode Switching

A 2 mode operation of the drive train has been implemented. To switch between engine mode and hydraulic mode a transfer logic is needed. For better feel for the driver when operating the vehicle and efficient drive train operation a smooth switching between the two modes is desirable.

When operating in hydraulic mode the engine is declutched and at idle. In order to reduce strain on the drive shaft and the clutch the engine and carrier shaft should be at similar speeds before engaging the clutch. To achieve this the engine control is enabled first, while P/M-T is still in control of the carrier speed. Once the engine and carrier

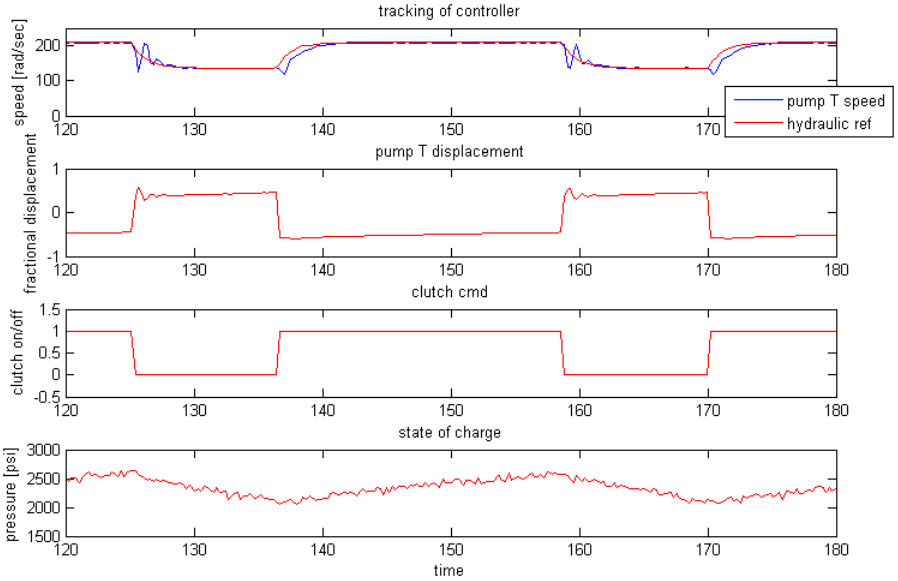


Figure 5.11: Performance of Switching Logic between Engine and Hydraulic Mode

shaft speeds are similar the clutch is engaged and the speed of the shaft is controlled by the engine. During engine mode the hydraulic mode control is disabled while P/M-T applies negative torque to the carrier shaft in order to charge the accumulator. The values in the hydraulic control loop are kept such that when the upper state of charge limit is reached tranfer to hydraulic mode control can be performed with a limited bump.

In Figure 5.11 the carrier speed together with the reference can be seen in the first graph. In engine mode the reference speed is set to 2000rpm, while the carrier speed in hydraulic mode is set to 1300rpm. To enable smooth switching between the two reference speeds a filter that slowly changes the reference speed once the mode is switched, was implemented. In the second graph the displacement of P/M-T can be seen. While the system operates in engine mode the hydraulic unit is pumping. The pressure, shown in the last plot, is then increased. The third graph shows the signal to the clutch. It can be seen that the clutch is engaged in enging mode and disengaged in hydraulic mode. It was found that switching from hydraulic mode to engine mode

there was no significant bump. When switching from engine mode to hydraulic mode oscillation in the speed of the carrier shaft was found. This could be due to the change in inertia when declutching the engine. To further improve the bumpless transfer from engine to hydraulic mode a ramping of the clutch should be considered. Both switching logics have sufficient performance to operate the hydraulic hybrid vehicle in modes. The switching logic has successfully been implemented in the Test Bed 3 vehicle at the University of Minnesota. During mode switch no noticable change in wheel speed was observed.

## 5.2 Driver Interface

In conventional vehicles the driver specifies the speed of the vehicle with the gas and brake pedal. With only one power source available the inputs from the driver go directly to the internal combustion engine in case of acceleration and to the friction brakes in case of deceleration. In a power split hybrid vehicle multiple power sources are available and can transmit power to the wheel. To enable the driver to operate the vehicle as a conventional vehicle a control unit is needed. Such a unit uses the desired torque specified by accelerator and brake pedal as an input and then specifies commands to the vehicle such that the drivers requests are satisfied.

The nature of the drive train of the Generation I vehicle is such that the torque to the wheel can be specified by the torque provided by P/M-S. This approximation has been shown in [34]. In the design of a user interface the relationship

$$T_{ext} = -u_S \tag{5.20}$$

will be used. The control unit uses the pedal command, which is a voltage signal, to specify the desired torque output of P/M-S. The displacement input to P/M-S is then found using the inverse Grandal pump model described in Section 2.5.2, where the displacement commanded is a function of the desired output torque, the pump/motor speed and the pressure difference between the hydraulic lines.

With this approach a driver interface was implemented that can be used to operate the vehicle in forward and reverse. Once switched into reverse gear the sign of the torque output of P/M-S is changed to transmit negative torque to the wheels. Using

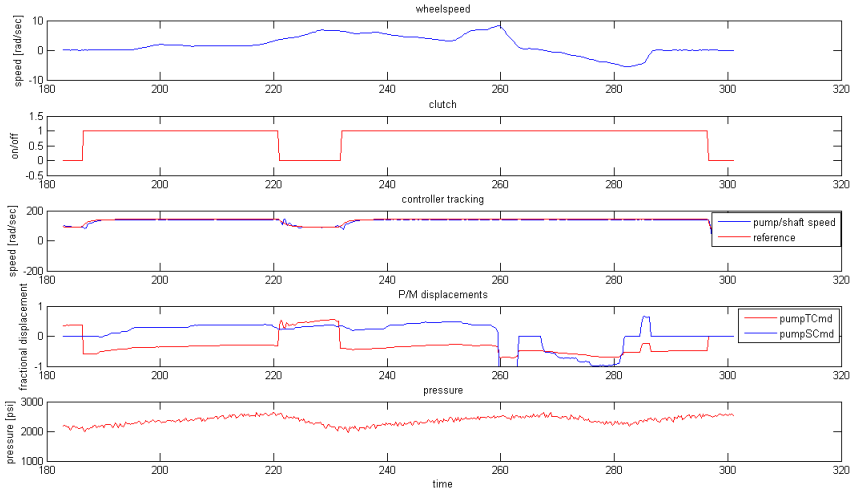


Figure 5.12: Data showing full functionality of the GenI vehicle

regenerative braking the kinetic energy usually lost when applying friction brakes can be recovered. For safety reasons the friction brakes had to remain in the vehicle. Therefore a brake knob was installed and used to specify the brake torque requested at the wheels. A torque proportional to the input voltage of the brake knob is applied to the wheels through P/M-S while the wheel speed is greater than zero. Similarly regenerative braking was implemented in reverse driving. Applying a positive torque to the wheels slows the wheels down while the speed is less than zero.

## 5.3 Road Test

A three level control strategy has been implemented on the Generation I hydraulic hybrid vehicle. Using an XPC target system the algorithms were downloaded on the vehicle and tested in real time. Without permit for public roads the parking lot and pedestrian streets surrounding the University of Minnesota ground were used as test areas. With the Polaris Ranger chassis a maximum speed of 22km/h was reached. In Figure 5.12 data from a general test run can be seen.

In this plot the rotational wheelspeed can be seen in the first graph. It is shown that

the vehicle is accelerated from stop to almost 10 rad/sec, which, with a wheel diameter of .62m, equates to approximately 22km/h. After slowing the vehicle down to a stop at time t=264sec the wheel speed turns negative. The vehicle is here operated in reverse.

In the second and third graph the engine and hydraulic mode can be observed. The second graph shows the clutch signal, where one implies that the clutch is engaged, while the clutch is released when the data shows 0. The control is operated in engine mode while the clutch is engaged. The third graph shows the carrier speed with the desired reference speed. It can be seen that the speed is set to a higher reference when operating in engine mode. The carrier is slowed down when P/M-T is in control.

Graph four shows the displacement command to the hydraulic units. In red P/M-T command is seen to be motoring when the vehicle is operated in hydraulic mode and pumping while the clutch is engaged and the engine is transmitting power. The displacement of P/M-T is adjusted to the loading torque of P/M-S on the carrier pump while operating in engine mode. In blue P/M-S command is shown. The hydrualic unit is transmitting positive torque when the vehicle is accelerated forward. To slow the vehicle down negative torque is provided to the wheels by P/M-S. Negative torque is also exerted while accelerating in reverse. Braking is performed with a positive displacement when the vehicle is operated at negative speed. The last graph shows the state of charge in the accumulator. In this test run the upper threshold was set to 2600psi and the lower threshold was kept at 2000psi pressure difference in the hydraulic lines. In engine mode the pressure increases while P/M-T is charging the energy storage. The stored energy is then re-used to accelerate the vehicle using P/M-S and in hydraulic mode using P/M-T to drive the carrier shaft.

## 5.4 Conclusion

The implementation of a three level control strategy on a power split hydraulic hybrid vehicle has been demonstrated. Control in each level has been designed, tested and implemented. A driver interface was designed such that vehicle operation is simplified for the user. Experimentally the vehicle has been shown to achieve forward and reverse driving. For future work it is suggested to design a drive cycle suitable for this vehicle.

Fuel measurements should then be taken to varify models of the vehicle and to emphasise system efficiency improvements through controls implementation. Once proper hardware is available a full mid level control should be implemented and various energy management strategies should be tested in the high level. A comparison of performance in fuel efficiency can then be drawn.

# Chapter 6

# Conclusion and Future Work

## 6.1 Review and Discussion

This thesis discussed the development, application and implementation of a three level control hierarchy. Two power split drive trains were modelled using the static relationships of the drive train as well as the inertia dynamics. The first, Generation I vehicle, is an input coupled power split hybrid drive train, the second, the Generation II vehicle, and output coupled power split hybrid vehicle. Modeling the drive train with engine and hydraulic components gave some insights to how hybrid vehicles can be configurated and how they operate.

In Chapter 3 a controls hierarchy was developed. Three levels of control were discussed. Seperating the management of the energy storage from the drive train optimization this startegy shows the impact of engine shifting on efficient drive train operation.

The application of the proposed strategy in off-line simulation as well as in real time implementation was shown. It was found that using a hierarchical control approach in the analysis of a hybrid drive train simplifies power train design and optimization. Using a Lagrange Optimization method the strategy was implemented in simulation to size hybrid drive trains, to find an optimal way to operate a power split drive train and to see the impact of hydraulic efficiency variations to fuel economy. It was found that sizing, modal operation and hydraulic efficiency improve overall efficiency of the hybrid vehicle. Also, drawing a comparison between the parallel, series and power split architecture, it was found that the power split configuration can perform as good or

better than other hybrid architectures over all ranges in hydraulic efficiency. Studies on the Generation II vehicle have shown that fuel consumption can be decreased by using hydro static transmissions over conventional 5-speed transmissions. Hybridizing the vehicle by adding energy storage capacity can improve fuel economy significant.

An implementation of the proposed hierarchical structure in real time has been shown in Chapter 5. It can be seen that the approach simplifies controls implementation on power split hybrid vehicles. Low level feedback controllers were developed for tracking of the specified optimal component operation. A user interface was designed such that the vehicle can be operated similarly to a conventional passenger vehicle. In road testing the operation of the vehicle was tested. Forward and reverse driving was achieved and regenerative braking can be performed.

This work has given insights into hybrid vehicle drive train analysis and design. The understanding gained in off-line analysis could be applied to the implementation in developing a fully functional power split hydraulic hybrid vehicle.

The primary accomplishment of this thesis work is the development of a controls strategy usable in simulation as well as in implementation on various hybrid vehicle drive trains. With this it contributes to literature by creating a framework for future control designs on any hybrid power train. This work shows the derivation and verification of the proposed controls startegy. Showing examples in simulation and implementation the use of this strategy is made clear.

Power split hybrid vehicles are known to be the new hybrid technology on the market. The vehicle configuration is shown to achieve more fuel savings then other configurations due to its drive train flexibility. With this flexibility the complexity of the control needed for optimal operation increases. While the developed control strategy can be used for any hybrid architecture this work focuses on the most complex case, the control of the power split vehicle.

Electric hybrid vehicles are known to the market but with technological improvements in fluid power the interest of the automotive industry for hydraulic hybrid vehicles is growing. Currently only used in heavy weight and frequent stop and go applications this technology could have potentials in passenger vehicles as well and compete in the market with its electric counterpart.

This research feeds directly into the Test Bed 3 research project and the control

algorithms designed in the scope of this thesis will be used in the future for further work on the hydraulic hybrid vehicle at the University of Minnesota. The framework developed can be used as a foundation to integrate and test other energy management strategies.

## 6.2 Suggestions for Future Work

The analysis of the Generation I and Generation II drive trains shown in Chapter 4 are performed assuming constant pressure. For sizing or to gain knowledge of a hydrid vehicle configuration this is appropriate but for fuel economy estimation more accurate values should be computed. Including pressure changes in the simulation adds an additional degree of freedom to the optimization, which results in an exponential increase in computational cost. The optimization problem becomes unsolvable using the Lagrange Multiplier Method. Therefore dynamic programming should be used to solve the complex problem.

In real time it is not feasable to turn the engine on and off frequently. As discussed in Section 4.2.2 for more realistic operation of the hybrid drive train in the analysis a penalty for turning the engine on and off should be added to the optimization. Simulations shown in this work energy storage size has not been considered. A major disadvantage of hydraulic hybrids is the energy density. Therefore a study on accumulator sizing should be performed to understand the effect of energy storage size on fuel consumption.

Using a forward facing control strategy the effect of the HSU restrictions should be analysed further to understand the optimal operation of the transmission. This understanding is needed for control design on the hybridized drive train of the Ford F150 vehicle.

With a fully functional vehicle a near future goal should be to measure fuel economy in the hydraulic hybrid vehicle at the University of Minnesota. Since federal drive cycles can not be demonstrated on this Polaris Ranger vehicle a drive cycle should be designed. Using real time fuel measurement vehicle models can be verified. Once vehicle hardware allows for implementation of full mid level control this should be done and various high level energy management strategies can be tested in their performance by measuring

fuel consumption over the designed drive cycle.

# References


[1] Porsche AG. Lohner porsche, 2010. http://www.porsche.com.

[2] Kemp W.H. *The Zero Carbon Car*. Aztext Press, 2007.

[3] A. Sciarretta; L. Guzzella. Control of hybrid electric vehicles. *IEEE Control Systems Magazine*, 2007.

[4] Y. Zhu; Y. Chen; G. Tian; H. Wu; Q. Chen. A four-step method to design an energy management strategy for hybrid vehicles. *Proceeding of the 2004 American Control Conference*, 2004.

[5] J. Liu; H. Peng. Control optimization for a power split hybrid vehicle. *Proceeding of the 2006 American Control Conference*, 2006.

[6] J. Liu; J. Peng. Modeling and control of a power split hybrid vehicle. *IEEE Transactions on Control System Technology*, 16(6), 2008.

[7] K. Ahn; S.W. Cha; J.M. Lee. Three types of simulation algorithms for evaluating the hev fuel efficiency. *SAE Technical Paper Series*, (2007-01-1771), 2007.

[8] K. Ahn; S. Cho; J.M. Lee. Optimal operation of the power-split hybrid electric vehilce powertrain. *Proceeding of ImechE, Part D: J. Automobile Engineering*, 222, 2008.

[9] P. Pisu; G. Rizzoni. A comparative study of supervisory control strategies for hybrid electric vehicles. *IEEE Transactions on Control Systems Technology*, 15(3):506–518, 2007.

[10] H.A. Borhan; A. Vahidi; A.M. Phillips; M.L. Kuang; I.V. Kolmanovsky. Predictive energy management of a power-split hybrid electric vehicle. *American Control Conference*, 2009.

[11] G. Hubbard. System level control of a hybrid-electric drivetrain. *Proceeding of the American Control Conference*, 1997.

[12] S.M.T. Bathaee; A.H. Gastaj; S.R. Emami; M. Mohammadian. A fuzzy-based supervisory robust control for parallel hybrid electric vehicles. *IEEE*, 2005.

[13] M. Huang; H. Yu. Optimal multilevel hierarchical control strategy for parallel hybrid electric vehicle. *IEEE*, 2006.

[14] M. Ellims J. Bridges; C.E. Wartnaby; D. Stannard; J. Styles. Frameworks for power and systems management in hybrid vehicles: Challenges and prospects. *SAE Technical Paper*, (2006-21-0005), 2006.

[15] Clive Tucker Pittsfield MA Lawrence R. Folsom, Pittsfield MA. Hydraulic machine, 03 2002.

[16] D.J. Lee; P.Y. Li. Passive decomposition for formation and maneuver control of multiple rigid-bodies. *ASME JDSMC*, pages 662–677, 2007.

[17] B. Zuurendonk. Advanced fuel consumption and emission modeling using willans line scaling techniques for engines. Technical report, Technische Universiteit Eindhoven, 2005.

[18] V. Ganesan. *Internal Combustion Engines.* The McGraw-Hill Company, third edition, 2007.

[19] P. Nachtwey. Hydraulics and pneumatics, technology zone, delta computer systems, vancouver, wash., 2010. http://www.hydraulicspneumatics.com.

[20] T. Kohmaescher. *Modelbildung, Analyse und Auslegung hydrostatischer Antriebsstrangkonzepte.* PhD thesis, RWTH Aachen, 2008.

[21] D.R. Grandall. The performance and efficiency of hydraulic pumps and motors. Master's thesis, University of Minnesota, January 2010.

[22] D. McCandlish; R.E. Dorey. The mathematical modeling of hydrostatic pumps and motors. *Proceedings of the Institution of Mechanical Engineers*, pages 165–174, 1984.

[23] Eaton Corporation. Hydraulic launch assist, 2010. http://www.eaton.com/EatonCom/.

[24] L. Guzzela; A. Sciarretta. *Vehicle Propulsion Systems. Introduction to Modeling and Optimization*. Springer-Verlag, 2005.

[25] G. Steinmauer; L. del Re. Optimal control of dual power sources. 2001.

[26] A. Kleimaier; D. Schrder. An approach for the online optimized control of a hybrid powertrain. 2002.

[27] M. Back. Prdiktive antriebsregelung zum energieoptimalen betrieb von hybridfahrzeugen. Master's thesis, Universitt Karlsruhe, 2005.

[28] C.C. Lin; H. Peng; J.W. Grizzle; J.M. Kang. Power management strategy for a parallel hybrid electric truck. *IEEE Transactions on Control Systems Technology*, 11(6):839–849, 2003.

[29] G. Paganelli; G. Ercole; A. Brahma; Y. Guezennec; G. Rizzoni. General supervisory control policy for the energy optimization of charge-sustaining hybrid electric vehicles. 2001.

[30] C. Musardo; G. Rizzoni; Y. Guezennec; B. Staccia. A-ecms: An adaptive algorithm for hybrid electric vehicle energy amangement. *European Journal for Control*, 11(4-5):509–524, 2005.

[31] C.C. Lin; H. Peng; J.W. Grizzle. A stochastic control strategy for hybrid electric vehicles. *Proc. 2004 American Control Conference*, pages 4710–4715, 2004.

[32] Z. Wu. The discrete lagrangian theory and its application to solve nonlinear discrete constrained optimization problems. Master's thesis, University of Illinois, 1998.

[33] D. Rizoulis; J. Burl; J. Beard. Control strategies for a series-parallel hybrid electric vehicle. *SAE Technical Paper*, (2001-01-1354), 2001.

[34] T.P. Sim; P.Y. Li. Analysis and control design of a hydro-mechanical hydraulic hybrid passenger vehicle. *ASME- Dynamic Systems and Control Conference*, 2009.

[35] Goodwin G.C.; Graebe S.F.; Salgado M.E. *Control System Design*. Prentice Hall, 2001.

[36] Franklin; Powell; Emami-Naeini. *Feedback Control of Dynamic Systems*. Prentice Hall, 2002.

# Appendix A

# Matlab Code

## A.1 Matlab Code for Generation I Simulations

### A.1.1 Experimentally Retrieved Pump Model

```
function [Q, Qideal]=flowmodel(x,w,dP)

%all calucations are with speed in rpm and max displacement D
    in cc/rev
%speed CCW is positive, CW is negative
%pumping if displacement opposite sign of speed
wSI=w;
w=w*60/(2*pi);%speed in rpm
wcheck=w;
xcheck=x;%x with sign for ideal flow calculation
%constants
D=28;%in cc per rev
DSI=2.8e-5/(2*pi);
Patmos=.1e6;%Pa
Cs=1.046e-8;%slip coefficient
B=1.02e9;%bulk modulus in Pa
```

```
Vr=.1;%Ratio of clearance volume to swept volume
K=50;
mu=-.000538*K+.05949;
wmax=4000;%rpm

%coefficients contains all coeff for model
%first row ccw pumping, second row cw pumping, third row ccw
    motoring,
%fourth row cw motoring
coefficients=[1.527,0.057,0,1.412,-.068;
     3.278,0,0,0.184,-.507;
     0.146,9.788,6.01,4.01,0.074;
     0,10.03,5.96,-10.1,0.204];

%pumping ccw
if(xcheck<=0 && wcheck>=0)
     row=1;
     a=coefficients(row,1);
     b=coefficients(row,2);
     e=coefficients(row,3);
     f=coefficients(row,4);
     n=coefficients(row,5);
     x=abs(x);
     w=abs(w);
     Q=w*D*x/1000-Cs*(dP/Patmos)^n*(a+b*(min(wmax,w)/wmax))*60*
         dP*D/(1000*2*pi*mu)-dP*w*D/(B*1e3)*(e*Vr+f*(1+x)/2);%lpm
     Q=-Q;
end
%pumping cw
if(xcheck>=0 && wcheck<=0)
     row=2;
     a=coefficients(row,1);
```

```
    b=coefficients(row,2);
    e=coefficients(row,3);
    f=coefficients(row,4);
    n=coefficients(row,5);
    x=abs(x);
    w=abs(w);
    Q=w*D*x/1000-Cs*(dP/Patmos)^n*(a+b*(min(wmax,w)/wmax))*60*
        dP*D/(1000*2*pi*mu)-dP*w*D/(B*1e3)*(e*Vr+f*(1+x)/2);%lpm
    Q=-Q;

end
%motoring ccw
if(xcheck>=0 && wcheck>=0)
    row=3;
    a=coefficients(row,1);
    b=coefficients(row,2);
    e=coefficients(row,3);
    f=coefficients(row,4);
    n=coefficients(row,5);
    x=abs(x);
    w=abs(w);
    Q=w*D*x/1000+Cs*(dP/Patmos)^n*(a+b*(min(wmax,w)/wmax))*60*
        dP*D/(1000*2*pi*mu)+dP*w*D/(B*1e3)*(e*Vr+f*(1+x)/2);%lpm

end
%motoring cw
if(xcheck<0 && wcheck<0)
    row=4;
    a=coefficients(row,1);
    b=coefficients(row,2);
    e=coefficients(row,3);
    f=coefficients(row,4);
```

```
    n=coefficients(row,5);
    x=abs(x);
    w=abs(w);
    Q=w*D*x/1000+Cs*(dP/Patmos)^n*(a+b*(min(wmax,w)/wmax))*60*
        dP*D/(1000*2*pi*mu)+dP*w*D/(B*1e3)*(e*Vr+f*(1+x)/2);%lpm
end

Q=Q/(1000*60);%in m^3/s
Qideal=wSI*DSI*xcheck;

end

%Dorey model from David grandals thesis

function[T,Tideal]=torquemodel(x,w,dP)

%all calucations are with speed in rpm and max displacement D
    in cc/rev
%speed CCW is positive, CW is negative
%pumping if displacement opposite sign of speed

w=w*60/(2*pi);%speed in rpm
wcheck=w;
xcheck=x;%includes sign for ideal toruqe calculation
%constants
D=28;%in cc per rev
DSI=2.8e-5/(2*pi);
Cv=2.163e5;%vicsous frictoin coefficient
Cf=.9702;%coulomb friciton coefficient
K=50;
mu=-.000538*K+.05949;
wmax=4000;%rpm
```

```
%coefficients contains all coeff for model
%first row ccw pumping, second row cw pumping, third row ccw
    motoring,
%fourth row cw motoring
coefficients=[.182,-.331,1.294,1.316;
     .178,-.223,1.012,.743;
     .139,-.522,1.556,.442;
     .184,-.459,1.103,.883];

%pumping ccw
if(xcheck<=0 && wcheck>=0)
     row=1;
     g=coefficients(row,1);
     h=coefficients(row,2);
     l=coefficients(row,3);
     m=coefficients(row,4);
     x=abs(x);
     w=abs(w);
     T=dP*D*x/(2*pi*1e6)+Cv*(l+m*x)*mu*w*D/(60e6)+Cf*(g+h*(w/
         wmax))*dP*D/(2*pi*1e6);
     T=-T;
     Tideal=dP*DSI*xcheck;
     T=min(T,Tideal);
end
%pumping Cw
if(xcheck>=0 && wcheck<=0)
     row=2;
     g=coefficients(row,1);
     h=coefficients(row,2);
     l=coefficients(row,3);
     m=coefficients(row,4);
```

```
    x=abs(x);
    w=abs(w);
%       p3=Cf*(g+h*(w/wmax))*dP*D/(2*pi*1e6)
%       p2=Cv*(l+m*x)*mu*w*D/(60e6)
    T=dP*D*x/(2*pi*1e6)+Cv*(l+m*x)*mu*w*D/(60e6)+Cf*(g+h*(w/
        wmax))*dP*D/(2*pi*1e6);
    Tideal=dP*DSI*xcheck;
    T=max(T,Tideal);
end
%motoring ccw
if(xcheck>0 && wcheck>=0)
    row=3;
    g=coefficients(row,1);
    h=coefficients(row,2);
    l=coefficients(row,3);
    m=coefficients(row,4);
    x=abs(x);
    w=abs(w);
%       p3=Cf*(g+h*(w/wmax))*dP*D/(2*pi*1e6)
%       p2=Cv*(l+m*x)*mu*w*D/(60e6)
    T=dP*D*x/(2*pi*1e6)-Cv*(l+m*x)*mu*w*D/(60e6)-Cf*(g+h*(w/
        wmax))*dP*D/(2*pi*1e6);
    Tideal=dP*DSI*xcheck;
    T=min(T,Tideal);
end
%motoring cw
if(xcheck<0 && wcheck<=0)
    row=4;
    g=coefficients(row,1);
    h=coefficients(row,2);
    l=coefficients(row,3);
    m=coefficients(row,4);
```

```
        x=abs(x);
        w=abs(w);
        T=dP*D*x/(2*pi*1e6)-Cv*(l+m*x)*mu*w*D/(60e6)-Cf*(g+h*(w/
            wmax))*dP*D/(2*pi*1e6);
        T=-T;
        Tideal=dP*DSI*xcheck;
        T=max(T,Tideal);
    end
    if(xcheck<0 && wcheck==0)
        row=4;
        g=coefficients(row,1);
        h=coefficients(row,2);
        l=coefficients(row,3);
        m=coefficients(row,4);
        x=abs(x);
        w=abs(w);
        T=dP*D*x/(2*pi*1e6)-Cv*(l+m*x)*mu*w*D/(60e6)-Cf*(g+h*(w/
            wmax))*dP*D/(2*pi*1e6);
    %       T=-T;
        Tideal=dP*DSI*xcheck;
        T=max(T,Tideal);
    end

    if(xcheck==0 && wcheck==0)
        T=0;
    end

    Tideal=dP*DSI*xcheck;

    end

    %calculate derived displacement
```

```
function [xder]=derivedDispl(x,w)
% w=400;
% x=-.2;
coefficients=[-0.414,-0.667,-0.022,1.30,0.130,0.045;
0.561,0.022,0.032,0.378,-0.053,0.021;
0.445,0.798,0.259,0.319,-1.05,0.316;
0.106,0.036,0.854,0.038,-0.203,0.117];

w=w*60/(2*pi);
wcheck=w;
xcheck=x;
wmax=4000;
xsign=x;
x=abs(x);

%pumping ccw
if(xcheck<=0 && wcheck>=0)
    row=1;
    a=coefficients(row,1);
    b=coefficients(row,2);
    c=coefficients(row,3);
    d=coefficients(row,4);
    e=coefficients(row,5);
    f=coefficients(row,6);
    w=abs(w);
    xder=a*x^2+b*(w/wmax)^2+c*x*(w/wmax)+d*x+e*(w/wmax)+f;
%       xder=-xder;
end
%pumping Cw
if(xcheck>=0 && wcheck<=0)
    row=2;
```

```
    a=coefficients(row,1);
    b=coefficients(row,2);
    c=coefficients(row,3);
    d=coefficients(row,4);
    e=coefficients(row,5);
    f=coefficients(row,6);
    w=abs(w);
    xder=a*x^2+b*(w/wmax)^2+c*x*(w/wmax)+d*x+e*(w/wmax)+f;
end
%motoring ccw
if(xcheck>0 && wcheck>=0)
    row=3;
    a=coefficients(row,1);
    b=coefficients(row,2);
    c=coefficients(row,3);
    d=coefficients(row,4);
    e=coefficients(row,5);
    f=coefficients(row,6);
    w=abs(w);
    xder=a*x^2+b*(w/wmax)^2+c*x*(w/wmax)+d*x+e*(w/wmax)+f;
end
%motoring cw
if(xcheck<0 && wcheck<=0)
    row=4;
    a=coefficients(row,1);
    b=coefficients(row,2);
    c=coefficients(row,3);
    d=coefficients(row,4);
    e=coefficients(row,5);
    f=coefficients(row,6);
    w=abs(w);
    xder=a*x^2+b*(w/wmax)^2+c*x*(w/wmax)+d*x+e*(w/wmax)+f;
```

```
%       xder=-xder;
end

xder=sign(xsign)*xder;
end
```

### A.1.2 Optimization Studies

```
% HMT static optimization, HMTopt4.m
% HMT in mode 1(using both pump/motors and engine clutched or
    declutched)
clear
rpm=2*pi/60;                %rad/s
psi=1e5/14.1;               %Pa
miles=1609.344;             %meters
airdens = 1.29;             %Air density STP     (kg/M^3)
slope = 0.0;                %Grade angle         (rad)
gallons=3.81;               %liters
%vehicle param
dia = .619;
R_B=1;%1/0.676;
gearsrat=[15.3  6.75];%[5.9  3.1]*2.66;
H_Reduct=12;%3.8;
eng_e=0.38;
%pump model
load pump21ccnolock
load pump14ccnolock
%pump T
T1=T1_21cc;
w=w_21cc;
x=x_21cc;
XX=XX_21cc;
Eloss=Eloss_21cc;
```

```
Q=Q_21cc;
P=P_21cc;
Eff=Eff_21cc;
[TT,PP,WW]=ndgrid(T1_21cc,P_21cc,w_21cc);        % Grid for XX
[PPP,XXX,WWW]=ndgrid(P_21cc,x_21cc,w_21cc);      % Grid for
    forward pump data (T, Q, Eloss etc).
[XX2,WW2]=ndgrid(x_21cc,w_21cc);
%pump S
T1_24cc=T1_14cc;
w_24cc=w_14cc;
x_24cc=x_14cc;
XX_24cc=XX_14cc;
Eloss_24cc=Eloss_14cc;
Q_24cc=Q_14cc;
P_24cc=P_14cc;
Eff_24cc=Eff_14cc;
[TT_24cc,PP_24cc,WW_24cc]=ndgrid(T1_14cc,P_14cc,w_14cc);        %
     Grid for XX
[PPP_24cc,XXX_24cc,WWW_24cc]=ndgrid(P_14cc,x_14cc,w_14cc);     %
     Grid for forward pump data (T, Q, Eloss etc).
[XX2_24cc,WW2_24cc]=ndgrid(x_14cc,w_14cc);
Pclist=find(P>3000*psi,1,'first');          %3000psi
%drive cycle
load allcyclesnew;
cyc=urban;
N=length(cyc.time);
V=[-15000:500:23000];                              %accumulator power
nV=length(V);
%create array to store values
StoreLoss=inf(N,nV);
StoreXe=NaN(N,nV);
StoreXb=NaN(N,nV);
```

```
StoreWe=NaN(N,nV);
Storeweng=NaN(N,nV);
StoreTeng=NaN(N,nV);
StoreEngEff=NaN(N,nV);
StoreTb=NaN(N,nV);
StoreWb=NaN(N,nV);
StoreTe=NaN(N,1);
StoreMode=ones(N,nV);
%engine (use willans line model 'engine(torque,speed)')
torq=[0:10:90]';
w1=[0:100:4500]*rpm;
Torque=torq*ones(size(w1));
ww=ones(length(torq),1)*w1;
[torque,speed]=ndgrid(torq,w1);
[eng_loss,eff_e]=engine(torque,speed);
maxeffengine=max(eff_e)
maxeng=max(maxeffengine);
heatcap=38.6e6;
maxeff=maxeng;
%maximum fuel economy achievable
fuelmin=(sum(cyc.power)/maxeff/heatcap);
d=cyc.distance(N);
mpgmax=(cyc.distance(N))/fuelmin*gallons/miles;
%gear
rat=gearsrat(1);
wc_cycle=cyc.w/2*rat/rpm; tc_cycle=2*cyc.torque/rat;
first_time=1; tic;
for k=1:N;
    k
    if rem(k,10)==0, toc; display(['k=',num2str(k)]); tic; end;
    wc=cyc.w(k)/2*rat/rpm; tc=2*cyc.torque(k)/rat;
    TBstart=find(T1 <= (tc-max(torq))*R_B,1,'last');
```

```
TBend=find(T1<tc*R_B,1,'last');
if isempty(TBstart), TBstart=1; end;
TBlistind=[TBstart:TBend];
TBlist=T1(TBlistind);
if (~any(TBlist==tc*R_B) & tc*R_B <= max(T1) ),
    if(tc*R_B<max(T1) && tc*R_B>min(T1))
    [TBlist,IX]=sort([TBlist,tc*R_B]);
    IX=find(IX==length(TBlist));
    tcind=round((tc*R_B-T1(1))/(T1(2)-T1(1)))+1;
    TBlistind(IX:length(TBlist))=[tcind,TBlistind(IX:length
        (TBlistind))];
    end;
end;
WBlistind=[find(w>0*rpm/R_B,1,'first'):find(w<4500*rpm/R_B
    ,1,'last')];
WBlist=w(WBlistind);
Wenglist=WBlist*R_B;
Tenglist=tc-TBlist/R_B;
%pump/motor S(initially called E)
WElist=2/rat*H_Reduct*(Wenglist-wc*rpm);
WElist1=WElist(find(WElist<0));
WElist2=WElist(find(WElist>=0));
TE=-cyc.torque(k)/H_Reduct;
xe=interpn(T1_24cc,P_24cc,w_24cc,XX_24cc,...
    TE*[-ones(size(WElist1'));ones(size(WElist2'))],...
    P_24cc(Pclist)*ones(size(WElist')),abs(WElist'));
xe = xe.*sign(WElist');
%area of no solution:
xe(isnan(xe))=2;
xe(find(abs(xe)>1))=2;
loss_E=interpn(XX2_24cc,WW2_24cc,squeeze(Eloss_24cc(Pclist
    ,:,:)),xe.*sign(WElist'),abs(WElist'));
```

```
Q_E=interpn(XX2_24cc,WW2_24cc,squeeze(Q_24cc(Pclist,:,:)),
    xe.*sign(WElist'),abs(WElist'));
%pump/motor T(initially called B)
xb=squeeze(XX(TBlistind,Pclist,WBlistind));
xbbb=size(xb);
if(xbbb(1)~=length(TBlistind))
     xb=xb';
end
[xjunk,wb2]=ndgrid(TBlistind,WBlist);
loss_B=interpn(XX2,WW2,squeeze(Eloss(Pclist,:,:)),xb,wb2);
Q_B=interpn(XX2,WW2,squeeze(Q(Pclist,:,:)),xb,wb2);
%engine
[T2,W2]=ndgrid(Tenglist,Wenglist);
[eng_loss,engine_eff]=engine(T2,W2);
%total system losses and power from accumulator
total_loss=eng_loss+loss_B+ones(length(TBlist),1)*loss_E';
P_acc = (Q_B+ones(length(TBlist),1)*Q_E')*P_24cc(Pclist);
if (first_time),
figure(1);
hold off;
[c1,h1]=contour(Wenglist/rpm,Tenglist,total_loss
    ,[10:10000:90000]); clabel(c1,h1); %total_loss
axis([0 4500 -50 75]);
set(h1,'EraseMode','xor');
hold on;
h0=plot(wc,tc,'b*');
h3=plot(wc,tc,'ro');
figure(2); hold off;
[c2,h2]=contour(Wenglist/rpm,Tenglist,P_acc,V); clabel(c2,
    h2);
axis([0 8000 -50 75]);
set(h2,'EraseMode','xor');
```

```
hold on;
h00=plot(wc,tc,'*');
h4=plot(wc,tc,'ro');
first_time=0;
else
  set(h2,'ZData',P_acc,'XData',Wenglist/rpm,'YData',
     Tenglist);
end;
% Process optimal power
c2=get(h2,'ContourMatrix'); % Get power to accumulator
   level curves
clear pacc;
kk=length(c2); kind=1; plevel=0;
previous=-inf;
if(kk==0)
    pacc.min=inf;
    pacc.teng=0;
    pacc.w=0;
    pacc.pow=0;
else
while kind<=kk,
    if c2(1,kind)~=previous;
        plevel=plevel+1;
        pacc.pow(plevel)=c2(1,kind);
        num=c2(2,kind);
        weng=c2(1,kind+1:kind+num)'*rpm;
        teng=c2(2,kind+1:kind+num)';
        loss=flipud(interpn(Tenglist,Wenglist,total_loss,
            teng,weng));
        [pacc.min(plevel),ind]=min(loss);
        pacc.w(plevel)=weng(ind); pacc.teng(plevel)=teng(
            ind);
```

```
    else
        num=c2(2,kind);
        weng=c2(1,kind+1:kind+num)'*rpm;
        teng=c2(2,kind+1:kind+num)';
        loss=flipud(interpn(Tenglist,Wenglist,total_loss,
            teng,weng));
        [minn,ind]=min(loss);
        if (minn < pacc.min(plevel))
            pacc.w(plevel)=weng(ind); pacc.teng(plevel)=
                teng(ind);
        end;
    end;
    previous=pacc.pow(plevel);
    kind=kind+num+1;
end;
end;
set(h3,'XData',pacc.w/rpm,'YData',pacc.teng);
set(h4,'XData',pacc.w/rpm,'YData',pacc.teng);
pacc.ew = 2/rat*H_Reduct*(pacc.w-wc*rpm);
pacc.ex = interpn(T1_24cc,P_24cc,w_24cc,XX_24cc,TE*sign(
    pacc.ew),P(Pclist)*ones(size(pacc.ew)),abs(pacc.ew));
pacc.ex = pacc.ex.*sign(pacc.ew);
pacc.bw = pacc.w/R_B;
pacc.tb = (tc-pacc.teng)*R_B;
pacc.bx = interpn(T1,P,w,XX,...
pacc.tb,P(Pclist)*ones(size(pacc.teng)),pacc.bw);
set(h444,'XDATA',abs(pacc.ew),'YDATA',pacc.ex.*sign(pacc.ew
    ));
set(h333,'XDATA',pacc.bw,'YDATA',pacc.bx);
Vind=interp1(V,1:nV,pacc.pow,'nearest');
StoreLoss(k,Vind)=pacc.min;
StoreXe(k,Vind)=pacc.ex;
```

```
        StoreWe(k,Vind)=pacc.ew;
        StoreXb(k,Vind)=pacc.bx;
        StoreWb(k,Vind)=pacc.bw;
        Storeweng(k,Vind)=pacc.w;
        StoreTeng(k,Vind)=pacc.teng;
        StoreTb(k,Vind)=pacc.tb;
        StoreTe(k)=TE;
        StoreEngEff(k,Vind)=eng_e*(pacc.teng.*pacc.w)./(pacc.teng.*
            pacc.w + pacc.min);
        minimumoftimepoint=min(StoreLoss(k,:));
        if(minimumoftimepoint>=1e10)
            ans=0;
        end
end;
%when vehicle stopped, turn all components off
ind=find(cyc.w==0);
ind2=find(cyc.torque(ind)==0);
index=ind(ind2);
if(isempty(find(StoreLoss(index,31)==0)))
    StoreLoss(index,31)=0;
    Storeweng(index,31)=0;
    StoreTeng(index,31)=0;
    StoreXb(index,31)=0;
    StoreWb(index,31)=0;
    StoreTb(index,31)=0;
    StoreTe(index,31)=0;
    StoreXe(index,31)=0;
    StoreWe(index,31)=0;
end
toc
opt_info='Newloss';
save NewOptim_HMT_resized_hway
```

```
% HMT static optimization, Mode3and32Parallel.m
% mode 2: pump S locked up: parallel mode
rpm=2*pi/60;                %rad/s
psi=1e5/14.1;               %Pa
miles=1609.344;             %meters
airdens = 1.29;             %Air density STP     (kg/M^3)
slope = 0.0;                %Grade angle         (rad)
%vehicle param
dia = .619;
R_B=1%1/0.676;
gearsrat=[15.3  6.75];%[5.9  3.1]*2.66;
H_Reduct=12;%3.8;
eng_e=0.38;
%gear
rat=gearsrat(2);
mode='n';
%pump/motor
load pump21ccwlock
T1=T1_21cc;
w=w_21cc;
x=x_21cc;
XX=XX_21cc;
Eloss=Eloss_21cc;
Q=Q_21cc;
P=P_21cc;
Eff=Eff_21cc;
%drive cycle
load allcyclesnew;
cyc=hway;
N=length(cyc.time);
%accumulator power
V=[-15000:500:23000];
```

```
nV=length(V);
%create array to store values
StoreLoss=inf(N,nV);
StoreXe=zeros(N,nV);
StoreXb=NaN(N,nV);
StoreWe=zeros(N,nV);
Storeweng=NaN(N,nV);
StoreTeng=NaN(N,nV);
StoreEngEff=NaN(N,nV);
StoreTb=NaN(N,nV);
StoreWb=NaN(N,nV);
StoreTe=zeros(N,1);
StoreMode=3*ones(N,nV);
%engine
torq=[0:10:70]';
w1=[0:100:4500]*rpm;
Torque=torq*ones(size(w1));
ww=ones(length(torq),1)*w1;
[eng_loss,eff_e]=engine1(Torque,ww);
[TT,PP,WW]=ndgrid(T1,P,w);   % Grid for XX
[PPP,XXX,WWW]=ndgrid(P,x,w);    % Grid for forward pump data (T,
    Q, Eloss etc).
[XX2,WW2]=ndgrid(x,w);
Pclist=find(P>3000*psi,1,'first');          %3000psi
first_time=1;
for k=1:N;
    %display(['k=',num2str(k)]);
    if rem(k,10)==0, toc; display(['k=',num2str(k)]); tic; end;
    wc=cyc.w(k)/2*rat/rpm;
    tc=2*cyc.torque(k)/rat;
    TBstart=find(T1 <= (tc-max(torq))*R_B,1,'last');
    TBend=find(T1<tc*R_B,1,'last');
```

```
if isempty(TBstart), TBstart=1; end;
TBlistind=[TBstart:TBend];
TBlist=T1(TBlistind);
if (~any(TBlist==tc*R_B) & tc*R_B <= max(T1) ),
      if(tc*R_B<max(T1) && tc*R_B>min(T1))
     [TBlist,IX]=sort([TBlist,tc*R_B]);
     IX=find(IX==length(TBlist));
     tcind=round((tc*R_B-T1(1))/(T1(2)-T1(1)))+1;
     TBlistind(IX:length(TBlist))=[tcind,TBlistind(IX:length
         (TBlistind))];
      end
end;
if(wc<4500)
WBlist=wc*rpm/R_B;
Wenglist=WBlist*R_B;
Tenglist=tc-TBlist/R_B;
xb=interpn(T1,P,w,XX,TBlist,P(Pclist),abs(WBlist'));
index=find(abs(xb)<=1);
xb=xb(index);
Tenglist=Tenglist(index);
ind2=find(abs(xb)<.000001);
xb(ind2)=0;
if(~isempty(xb))
loss_B=interpn(XX2,WW2,squeeze(Eloss(Pclist,:,:)),xb,abs(
    WBlist'));
Q_B=interpn(XX2,WW2,squeeze(Q(Pclist,:,:)),xb,abs(WBlist'))
    ;
[eng_loss,engine_eff]=engine(Tenglist',(Wenglist*ones(size(
    Tenglist)))');
total_loss=eng_loss+loss_B;
P_acc = (Q_B)*P(Pclist);
total_loss(isnan(total_loss))=inf;
```

```
        Vind=interp1(V,1:nV,P_acc,'nearest');
        index=find((~isnan(Vind)));
        Vind=Vind(index);
        StoreLoss(k,Vind)=total_loss(index);
        StoreXb(k,Vind)=xb(index);
        StoreWb(k,Vind)=WBlist;
        Storeweng(k,Vind)=Wenglist;
        StoreTeng(k,Vind)=Tenglist(index);
        StoreTb(k,Vind)=TBlist(index);
        StoreEngEff(k,Vind)=(Tenglist(index).*Wenglist)./(Tenglist(
            index).*Wenglist+total_loss(index)');
        end
        end
end;
ind=find(cyc.w==0);
ind2=find(cyc.torque(ind)==0);
index=ind(ind2);
%when vehicle at stop and no torque required turn components
    off
if(isempty(find(StoreLoss(index,31)==0)))
    StoreLoss(index,31)=0;
    Storeweng(index,31)=0;
    StoreTeng(index,31)=0;
    StoreXb(index,31)=0;
    StoreWb(index,31)=0;
    StoreTb(index,31)=0;
end
%find engine declutched mode
for(k=1:N)
        ii=find(StoreTeng(k,:)<.5);
        StoreMode(k,ii)=32;
end
```

```
opt_info='Newloss';
save NewOptim_resized_parallel_gear2_hway StoreLoss StoreXb
    StoreXe StoreWe StoreTe StoreMode StoreWb Storeweng
    StoreTeng StoreTb StoreEngEff V opt_info

% HMT static optimization, Mode4Blocked.m
% mode four: HMT only running on pump S, T locked up-> shaft
    locked up.
%pump/motor
load pump14ccnolock
T1_15cc=T1_14cc;
w_15cc=w_14cc;
x_15cc=x_14cc;
XX_15cc=XX_14cc;
Eloss_15cc=Eloss_14cc;
Q_15cc=Q_14cc;
P_15cc=P_14cc;
Eff_15cc=Eff_14cc;
%parameters
rpm=2*pi/60;              %rad/s
psi=1e5/14.1;             %Pa
miles=1609.344;           %meters
airdens = 1.29;           %Air density STP     (kg/M^3)
slope = 0.0;              %Grade angle         (rad)
%drive cycle
load allcyclesnew;
cyc=hway;
N=length(cyc.time);
%accumulator power
V=[-15000:500:23000];
nV=length(V);
%create array to store values
```

```
StoreLoss=inf(N,nV);
StoreXe=NaN(N,nV);
StoreXb=zeros(N,nV);
StoreWe=NaN(N,nV);
Storeweng=zeros(N,nV);
StoreTeng=zeros(N,nV);
StoreEngEff=zeros(N,nV);
StoreTb=zeros(N,nV);
StoreWb=zeros(N,nV);
StoreTe=zeros(N,1);
StoreMode=4*ones(N,nV);
H_R=12;%4.8673;%7.5347;
Pclist=find(P_15cc>3000*psi,1,'first');          %3000psi
[XX2_15cc,WW2_15cc]=ndgrid(x_15cc,w_15cc);
for k=1:N
    k
    w_E= -H_R*cyc.w(k);
    T_E=-cyc.torque(k)/H_R;
    if(abs(w_E)<5000*2*pi/60)
    xe=interpn(T1_15cc,P_15cc,w_15cc,XX_15cc,T_E*sign(w_E),
        P_15cc(Pclist),abs(w_E));
    xe = xe.*sign(w_E);
    loss_E=interpn(XX2_15cc,WW2_15cc,squeeze(Eloss_15cc(Pclist
        ,:,:)),xe.*sign(w_E),abs(w_E));
    Q_E=interpn(XX2_15cc,WW2_15cc,squeeze(Q_15cc(Pclist,:,:)),xe
        .*sign(w_E),abs(w_E));
    Pacc=Q_E*P_15cc(Pclist);
    Vind=interp1(V,1:nV,Pacc,'nearest');
    if(~isnan(Vind))
     StoreLoss(k,Vind)=loss_E;
     StoreXe(k,Vind)=xe;
     StoreWe(k,Vind)=w_E;
```

```
      StoreTe(k)=T_E;
    end
    end
end
opt_info='Newloss';
save NewOptim_resized_series_hway StoreLoss StoreXb StoreXe
    StoreWe StoreTe StoreMode StoreWb Storeweng StoreTeng
    StoreTb StoreEngEff V opt_info

%DP2.m
%program to find optimal vehicle operation over a drive cycle
global StoreLoss N V;
load NewOptim_HMT_resized_urban_twogears; %Optim_HMT_28cc_new
load allcyclesnew;
cyc=urban;
N=length(cyc.time);
range=1:N;
N=length(cyc.time(range));
%lagrange optimization
StoreLoss=StoreLoss(range,:);
lam=fminsearch(@(lam) onestep(lam,N),-3.532)
%final cost
J=StoreLoss'+lam*V'*ones(1,N);
%looking at outputs
[ll,Vlist]=min(J);
Vlist(range)=Vlist;
Power=V(Vlist);
ll(find(ll==inf))=0;
totalloss=sum(ll)
poweraccumulator=sum(Power)
mode='n';
figure(1)
```

```
plot(cumsum(Power));
xlabel('time in drive cycle');
ylabel('energy in accumulator [J]');
title('state of charge in accumulator');
heatcap=38.6e6; %43.2e6; %J/liter
work=sum(cyc.power(range));
if mode=='n'
    fuel=(totalloss+work)/(heatcap);
else
    fuel=(totalloss+work)/(eng_e*heatcap);
end;
miles=1609; %m
gallons=3.81; %liters
mpg=diff(cyc.distance(range([1,N])))/fuel*gallons/miles

% Unconstrained optimization via Lagrange multiplier for EPA
   cycle
function [total]=onestep(lam,n)
global StoreLoss N V list
J=StoreLoss'+lam*V'*ones(1,N);
J=J(:,1:n);
[ll,list]=min(J);
total=(sum(V(list)))^2;
```

## A.2 Matlab Code for Generation II Simulations

### A.2.1 Folsom Hydraulic Pump Model

```
function [flow,leak]=flowLossonePump(x,w,P)
parameters_04017r1
areas_04017r1
cop_04017r1
%convert values from SI to english units:
dsp=x'*222/16.39;
```

```
s=w'*60/(2*pi);
phsu=P'/6894.75;
ang=asin(dsp/(pba*tpscd*np))*180/pi;
                                                    %calculate pump
    angle from displacement
%calculate torqueloss
if(sign(w*x)==-1)%pumping
        [TLcb,cbl,hh,hl,prh,prl] = cb_thrbrg_04017r1(phsu,abs(s),
            dopuckp);                               % Cylinder block
            thrust bearing function
        TLcbp = TLcb;
        [pllrp,plhrp,TLtp,lprh,lprl,lkh,lkl,tpl,mh,ml,hh,hl,prh,
            prl] = tqplate_loss_04017r1_1(dop,phsu,abs(s),ang);
            % Torque plate loss function, pump inputs
        TLtpp = TLtp;
        leak=TLtpp+TLcbp;
        %convert from english to SI units
        flowideal=(s.*dsp'/231)*.0037854;
        loss=leak*.0037854;
         flow = ((s.*dsp'/231)+leak)*.0037854;
         ans=0;
else%motoring
         [TLcb,cbl,hh,hl,prh,prl] = cb_thrbrg_04017r1(phsu,abs(s
             '),dopuckm);                           % Cylinder block
             thrust bearing function
         TLcbm = TLcb;
         [pllr,plhr,TLtp,lprh,lprl,lkh,lkl,tpl,mh,ml,hh,hl,prh,
             prl] = tqplate_loss_04017r1_1(dom,phsu,abs(s'),ang);
                % Torque plate loss function, motor inputs
         TLtpm = TLtp;
         leak=TLtpm+TLcbm;
         %convert from english to SI units
```

```
        flow = ((s.*dsp'/231)+leak).*.0037854;%[m^3/min]
end
if(x==0)
    flow=0;
end

function [T,loss]=torqueLossonePump(x,w,P)
parameters_04017r1
areas_04017r1
cop_04017r1
D=222e-6;
Tideal=abs(P*D*x/(2*pi));
%convert values from SI to english units:
dsp=x'*222/16.39;
s=w'*60/(2*pi);
phsu=P'/6894.75;
ang=asin(dsp/(pba*tpscd*np))*180/pi;
                                        %calculate pump
    angle from displacement
st = tpscd*sin(ang*pi/180)/12*2;
                                            % Pump
   piston stroke (ft/rev)
xxx=x;
%calculate torqueloss
if(sign(w*x)==-1)%pumping
Q = abs(s.*dsp'/231);

   % Flow rate, pump (gpm)
[m,n] = size(s);
% [pdp,pdm] = pist_drag_04017r1(abs(sp),abs(sm'),abs(stp),stm);
                                    % Piston drag loss function
```

```
cfp = 0.000028416*mpo*pcd/2*abs(s).^2;                    % Pump
    centrifugal force (lbf)
ffp = cfp*pcf;                                            % Pump
    friction force (lbf)
hplp = ffp.*abs(st).*abs(s)/33000*np;                     %
    Pump horsepower loss (hp)
pdp = hplp./abs(s)*5252;                                  % Pump
    piston drag (lbf-ft)
% [prdp,prdm] = pist_ring_drag_04017r1(phsu,abs(sp),abs(sm'),
    abs(stp),stm);                          % Piston ring drag loss
    function
pmuv = pmu*ones(m,1);                                     %
    Makeup pressure, vector form (psi)
rfhp = phsu*par;                                          %
    High pressure ring force (lbf)
rflp = pmuv*par;                                          %
    Low pressure ring force (lbf)
ffhp = rfhp*pcf;                                          %
    High pressure friction force (lbf)
fflp = rflp*pcf;                                          %
    Low pressure friction force (lbf)
hplp = ffhp.*abs(st).*abs(s)*nph/(550*60) + fflp.*abs(st).*abs(
    s)*npl/(550*60); % Pump horsepower loss (hp)
prdp = hplp./abs(s)*5252;
                                                  % Pump torque loss (
    lbf-ft)
% [sjlp,sjlm,pvp,pvm] = spher_joint_loss_04017r1(phsu,abs(sp),
    abs(sm'),abs(pang), mang);        % Spherical joint loss
    function
ca = pi/4*(pd^2 - phd^2);                                 %
    Clamp area (in^2)
```

```
sa = pi/4*(gd^2 - phd^2) + pi/4*(ds^2 - gd^2)*sjpd;          %
    Separating area (in^2)
jfh = phsu*(ca - sa);                                        %
    High pressure joint force (lbf)
jfl = pmuv*(ca - sa);                                        %
    Low pressure joint force (lbf)
ffh = jfh*pcf;                                               %
    High pressure friction force (lbf)
ffl = jfl*pcf;                                               %
    Low pressure friction force (lbf)
jdp = pi*ds*abs(ang)*4/(360*12);
                                        % Pump joint travel (in/
    rev)
hplp = ffh.*jdp.*abs(s)*nph/(550*60) + ffl.*jdp.*abs(s)*npl
    /(550*60); % Pump horsepower loss (hp)
sjlp = hplp./abs(s)*5252;
                                                % Pump spherical
    joint loss (lbf-ft)
% [TLcb, cbl, hh, hl, prh, prl] = cb_thrbrg_04017r1(phsu, abs(sp),
    dopuckp);                   % Cylinder block thrust bearing
    function
pll = (plod-plid)/2;
                                                             %
     Puck land length (in)
plw = pi*plid;

   % Puck land width (in)
prh = (phsu*pba+pkspl)/puckpa;
                                                        % High
    recess pressure (psi)
[m,n] = size(prh);
prl = (pmu*pba+pkspl)/puckpa*ones(m,n);
```

```
for i = 1:m
    if prl(i) > pmu
        prl(i) = pmu - .00001;
    end
end
plhp = pi*dopuckp^2/4*cdch*(2/dens*(phsu-prh)).^0.5*60;
                                        % High pressure puck
    leakage
pllp = pi*dopuckp^2/4*cdch*(2/dens*(pmu-prl)).^0.5*60;
                                    % Low pressure puck leakage
a = prh*plpd*plw*60/(12*visc*pll);
                                                % Equations for
    finding roots of hh (see hand writeup)
b = zeros(m,n);
c = zeros(m,n);
d = -plhp;
for i = 1:m
    hh1(i,:) = [a(i) b(i) c(i) d(i)];
    hh2(:,i) = roots(hh1(i,:));
end
hh = hh2(3,:);

   % High pressure film thickness (in)
a = prl*plpd*plw*60/(12*visc*pll);
                                                % Equations for
    finding roots of hl (see writeup)
b = zeros(m,n);
c = zeros(m,n);
d = -pllp;
for i = 1:m
    hl1(i,:) = [a(i) b(i) c(i) d(i)];
    hl2(:,i) = roots(hl1(i,:));
```

```
end
hl = hl2(3,:);

   % Low pressure film thickness
tlc = visc1*(plod^4+2*plod^3*plid-2*plod*plid^3-plid^4)
   /28013.28;                  % Torque loss constant
cblh = (abs(s)*tlc*nph)./(hh'*12);
                                                  % Puck
   drag, high pressure (lbf-ft)
cbll = (abs(s)*tlc*npl)./(hl'*12);
                                                  % Puck
   drag, low pressure (lbf-ft)
cbl = cblh+cbll;

   % Puck drag, total (lbf-ft)
cblp = cbl;

   % Puck drag, pump (lbf-ft)
% [fl] = flow_loss_04017r1(Q);
                                                    % Flow
   loss function
ifr = [0.00; 17.9854727272727; 36.2747672727273;
   54.4853454545455; 72.7777818181818; 91.03];
tlt = [0.00; 0.86286834656211; 1.89340040374819;
   4.18853919164347; 7.15005702851427; 10.7];
fl_pabax = interp1(ifr,tlt,Q,'spline');          % PABAX flow
   loss
fl = fl_pabax*flcalc;                            % Adjusted flow
    loss
flp = fl;

   % Pump and motor flow loss (lbf-ft)
```

```
% [pllrp,plhrp,TLtp,lprh,lprl,lkh,lkl,tpl,mh,ml,hh,hl,prh,prl]
    = tqplate_loss_04017r1(dop,Q,phsu,abs(sp),pang);    % Torque
    plate loss function, pump inputs
prl = 10*ones(m,1);
                                                        %
    Initial value for low recess pressure (psi)
moment_cond = 0;
                                                        %
    Initial moment condition (0=false)
while moment_cond == 0
% Land widths and lengths (in)
kilg = kio-kii;
                                                        %
    Inside kidney land length
kolg = koo-koi;
                                                        %
    Outside kidney land length
obgilg = obgio-obgii;
                                                        % Inside
    overbalance groove land length
obgolg = obgoo-obgoi;
                                                        % Outside
    overbalance groove land length
kiw = 2*pi*kii;
                                                        %
    Kidney inside land width (circumference based on inside
    radius)
kow = 2*pi*koi;
                                                        %
    Kidney outside land width (circumference based on inside
    radius)
```

```
obgiw = 2*pi*obgii;
                                                    % Inside
    overbalance groove width (circumference based on inside
    radius)
obgow = 2*pi*obgoi;
                                                    %
    Outside overbalance groove width (circumference based on
    inside radius)
% Pressures (psi)
klpl = pmu*ldp;
                                                    %
    Kidney lands pressure, low
klph = phsu*ldp;
                                                    %
    Kidney lands pressure, high
obgpl = prl;
                                                    %
     Initial overbalance groove pressure, low
obglpl = prl*ldp;
                                                    %
    Initial ob land pressure, low
kpl = pmu;

    % Kidney pressure, low
kph = phsu;

    % Kidney pressure, high
ppl = pmu;

    % Piston pressure, low
```

```
pph = phsu;

   % Piston pressure, high
% Loads (lbf)
obgill = obglpl*obgial;
                                                    % Initial
   inside obg land load, low pressure
obgoll = obglpl*obgoal;
                                                    % Initial
   outside ob land load, low pressure
kill = klpl*kial;
                                                        %
   Inside kidney land load, low pressure
kilh = klph*kiah;
                                                        %
   Inside kidney land load, high pressure
koll = klpl*koal;
                                                        %
   Outside kidney land load, low pressure
kolh = klph*koah;
                                                        %
   Outside kidney land load, high pressure
obgll = obgpl*obgal;
                                                    % Initial
    ob groove load, low pressure
kall = kpl*(kaal);
                                                        %
   Kidney annulus load, low pressure
kalh = kph*(kaah);
                                                        %
   Kidney annulus load, high pressure
```

```
pll = ppl*pal*cos(ang*pi/180);
                                                    % Piston load,
    low pressure
plh = pph*pah.*cos(ang*pi/180);
                                                   % Piston load,
    high pressure
ffp = 0; fflp = 0; ffhp = 0;
                                                    % PISTON AND
    PISTON RING FRICTION FORCE NO LONGER USED IN PISTON LOAD
    CALCS
pllr = pll-ffp-fflp;
                                                              %
    Resultant piston load, low pressure
plhr = plh+ffp+ffhp;
                                                              %
    Resultant piston load, high pressure
% Moments, high pressure pivot (lbf-in)
obgimhl = -obgill*obgicophl;
                                                    % Initial inside
    ob land moment, hpp, lp
obgomhl = -obgoll*obgocophl;
                                                    % Initial outside
     ob land moment, hpp, lp
kimhl = -kill*kicophl;
                                                          % Inside
    kidney land moment, hpp, lp
kimhh = -kilh*kicophh;
                                                          % Inside
    kidney land moment, hpp, hp
komhl = -koll*kocophl;
                                                          % Outside
    kidney land moment, hpp, lp
```

```
komhh = -kolh*kocophh;
                                                    % Outside
    kidney land moment, hpp, hp
obgmhl = -obgll*obgcophl;
                                                % Initial ob
    groove moment, hpp, lp
kamhl = -kall*kacophl;
kamhh = -kalh*kacophh;
pmhl = pllr*pcophl;
                                                    % Piston
     moment, hpp, lp
pmhh = plhr*pcophh;
                                                    % Piston
     moment, hpp, hp
mhl = (kamhl+obgimhl+obgomhl+kimhl+komhl+obgmhl+pmhl);
                        % Initial moment, high pressure pivot, low
    pressures
mhh = (kamhh+kimhh+komhh+pmhh);
                                                % Moment, high
    pressure pivot, high pressures (knowns only)
% Moments, low pressure pivot (lbf-in)
obgimll = -obgill*obgicopll;
                                                % Initial inside
    ob land moment, lpp, lp
obgomll = -obgoll*obgocopll;
                                                % Initial outside
     ob land moment, lpp, lp
kimll = -kill*kicopll;
                                                    % Inside
    kidney land moment, lpp, lp
```

```
kimlh = -kilh*kicoplh;
                                                    % Inside
    kidney land moment, lpp, hp
komll = -koll*kocopll;
                                                    % Outside
    kidney land moment, lpp, lp
komlh = -kolh*kocoplh;
                                                    % Outside
    kidney land moment, lpp, hp
obgmll = -obgll*obgcopll;
                                                % Initial ob
    groove moment, lpp, lp
kamll = -kall*kacopll;
kamlh = -kalh*kacoplh;
pmll = pllr*pcopll;
                                                    % Piston
     moment, lpp, lp
pmlh = plhr*pcoplh;
                                                    % Piston
     moment, lpp, hp
mll = (obgmll+obgimll+obgomll+kamll+kimll+komll+pmll);
                    % Initial moment, low pressure pivot, low
    pressures
mlh = (kamlh+kimlh+komlh+pmlh);
                                                % Moment, low
    pressure pivot, high pressures (knowns only)
% Calculation of overbalance groove pressure, high (psi)
prh = (mhl+mhh+mll+mlh)/(obgah*(obgcophh+obgcoplh)+ldp*obgiah*(
    obgicophh+obgicoplh)+ldp*obgoah*(obgocophh+obgocoplh));
lprh = nph*pi*dop^2/4*cdch*(2/dens*(phsu-prh)).^(1/2)*60;
                    % Leakage, overbalance groove, high
    pressure (in^3/min)
```

```
hh = (lprh*24*visc./(prh*ldp*60*(obgiw/obgilg+obgow/obgolg)))
    .^(1/3);    % Film thickness, high pressure side (in)
hl = hh;

    % Film thickness, low pressure side (in)
aa = hh.^3*dens*ldp/(npl^2*pi^2*dop^4*cdch^2*visc*60*3)*(obgow/
    obgolg+obgiw/obgilg);
bb = 1;
cc = -(hh.^3*pmu*ldp*60/(visc*24)*(obgow/obgolg+obgiw/obgilg));
for i = 1:m
lprl1(i,:) = [aa(i) bb cc(i)];
lprl2(:,i) = roots(lprl1(i,:));
                                        % Roots for low
    recess pressure leakage
end
lprl = lprl2(2,:)';
                                                        %
    Leakage, overbalance groove, low pressure (in^3/min)
prl = pmu-lprl.^2*dens*8/(npl^2*pi^2*dop^4*cdch^2*60^2);
                        % Low recess pressure (psi)
% Recalculation of pressures, loads, moments dependent on prl
obgpl = prl;
                                                            %
     Overbalance groove pressure, low
obglpl = prl*ldp;
                                                        %
    Overbalance land pressure, low
obgill = obglpl*obgial;
                                                % Inside ob
    land load, low pressure
```

```
obgoll = obglpl*obgoal;
                                                    % Outside ob
    land load, low pressure
obgll = obgpl*obgal;
                                                    %
   Overbalance groove load, low pressure
obgimhl = -obgill*obgicophl;
                                                    % Inside ob land
   moment, hpp, lp
obgomhl = -obgoll*obgocophl;
                                                    % Outside ob land
    moment, hpp, lp
obgmhl = -obgll*obgcophl;
                                                    % Overbalance
   groove moment, hpp, lp
obgimll = -obgill*obgicopll;
                                                    % Inside ob land
   moment, lpp, lp
obgomll = -obgoll*obgocopll;
                                                    % Outside ob land
    moment, lpp, lp
obgmll = -obgll*obgcopll;
                                                    % Overbalance
   groove moment, lpp, lp
% Undefined loads and moments
obgilh = prh*ldp*obgiah;
                                                    % Inside ob
   land load, high pressure (lbf)
obgolh = prh*ldp*obgoah;
                                                    % Outside ob
   land load, high pressure (lbf)
```

```
obglh = prh*obgah;
                                                    % Ob
    groove load, high pressure (lbf)
obgimhh = -obgilh*obgicophh;
                                                % Inside ob land
    moment, hpp, hp (lbf-in)
obgomhh = -obgolh*obgocophh;
                                                % Outside ob land
     moment, hpp, hp (lbf-in)
obgmhh = -obglh*obgcophh;
                                                   % Ob groove
    moment, hpp, hp (lbf-in)
obgimlh = -obgilh*obgicoplh;
                                                % Inside ob land
    moment, lpp, hp (lbf-in)
obgomlh = -obgolh*obgocoplh;
                                                % Outside ob land
     moment, lpp, hp (lbf-in)
obgmlh = -obglh*obgcoplh;
                                                   % Ob groove
    moment, lpp, hp (lbf-in)
% Recalculation of total high pressure pivot and low pressure
    pivot moments
mhh = kamhh+kimhh+komhh+obgimhh+obgomhh+obgmhh+pmhh;
                          % Moment, hpp, hp (lbf-in)
mhl = (kamhl+obgimhl+obgomhl+kimhl+komhl+obgmhl+pmhl);
                         % Moment, hpp, lp (lbf-in)
mh = (mhl+mhh)/12;
                                                    %
    Moment, high pressure pivot (lbf-ft)
mlh = kamlh+kimlh+komlh+obgimlh+obgomlh+obgmlh+pmlh;
                          % Moment, lpp, hp (lbf-in)
```

```
mll = (kamll+obgimll+obgomll+kimll+komll+obgmll+pmll);
                        % Moment, lpp, lp (lbf-in)
ml = (mll+mlh)/12;
                                                        %
    Moment, low pressure pivot (lbf-ft)
cond = abs(abs(mh)-abs(ml));
                                                % Condition
    statement for while loop
moment_cond = all(cond <= 0.01);
                                            % Condition to exit
    while loop --> moment_delta < 0.1

    % for each step --> moment_cond = 1 when this is the case
end
pistloadtotal = pllr + plhr;
tqplateload = kall+kalh+obgll+obglh+obgill+obgilh+obgoll+obgolh
    +kill+kilh+koll+kolh;
% Loss Calculations
% Leakage calculations - all leakages in gpm
hl = hh;
lprh = lprh/231;
                                                        %
    High recess pressure leakage (gpm)
lprl = lprl/231;
                                                        % Low
     recess pressure leakage (gpm)
Lkih = kiw*hh.^3.*phsu*ldp*60/(visc*kilg*24*231);
                            % Inside kidney land leak, hp (gpm)
Lkil = kiw*hh.^3*pmu*ldp*60/(visc*kilg*24*231);
                           % Inside kidney land leak, lp (gpm)
```

```
Lkoh = kow*hh.^3.*phsu*ldp*60/(visc*kolg*24*231);
                                % Outside kidney land leak, hp (gpm
    )
Lkol = kow*hh.^3*pmu*ldp*60/(visc*kolg*24*231);
                               % Outside kideny land leak, lp (gpm)
lkh = Lkih+Lkoh;
                                                                  %
    High pressure kidney leakage (gpm)
lkl = Lkil+Lkol;
                                                                  % Low
     pressure kidney leakage (gpm)
TLhp = lkh+lprh;
                                                                  %
    Torque plate leakage, high pressure (gpm)
TLlp = lkl+lprl;
                                                                  %
    Torque plate leakage, low pressure (gpm)
TLtp = TLhp+TLlp;
                                                                 %
    Torque plate leakage, total (gpm)
% Torque Loss Calculations
% Torque loss constant
tlc = visc*pi^2/120*((obgoo^4+2*obgoo^3*obgoi-2*obgoo*obgoi^3-
    obgoi^4)+(obgio^4+2*obgio^3*obgii-2*obgio*obgii^3-obgii^4)+(
    koo^4+2*koo^3*koi-2*koo*koi^3-koi^4)+(kio^4+2*kio^3*kii-2*
    kio*kii^3-kii^4)+(tpore^4+2*tpore^3*tpoie-2*tpore*tpoie^3-
    tpoie^4));
tpl = abs(s).*tlc./(hh*12);
plt = plhr+pllr;
tpltotal = obgilh+obgolh+obglh+obgill+obgoll+obgll+kall+kalh+
    kill+kilh+koll+kolh ;     % Total torque plate (separating)
    load (lbf)
```

```
[plt tpltotal];
tplp = tpl;

   % Torque loss, pump torque plate interface (lbf-ft)
ptl = pdp+prdp+sjlp+cblp+flp+tplp;
                                                    % Pump
   torque loss (lbf-ft)
Tlosspump=1/0.73756*(ptl');%Nm
T=Tideal+Tlosspump;
if(xxx>=0)
    T=T;
else
    T=-T;
end
loss=Tlosspump;
else%motoring
Q = abs(s.*dsp'/231);

   % Flow rate, pump (gpm)
[m,n] = size(s);
% [pdp,pdm] = pist_drag_04017r1(abs(sp),abs(sm'),abs(stp),stm);
                                % Piston drag loss function
cfm = 0.000028416*mpo*pcd/2*abs(s).^2;              % Motor
   centrifugal force (lbf)
ffm = cfm*pcf;                                  % Motor
   friction force (lbf)
hplm = ffm.*abs(st).*abs(s)/33000*np;                    %
   Motor horsepower loss (hp)
x=abs(s);
for i = 1:m
if x(i) <= 0.0000001
    pdm(i) = 0;
```

```
else pdm(i) = hplm(i)/x(i)*5252;                    % Motor piston
    drag (lbf-ft)
end
end
pdm = pdm';
% [prdp,prdm] = pist_ring_drag_04017r1(phsu,abs(sp),abs(sm'),
    abs(stp),stm);                    % Piston ring drag loss
    function
pmuv = pmu*ones(m,1);                                          %
    Makeup pressure, vector form (psi)
rfhp = phsu*par;
    % High pressure ring force (lbf)
rflp = pmuv*par;                                               %
    Low pressure ring force (lbf)
ffhp = rfhp*pcf;                                               %
    High pressure friction force (lbf)
fflp = rflp*pcf;                                               %
    Low pressure friction force (lbf)
hplm = ffhp.*abs(st).*abs(s)*nph/(550*60) + fflp.*st.*abs(s)*
    npl/(550*60);    % Motor horsepower loss (hp)
x=abs(s);
for i = 1:m
if x(i) <= 0.001
     prdm(i) = 0;
else prdm(i) = hplm(i)/x(i)*5252;                              %
    Motor torque loss (lbf-ft)
end
end
prdm = prdm';
% [sjlp,sjlm,pvp,pvm] =
% spher_joint_loss_04017r1(phsu,abs(sp),abs(sm'),abs(pang),
    mang);        % Spherical joint loss function
```

```
pmuv = pmu*ones(m,1);                                                    %
    Makeup pressure, vector form (psi)
ca = pi/4*(pd^2 - phd^2);                                                %
    Clamp area (in^2)
sa = pi/4*(gd^2 - phd^2) + pi/4*(ds^2 - gd^2)*sjpd;                      %
    Separating area (in^2)
cona = pi/4*(ds^2-shd^2);                                                %
    Contact area (in^2)
jfh = phsu*(ca - sa);
    % High pressure joint force (lbf)
jfl = pmuv*(ca - sa);                                                    %
    Low pressure joint force (lbf)
cph = jfh/cona;                                                          %
    High contact pressure (psi)
cpl = jfl/cona;                                                          %
    Low contact pressure (psi)
ffh = jfh*pcf;                                                           %
    High pressure friction force (lbf)
ffl = jfl*pcf;                                                           %
    Low pressure friction force (lbf)
jdm = pi*ds*ang*4/(360*12);                                              %
     Motor joint travel (in/rev)
jsm = jdm.*abs(s)/12;
                                                    % Joint speed
    motor (ft/min)
hplm = ffh.*jdm.*abs(s)*nph/(550*60) + ffl.*jdm.*abs(s)*npl
    /(550*60); % Motor horsepower loss (hp)
x=abs(s);
for i = 1:m
if x(i) <= 0.001
     sjlm(i) = 0;
```

```
else sjlm(i) = hplm(i)/x(i)*5252;                                    %
    Motor spherical joint loss (lbf-ft)
end
end
sjlm = abs(sjlm)';
% [TLcb, cbl, hh, hl, prh, prl] = cb_thrbrg_04017r1(phsu, abs(sm'),
    dopuckm);
%% Cylinder block thrust bearing function
pll = (plod-plid)/2;
                                                                     %
     Puck land length (in)
plw = pi*plid;

    % Puck land width (in)
bal = puckpa/pba;

    % Overbalance
prh = (phsu*pba+pkspl)/puckpa;
                                                          % High
    recess pressure (psi)
[m,n] = size(prh);
prl = (pmu*pba+pkspl)/puckpa*ones(m,n);
for i = 1:m
     if prl(i) > pmu
          prl(i) = pmu - .00001;
     end
end
plhp = pi*dopuckm^2/4*cdch*(2/dens*(phsu-prh)).^0.5*60;
                                              % High pressure puck
    leakage
```

```
tlhp = plhp*nph;

   % High pressure total leakage
pllp = pi*dopuckm^2/4*cdch*(2/dens*(pmu-prl)).^0.5*60;
                                    % Low pressure puck leakage
tllp = pllp*npl;

   % Low pressure total leakage
TLcb = (tlhp + tllp)/231;
                                                          %
   Leakage per interface (gpm)
a = prh*plpd*plw*60/(12*visc*pll);
                                                  % Equations for
    finding roots of hh (see hand writeup)
b = zeros(m,n);
c = zeros(m,n);
d = -plhp;
for i = 1:m
    hh1(i,:) = [a(i) b(i) c(i) d(i)];
    hh2(:,i) = roots(hh1(i,:));
end
hh = hh2(3,:);

   % High pressure film thickness (in)
a = prl*plpd*plw*60/(12*visc*pll);
                                                  % Equations for
    finding roots of hl (see writeup)
b = zeros(m,n);
c = zeros(m,n);
d = -pllp;
for i = 1:m
    hl1(i,:) = [a(i) b(i) c(i) d(i)];
```

```
    hl2(:,i) = roots(hl1(i,:));
end
hl = hl2(3,:);

   % Low pressure film thickness
tlc = visc1*(plod^4+2*plod^3*plid-2*plod*plid^3-plid^4)
   /28013.28;                  % Torque loss constant
cblh = (abs(s)*tlc*nph)./(hh'*12);
                                                  % Puck
   drag, high pressure (lbf-ft)
cbll = (abs(s)*tlc*npl)./(hl'*12);
                                                  % Puck
   drag, low pressure (lbf-ft)
cbl = cblh+cbll;

   % Puck drag, total (lbf-ft)
cblm = cbl;

   % Puck drag, motor (lbf-ft)
% [fl] = flow_loss_04017r1(Q);

   % Flow loss function
ifr = [0.00; 17.9854727272727; 36.2747672727273;
   54.4853454545455; 72.7777818181818; 91.03];
tlt = [0.00; 0.86286834656211; 1.89340040374819;
   4.18853919164347; 7.15005702851427; 10.7];
fl_pabax = interp1(ifr,tlt,Q,'spline');          % PABAX flow
   loss
fl = fl_pabax*flcalc;                            % Adjusted flow
    loss
```

```
flm = fl;

    % Pump and motor flow loss (lbf-ft)
% [pllr,plhr,TLtp,lprh,lprl,lkh,lkl,tpl,mh,ml,hh,hl,prh,prl] =
    tqplate_loss_04017r1(dom,Q,phsu,abs(sm'),mang);      % Torque
    plate loss function, motor inputs
%v,w,x,y,z
v=dom;
x=phsu;
y=abs(s);
z=ang;
prl = 10*ones(m,1);
                                                          %
    Initial value for low recess pressure (psi)
moment_cond = 0;
                                                            %
    Initial moment condition (0=false)
while moment_cond == 0
% Land widths and lengths (in)
kilg = kio-kii;
                                                             %
    Inside kidney land length
kolg = koo-koi;
                                                             %
    Outside kidney land length
obgilg = obgio-obgii;
                                                          % Inside
    overbalance groove land length
obgolg = obgoo-obgoi;
                                                          % Outside
    overbalance groove land length
```

```
kiw = 2*pi*kii;
                                                              %
    Kidney inside land width (circumference based on inside
    radius)
kow = 2*pi*koi;
                                                              %
    Kidney outside land width (circumference based on inside
    radius)
obgiw = 2*pi*obgii;
                                                          % Inside
     overbalance groove width (circumference based on inside
    radius)
obgow = 2*pi*obgoi;
                                                          %
    Outside overbalance groove width (circumference based on
    inside radius)
% Pressures (psi)
klpl = pmu*ldp;
                                                              %
    Kidney lands pressure, low
klph = x*ldp;
                                                               %
    Kidney lands pressure, high
obgpl = prl;
                                                                %
     Initial overbalance groove pressure, low
obglpl = prl*ldp;
                                                              %
    Initial ob land pressure, low
kpl = pmu;

    % Kidney pressure, low
```

```
kph = x;

    % Kidney pressure, high
ppl = pmu;

    % Piston pressure, low
pph = x;

    % Piston pressure, high
% Loads (lbf)
obgill = obglpl*obgial;
                                                    % Initial
    inside obg land load, low pressure
obgoll = obglpl*obgoal;
                                                    % Initial
    outside ob land load, low pressure
kill = klpl*kial;
                                                        %
    Inside kidney land load, low pressure
kilh = klph*kiah;
                                                        %
    Inside kidney land load, high pressure
koll = klpl*koal;
                                                        %
    Outside kidney land load, low pressure
kolh = klph*koah;
                                                        %
    Outside kidney land load, high pressure
obgll = obgpl*obgal;
                                                    % Initial
     ob groove load, low pressure
```

```
kall = kpl*(kaal);
                                                    %
    Kidney annulus load, low pressure
kalh = kph*(kaah);
                                                    %
    Kidney annulus load, high pressure
pll = ppl*pal*cos(z*pi/180);
                                                % Piston load,
    low pressure
plh = pph*pah.*cos(z*pi/180);
                                               % Piston load,
    high pressure
ffp = 0; fflp = 0; ffhp = 0;
                                                % PISTON AND
    PISTON RING FRICTION FORCE NO LONGER USED IN PISTON LOAD
    CALCS
pllr = pll-ffp-fflp;
                                                    %
    Resultant piston load, low pressure
plhr = plh+ffp+ffhp;
                                                    %
    Resultant piston load, high pressure
% Moments, high pressure pivot (lbf-in)
obgimhl = -obgill*obgicophl;
                                                % Initial inside
    ob land moment, hpp, lp
obgomhl = -obgoll*obgocophl;
                                                % Initial outside
     ob land moment, hpp, lp
kimhl = -kill*kicophl;
                                                    % Inside
    kidney land moment, hpp, lp
```

```
kimhh = -kilh*kicophh;
                                                    % Inside
    kidney land moment, hpp, hp
komhl = -koll*kocophl;
                                                    % Outside
    kidney land moment, hpp, lp
komhh = -kolh*kocophh;
                                                    % Outside
    kidney land moment, hpp, hp
obgmhl = -obgll*obgcophl;
                                                % Initial ob
    groove moment, hpp, lp
kamhl = -kall*kacophl;
kamhh = -kalh*kacophh;
pmhl = pllr*pcophl;
                                                    % Piston
     moment, hpp, lp
pmhh = plhr*pcophh;
                                                    % Piston
     moment, hpp, hp
mhl = (kamhl+obgimhl+obgomhl+kimhl+komhl+obgmhl+pmhl);
                    % Initial moment, high pressure pivot, low
    pressures
mhh = (kamhh+kimhh+komhh+pmhh);
                                                % Moment, high
    pressure pivot, high pressures (knowns only)
% Moments, low pressure pivot (lbf-in)
obgimll = -obgill*obgicopll;
                                                % Initial inside
    ob land moment, lpp, lp
```

```
obgomll = -obgoll*obgocopll;
                                                    % Initial outside
    ob land moment, lpp, lp
kimll = -kill*kicopll;
                                                    % Inside
   kidney land moment, lpp, lp
kimlh = -kilh*kicoplh;
                                                    % Inside
   kidney land moment, lpp, hp
komll = -koll*kocopll;
                                                    % Outside
   kidney land moment, lpp, lp
komlh = -kolh*kocoplh;
                                                    % Outside
   kidney land moment, lpp, hp
obgmll = -obgll*obgcopll;
                                                  % Initial ob
   groove moment, lpp, lp
kamll = -kall*kacopll;
kamlh = -kalh*kacoplh;
pmll = pllr*pcopll;
                                                    % Piston
    moment, lpp, lp
pmlh = plhr*pcoplh;
                                                    % Piston
    moment, lpp, hp
mll = (obgmll+obgimll+obgomll+kamll+kimll+komll+pmll);
                      % Initial moment, low pressure pivot, low
   pressures
mlh = (kamlh+kimlh+komlh+pmlh);
                                                % Moment, low
   pressure pivot, high pressures (knowns only)
```

```
% Calculation of overbalance groove pressure, high (psi)
prh = (mhl+mhh+mll+mlh)/(obgah*(obgcophh+obgcoplh)+ldp*obgiah*(
    obgicophh+obgicoplh)+ldp*obgoah*(obgocophh+obgocoplh));
lprh = nph*pi*v^2/4*cdch*(2/dens*(x-prh)).^(1/2)*60;
                        % Leakage, overbalance groove, high
    pressure (in^3/min)
hh = (lprh*24*visc./(prh*ldp*60*(obgiw/obgilg+obgow/obgolg)))
    .^(1/3);    % Film thickness, high pressure side (in)
hl = hh;

    % Film thickness, low pressure side (in)
aa = hh.^3*dens*ldp/(npl^2*pi^2*v^4*cdch^2*visc*60*3)*(obgow/
    obgolg+obgiw/obgilg);
bb = 1;
cc = -(hh.^3*pmu*ldp*60/(visc*24)*(obgow/obgolg+obgiw/obgilg));
for i = 1:m
lprl1(i,:) = [aa(i) bb cc(i)];
lprl2(:,i) = roots(lprl1(i,:));
                                            % Roots for low
    recess pressure leakage
end
lprl = lprl2(2,:)';
                                                          %
    Leakage, overbalance groove, low pressure (in^3/min)
prl = pmu-lprl.^2*dens*8/(npl^2*pi^2*v^4*cdch^2*60^2);
                        % Low recess pressure (psi)
% Recalculation of pressures, loads, moments dependent on prl
obgpl = prl;
                                                          %
     Overbalance groove pressure, low
```

```
obglpl = prl*ldp;
                                                    %
    Overbalance land pressure, low
obgill = obglpl*obgial;
                                                    % Inside ob
    land load, low pressure
obgoll = obglpl*obgoal;
                                                    % Outside ob
     land load, low pressure
obgll = obgpl*obgal;
                                                    %
    Overbalance groove load, low pressure
obgimhl = -obgill*obgicophl;
                                                    % Inside ob land
    moment, hpp, lp
obgomhl = -obgoll*obgocophl;
                                                    % Outside ob land
     moment, hpp, lp
obgmhl = -obgll*obgcophl;
                                                    % Overbalance
    groove moment, hpp, lp
obgimll = -obgill*obgicopll;
                                                    % Inside ob land
    moment, lpp, lp
obgomll = -obgoll*obgocopll;
                                                    % Outside ob land
     moment, lpp, lp
obgmll = -obgll*obgcopll;
                                                    % Overbalance
    groove moment, lpp, lp
% Undefined loads and moments
```

```
obgilh = prh*ldp*obgiah;
                                                    % Inside ob
    land load, high pressure (lbf)
obgolh = prh*ldp*obgoah;
                                                    % Outside ob
    land load, high pressure (lbf)
obglh = prh*obgah;
                                                        % Ob
    groove load, high pressure (lbf)
obgimhh = -obgilh*obgicophh;
                                                  % Inside ob land
    moment, hpp, hp (lbf-in)
obgomhh = -obgolh*obgocophh;
                                                  % Outside ob land
     moment, hpp, hp (lbf-in)
obgmhh = -obglh*obgcophh;
                                                     % Ob groove
    moment, hpp, hp (lbf-in)
obgimlh = -obgilh*obgicoplh;
                                                  % Inside ob land
    moment, lpp, hp (lbf-in)
obgomlh = -obgolh*obgocoplh;
                                                  % Outside ob land
     moment, lpp, hp (lbf-in)
obgmlh = -obglh*obgcoplh;
                                                     % Ob groove
    moment, lpp, hp (lbf-in)
% Recalculation of total high pressure pivot and low pressure
    pivot moments
mhh = kamhh+kimhh+komhh+obgimhh+obgomhh+obgmhh+pmhh;
                          % Moment, hpp, hp (lbf-in)
```

```
mhl = (kamhl+obgimhl+obgomhl+kimhl+komhl+obgmhl+pmhl);
                        % Moment, hpp, lp (lbf-in)
mh = (mhl+mhh)/12;
                                                        %
    Moment, high pressure pivot (lbf-ft)
mlh = kamlh+kimlh+komlh+obgimlh+obgomlh+obgmlh+pmlh;
                          % Moment, lpp, hp (lbf-in)
mll = (kamll+obgimll+obgomll+kimll+komll+obgmll+pmll);
                        % Moment, lpp, lp (lbf-in)
ml = (mll+mlh)/12;
                                                        %
    Moment, low pressure pivot (lbf-ft)
cond = abs(abs(mh)-abs(ml));
                                                % Condition
    statement for while loop
moment_cond = all(cond <= 0.01);
                                              % Condition to exit
    while loop --> moment_delta < 0.1

    % for each step --> moment_cond = 1 when this is the case
end
pistloadtotal = pllr + plhr;
tqplateload = kall+kalh+obgll+obglh+obgill+obgilh+obgoll+obgolh
    +kill+kilh+koll+kolh;
% Loss Calculations
% Leakage calculations - all leakages in gpm
hl = hh;
lprh = lprh/231;
                                                        %
    High recess pressure leakage (gpm)
```

```
lprl = lprl/231;
                                                    % Low
    recess pressure leakage (gpm)
Lkih = kiw*hh.^3.*x*ldp*60/(visc*kilg*24*231);
                                % Inside kidney land leak, hp (gpm)
Lkil = kiw*hh.^3*pmu*ldp*60/(visc*kilg*24*231);
                               % Inside kidney land leak, lp (gpm)
Lkoh = kow*hh.^3.*x*ldp*60/(visc*kolg*24*231);
                                % Outside kidney land leak, hp (gpm
   )
Lkol = kow*hh.^3*pmu*ldp*60/(visc*kolg*24*231);
                               % Outside kideny land leak, lp (gpm)
lkh = Lkih+Lkoh;
                                                    %
   High pressure kidney leakage (gpm)
lkl = Lkil+Lkol;
                                                    % Low
    pressure kidney leakage (gpm)
TLhp = lkh+lprh;
                                                    %
   Torque plate leakage, high pressure (gpm)
TLlp = lkl+lprl;
                                                    %
   Torque plate leakage, low pressure (gpm)
% Torque Loss Calculations
% Torque loss constant
tlc = visc*pi^2/120*((obgoo^4+2*obgoo^3*obgoi-2*obgoo*obgoi^3-
   obgoi^4)+(obgio^4+2*obgio^3*obgii-2*obgio*obgii^3-obgii^4)+(
   koo^4+2*koo^3*koi-2*koo*koi^3-koi^4)+(kio^4+2*kio^3*kii-2*
   kio*kii^3-kii^4)+(tpore^4+2*tpore^3*tpoie-2*tpore*tpoie^3-
   tpoie^4));
tpl = y.*tlc./(hh*12);
```

```
plt = plhr+pllr;
tpltotal = obgilh+obgolh+obglh+obgill+obgoll+obgll+kall+kalh+
    kill+kilh+koll+kolh ;     % Total torque plate (separating)
    load (lbf)
[plt tpltotal];%
tplm = tpl;

    % Torque loss, motor torque plate interface (lbf-ft)
mtl = pdm+prdm+sjlm+cblm+flm+tplm;
Tlossmotor=1/0.73756*(mtl');%Nm
T=Tideal-Tlossmotor;
if(xxx>0)
    T=T;
else
    T=-T;
end
loss=Tlossmotor;
end
```

### A.2.2 Optimization Studies

```
%restrictionsinArchitecture.m
%plot drive cycle
load allcyclesFord
load indexengine
load enginemap4_6_3Vl
cyc=urban;
N=length(cyc.w);
r=(70+34)/34;
R1=r/(r-1);
R2=(r-1)/r;
R3=(r-1)*(r-1)/(r^2);
Rf=3.31;
```

```
%hybrid with restrictions
if 0
for(k=1:N)
    ww=cyc.w(k)*Rf;
    Tw=-cyc.torque(k)/Rf;
    if(cyc.torque(k)>0)
        %engine operation
        engspeed=[90:5:500];
        engtorque=[50:5:400];
        [engW,engT]=ndgrid(engspeed,engtorque);
        wheelw=ones(size(engW))*ww;
        wheelT=ones(size(engW))*Tw;
        %P/M operation
        wT=R1*wheelw;
        wS=wheelw-R1*engW;
        TT=-R2*wheelT-R3*engT;
        TS=R2*engT;
        effi=interpn(T_nm,omega_rads,efficiency,engT,engW);
        [l,h]=size(engW);
        for(j=1:l)
        for(i=[1:h])
            maxT=interp1(maxcurveomega_rads,maxcurveT_nm,engW(j
                ,i));
            if(maxT<engT(j,i))
                effi(j,i)=0;
            end
        end
        end
        for(j=1:length(effi))
            iip=find(TT(j,:)>0);
            iif1=find(TS(j,iip)<-48);
            ix1=iip(iif1);
```

```
            effi(j,ix1)=0;
            iin=find(TT(j,:)<0);
            iif2=find(TS(j,iin)>48);
            ix2=iin(iif2);
            effi(j,ix2)=0;
        end
        [val,i1]=max(effi);
        [val2,i2]=max(val);
        i1=i1(i2);
        eff(k)=effi(i1,i2);
        wengact(k)=engW(i1,i2);
        Tengact(k)=engT(i1,i2);
        wTact(k)=wT(i1,i2);
        wSact(k)=wS(i1,i2);
        TTact(k)=TT(i1,i2);
        TSact(k)=TS(i1,i2);
    else
        %braking regeneration
        wengact(k)=0;
        Tengact(k)=0;
        eff(k)=0;
        TTact(k)=R2*cyc.torque(k)/Rf;
        TSact(k)=0;
        wSact(k)=cyc.w(k)*Rf;
        wTact(k)=R1*cyc.w(k)*Rf;
    end
end
enginespeed=(cyc.w*Rf)*1/R1;
enginetorque=(cyc.torque/Rf)*R2/R3;
figure(1)
contour(omega_rads,T_nm,efficiency);hold on;
plot(maxcurveomega_rads,maxcurveT_nm);
```

```
plot(enginespeed,enginetorque,'*b');
plot(weng,Teng,'*r');
title('drive cycle at engine-mechanical only');
ylabel('engine torque [Nm]');
xlabel('engine speed [rad/s]');
axis([0 400 0 800])
wengrestrict=weng;
Tengrestrict=Teng;
figure(2)
plot(wS,TS,'*b');
title('P/M-S');
xlabel('speed [rad/s]');
ylabel('torque [Nm]');
figure(3)
plot(wT,TT,'*b');
title('P/M-T');
xlabel('speed [rad/s]');
ylabel('torque [Nm]');
ii=find(eff~=0);
meanengeff=sum(eff(ii))/length(ii)
end
%% for hybrid without restirctions
if 0
for(k=1:N)
    if(cyc.torque(k)>0)
        ww=cyc.w(k)*Rf;
        Tw=-cyc.torque(k)/Rf;
        %engine optimal
        optengspeed=141;
        optengtorque=358;
        weng(k)=optengspeed;
        Teng(k)=optengtorque;
```

```
        %P/M operation
        wT(k)=R1*ww;
        wS(k)=ww-R1*optengspeed;
        TT(k)=-R2*Tw-R3*optengtorque;
        TS(k)=R2*optengtorque;
        eff(k)=interpn(T_nm,omega_rads,efficiency,optengtorque,
            optengspeed);
    else
        %braking regeneration
        weng(k)=0;
        Teng(k)=0;
        eff(k)=0;
        TT(k)=R2*cyc.torque(k)/Rf;
        TS(k)=0;
        wS(k)=cyc.w(k)*Rf;
        wT(k)=R1*cyc.w(k)*Rf;
    end
end
enginespeed=(cyc.w*Rf)*1/R1;
enginetorque=(cyc.torque/Rf)*R2/R3;
figure(1)
contour(omega_rads,T_nm,efficiency);hold on;
plot(maxcurveomega_rads,maxcurveT_nm);
plot(enginespeed,enginetorque,'*b');
plot(weng,Teng,'*r');
title('drive cycle at engine-mechanical only');
ylabel('engine torque [Nm]');
xlabel('engine speed [rad/s]');
axis([0 400 0 800])
figure(2)
plot(wS,TS,'*b');
title('P/M-S');
```

```
xlabel('speed [rad/s]');
ylabel('torque [Nm]');
figure(3)
plot(wT,TT,'*b');
title('P/M-T');
xlabel('speed [rad/s]');
ylabel('torque [Nm]');
ii=find(eff~=0);
meanengeff=sum(eff(ii))/length(ii)
figure(5)
subplot(121)
hold on;
plot(enginespeed,enginetorque,'*b');
plot(weng,Teng,'*r');
contour(omega_rads,T_nm,efficiency);
plot(maxcurveomega_rads,maxcurveT_nm);
title('drive cycle at engine-hybrid');
legend('drive cycle at engine-mechanical only','optimal engine
    operation for hybrid');
ylabel('engine torque [Nm]');
xlabel('engine speed [rad/s]');
axis([0 400 0 600])
subplot(122)
hold on;
plot(enginespeed,enginetorque,'*b');
plot(wengrestrict,Tengrestrict,'*r');
contour(omega_rads,T_nm,efficiency);
plot(maxcurveomega_rads,maxcurveT_nm);
title('drive cycle at engine-hybrid with restrictions');
legend('drive cycle at engine-mechanical only','optimal engine
    operation for hybrid with restrictions');
ylabel('engine torque [Nm]');
```

```
xlabel('engine speed [rad/s]');
axis([0 400 0 600])
ans=0;
end
if 0
%find optimal points for CVT
for(k=1:N)
    power=cyc.power(k);
    if(power>0)
        ww=cyc.w(k)*Rf;
        Tw=-cyc.torque(k)/Rf;
        engspeed=[100:5:500];
        ls=length(engspeed);
        engtorque=power./engspeed;
        eff=interpn(T_nm,omega_rads,efficiency,engtorque,
            engspeed);
        for(i=1:ls)
            maxT=interp1(maxcurveomega_rads,maxcurveT_nm,
                engspeed(i));
            if(maxT<engtorque(i))
                eff(i)=0;
            end
        end
        [i,u]=max(eff);
        weng(k)=engspeed(u);
        Teng(k)=engtorque(u);
        eff(k)=i;
        wT(k)=R1*ww;
        wS(k)=ww-R1*weng(k);
        TT(k)=-R2*Tw-R3*Teng(k);
        TS(k)=R2*Teng(k);
    else
```

```
            weng(k)=0;
            Teng(k)=0;
            eff(k)=0;
            TT(k)=0;
            TS(k)=0;
            wS(k)=0;
            wT(k)=0;
        end
end
enginespeed=(cyc.w*Rf)*1/R1;
enginetorque=(cyc.torque/Rf)*R2/R3;
figure(1)
hold on;
plot(enginespeed,enginetorque,'*b');
plot(weng,Teng,'*r');
contour(omega_rads,T_nm,efficiency);
plot(maxcurveomega_rads,maxcurveT_nm);
title('optimal operation for CVT');
ylabel('engine torque [Nm]');
xlabel('engine speed [rad/s]');
legend('drive cycle at engine-mechanical only','optimal engine
    operation for CVT');
axis([0 400 0 600])
figure(2)
plot(wS,TS,'*b');
title('P/M-S');
xlabel('speed [rad/s]');
ylabel('torque [Nm]');
figure(3)
plot(wT,TT,'*b');
title('P/M-T');
xlabel('speed [rad/s]');
```

```
ylabel('torque [Nm]');
ii=find(eff~=0);
meanengeff=sum(eff(ii))/length(ii)
ans=0;
end
enginespeed=(cyc.w*Rf)*1/R1;
enginetorque=(cyc.torque/Rf)*R2/R3;
plot(enginespeed,enginetorque,'*r');
figure(1)
plot(cyc.w,cyc.torque,'*b');hold on;
plot(cyc.w(ix),cyc.torque(ix),'*r');
figure(2)
plot(enginespeed,enginetorque,'*r');
title('drive cycle at engine-mechanical only');
ylabel('engine torque [Nm]');
xlabel('engine speed [rad/s]');
figure(3)
contour(omega_rads,T_nm,efficiency);hold on;
plot(maxcurveomega_rads,maxcurveT_nm);
plot(enginespeed,enginetorque,'*b');
title('drive cycle at engine-mechanical only');
ylabel('engine torque [Nm]');
xlabel('engine speed [rad/s]');
axis([0 400 0 800])
optengspeed=150;
optengtorque=350;
ww=cyc.w*Rf;
Tw=-cyc.torque/Rf;
wT=R1*ww;
wS=ww-R1*optengspeed;
TT=-R2*Tw-R3*optengtorque;
TS=R2*optengtorque*ones(length(TT),1);
```

```
inzero=find(cyc.torque~=0);
TTpos=find(TT(inzero)>0);
TTneg=find(TT(inzero)<0);
P=2000*6894.75;
Tmax=P*222e-6*.1/(2*pi);
n1=find(TS(inzero(TTpos))<-Tmax);%never happens because engine
    torque positive!
n2=find(TS(inzero(TTneg))>Tmax);
notpos1=inzero(TTpos(n1));
notpos2=inzero(TTneg(n2));
brakeindex=find(Tw>0)
figure(3)
plot(ww,-Tw,'*b',...
     ww(notpos2),-Tw(notpos2),'*r',...
     ww(brakeindex),-Tw(brakeindex),'*g');
legend('possible to shift to engine optimal','not possible to
    shift to engine optimal','braking');
xlabel('engine speed [rad/sec]');
ylabel('engine torque [Nm]');
title('urban drive cycle');
wmech=ww*1/R1;
Tmech=Tw*-1*R2/R3;
figure(4)
plot(wmech,Tmech,'*b',...
     wmech(notpos2),Tmech(notpos2),'*r',...
     wmech(brakeindex),Tmech(brakeindex),'*g');
legend('possible to shift to engine optimal','not possible to
    shift to engine optimal','braking');
xlabel('engine speed [rad/sec]');
ylabel('engine torque [Nm]');
title('urban drive cycle');
```